



Determination of pollutions in the surface of water samples from Ogbajarajara river, Nigeria by spectrophotometer and atomic absorption spectrometry before evaluation of health risk assessment

Stanley Chukwuemeka Ihenetu ^{a,*}, Victor Obinna Njoku^a, Francis Chizoruo Ibe^a, Gang Li^b,
Arinze Chinweuba^c and Christian Ebere Enyoh^{a,d}

^a Department of Chemistry, Faculty of Physical Sciences, Imo State University, P.M.B 2000 Owerri, Nigeria

^b CAS Key Laboratory of Urban Environmental and Health, Institute of Urban Environment, Chinese Academy of Science, 1799 Jimei Road, Xiamen 361021, China

^c Chemistry Department, Chukwuemeka odimegwu Ojukwu University Uli, Anambra Nigeria

^d Graduate School of Science and Engineering, Saitama University, 255 Shimo-Okubo, Sakura-ku, Saitama 8570-338, Japan

ARTICLE INFO:

Received 19 Nov 2021

Revised form 21 Jan 2022

Accepted 15 Feb 2022

Available online 30 Mar 2022

Keywords:

Heavy metal,
Environment,
Pollution,
Surface water,
Spectrophotometer,
Atomic absorption spectrometry

ABSTRACT

Determination of environmental pollution in the surface water is very important. So, in this study, determination, and health risk assessment were evaluated. The pollutions such as anions, cations, and heavy metals were analyzed in surface water by photometer spectrometry and atomic absorption spectrometry (AAS). Other parameters such as pH and TDS were determined. The results showed us, the electrical conductivity (EC) in this study falls between $100.68 \pm 1.0 - 194.74 \pm 1.4 \mu\text{s cm}^{-1}$ in the dry and wet season. The pH value in this study for the two seasons varied from 5.57 ± 0.22 to 5.73 ± 0.28 which shows a little acidity. In the current study, TDS for wet and dry seasons goes from $122.17 \pm 1.74 \text{ mg L}^{-1}$ to $63.80 \pm 0.86 \text{ mg L}^{-1}$. This may conceivably be a sign of typical pollution from the runoff of soils in the study area. The high phosphate levels in both wet and dry seasons are recorded from 60.74 ± 0.61 to $60.27 \pm 0.38 \text{ mg L}^{-1}$ in both seasons. Iron values observed range from 8.42 ± 0.06 to $6.28 \pm 0.11 \text{ mg L}^{-1}$ in the wet and dry season, Cu was recorded between $0.08 \pm 0.01 - 0.07 \pm 0.01 \text{ mg L}^{-1}$, Mn recorded from 0.07 ± 0.01 to $0.06 \pm 0.01 \text{ mg L}^{-1}$, Zn recorded between $2.29 \pm 0.09 - 1.15 \pm 0.09 \text{ mg L}^{-1}$, and Pb recorded from 0.69 ± 0.09 to $0.40 \pm 0.18 \text{ mg L}^{-1}$ while Cd and Ni were not detected in the study. Water quality index (WQI) values were determined as 549 for wet and 328 for the dry season, the hazard indices for both seasons are below one. The outcomes in this present study showed that the level of Pb in the surface water could present a carcinogenic risk to both adults and children. All heavy metals results were validated by electrothermal atomic absorption spectrometry (ET-AAS).

1. Introduction

As a universal solvent, water exists as a solid, liquid, and gaseous state. Water is mostly used in

a liquid state. Since water is crucial for all known types of life, ensuring our water is clean and preserved should be the most significant and head for this present generation and the next generation to come [1]. Water can be viewed as a chemical substance that is fundamental for all known types of life. So, the pollution in water must be analyzed

*Corresponding Author: Stanley Chukwuemeka Ihenetu

Email: ihenetustanley@yahoo.com

<https://doi.org/10.24200/amecj.v5.i01.162>

by analytical methods [2]. For the most part, surface waters comprise streams, rivers, reservoirs, lakes, and wetlands. Stream is applied to epitomize other streaming surface waters, beginning from creeks to the huge rivers [3]. Water pollution is a serious biological and chemical hazard. At the point when water is polluted, it then represents an unsafe impact on all creatures and the wellbeing of humans. At the point when poisonous constituents break down in waterways of each kind like oceans, lakes, and rivers, the water becomes polluted. Poisons consistently defame the surface water, which stands a genuine risk to families that use the polluted water.

Recently, the researchers used supported liquid extraction (SLE), the micro solid-phase extraction (MSPE), liquid-liquid microextraction (LLME), (liquid-liquid extraction) LLE, Liquid-phase membrane extraction (LPME) for metal, pesticides, carboxylic acids, and phenol in water matrixes. Also, many metals and VOCs were determined by different ionic liquids and adsorbents. Cloud point extraction (CPE) has been utilized for the preconcentration of cobalt, mercury, and nickel, after the arrangement of a complex with 1-(2-thiazolylazo)-2-naphthol (TAN), and later examination by flame atomic absorption spectrometry utilizing octylphenoxypolyethoxyethanol (Triton X-114) as surfactant [3,4]. The inhabitants of this area depend on the Ogbajajara River [Og] for their domestic and recreational purposes without proper knowledge of the river water quality and possible health implications. The introduction of surface water pollution in rural areas is due to different anthropogenic activities villagers do on the surface water and the washing away of surface soil directly to the surface water after manures are applied straightforwardly on the farmland. Quick urbanization leads to rigorous anthropogenic activities and the consumption of resources and energy in urban areas [4]. Individuals from these communities in Nwangele Local Government rely upon the surface water for their homegrown exercises with not much pipe-borne water around the communities which is situated in a further place for

the residents to get to. This fact, therefore, propelled the necessity of this study to find out the quality of surface water from the Ogbajajara river in the Nwangele local government area. It is therefore accepted that in the consumption of surface water, certain tests should have been completed before consumption in guidelines with the standards of the World Health Organization (WHO) and Federal Ministry of Environment (FMEv). [5], evaluated the water quality of the Nwangele River located in the Southeast area of Nigeria and concluded that the river is slightly polluted with heavy metals and the present river studied has a flow with Nwangele River. [6], researched the effectiveness of the water quality index in Izombe in the Imo state of Nigeria. The scientific research was done in areas where gas flaming is unremitting to build up pollution levels in rainwater and boreholes as they are viewed as the two significant establishments of water supply in the area. The grouping of pollution among the examined water assets was accomplished by contrasting the result of physicochemical tracers and that of WHO norms for drinking water. The Ogbajajara is a well-known river in the Nwangele local government area of the Imo State Nigeria. The major occupation in this area includes farming with few traders. The farming activities have an important bearing on the ecology of the area. Daily activities in this river include; washing and fermentation of cassava. Other activities are washing clothes, motorcycles, and cars, kitchen utensils, bathing, fishing, and road construction near the rivers. Recently many technologies such as the spectrophotometer [7], atomic absorption spectrometry [8], HPLC [9], gas chromatography [10], and electrochemistry were used for the determining of pollutions. The sole aim of this work is the determination of pollution in surface waters and the evaluation of human risk assessment due to the presence of heavy metals in surface water sources in this area.

2. Experimental

2.1. Study Area

The research area is the Ogbajajara River located

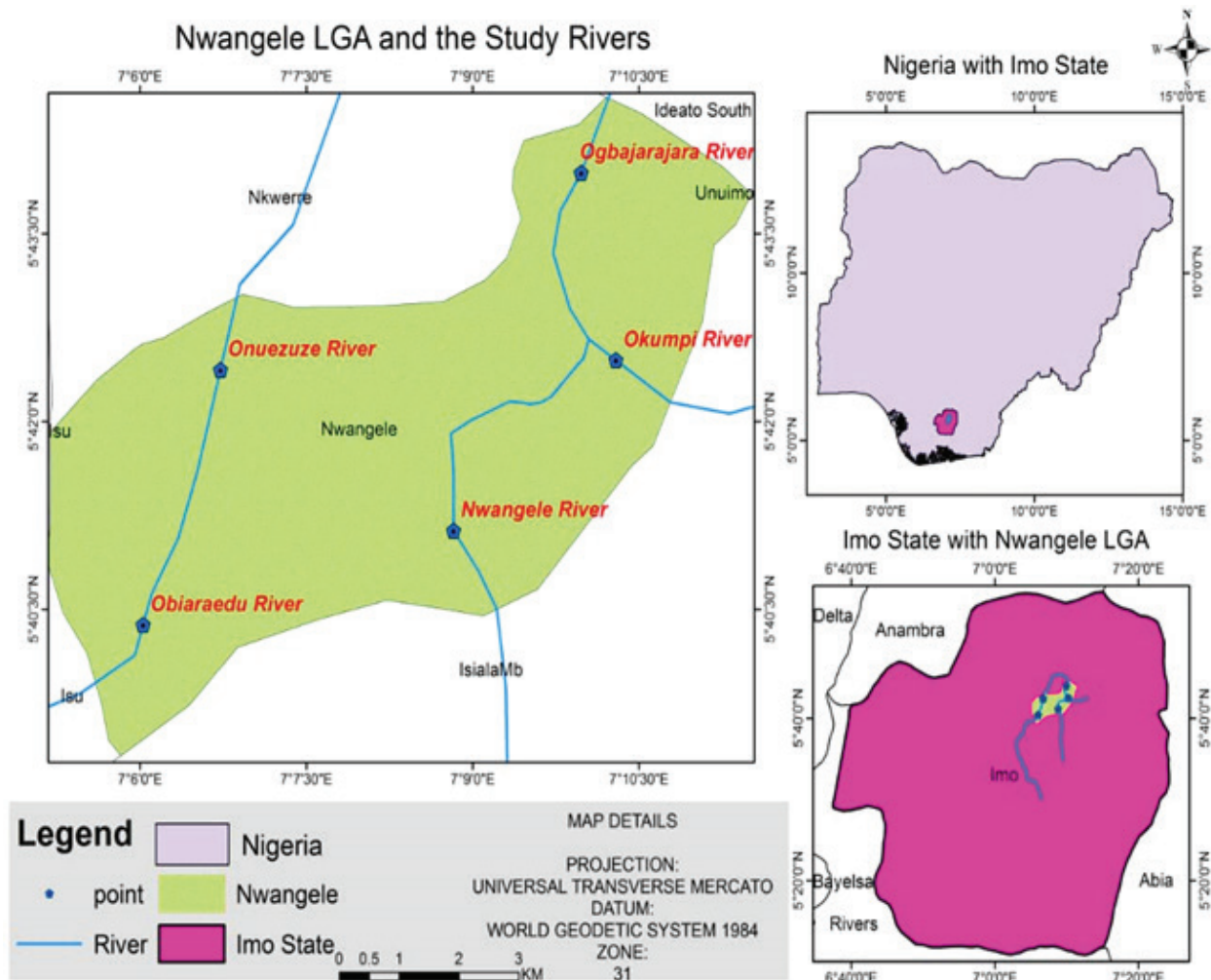


Fig. 1. Map of the Nwangele L.G.A. and its environs showing the Ogbajarajara River

in the Nwangele local government area of Imo state. The Nwangele is in the tropical rainforest region and it has two different seasons which are the dry and wet seasons. The wet season changes from April completely through October with top occurrence in June and September through the dry season starts in November entirely through March yearly. Nwangele has its headquarter in Amaigbo and an area of 63 km² (24 sq mi) and a populace of 128,472 as of the 2006 census (Fig.1). The geology of the Nwangele area includes plain soil which is about 0.05-2.0 mm in size and it is to some degree permeable, deep, and profoundly leached. Nwangele Local Government has numerous networks including Abba community, Isu Community, Umuozu community, Abajah community, and Amaigbo community. Topographically, the area

falls between directions of latitude 5.7045779011-5.7111225452 and longitude of 7.13319502340-7.4222545475. The occupants of these areas are dominantly Igbos and they are Christians with not very many conservatives and other religions. Their significant occupation is farming with not many traders. The farming exercises have a significant bearing on the ecology of the area. Daily exercises in this river incorporate; washing and aging of cassava. Different exercises are washing clothes, bikes, cars, cooking wares, bathing, and fishing.

2.2. Sample Collection

Ten surface water samples were collected randomly within the dry and wet seasons during the research period. Sampling was carried out for both dry and wet seasons and specified as Ogd and Ogd, where

Ogw will be for wet and Ogd will be for dry season respectively. The samples were collected using a clean plastic bottle from the surface waters. Five [5] samples were collected from the river to make up a composite sampling technique. The plastic bottles used for the collection of the surface water samples were appropriately marked and cleaned before sample collection by soaking it in 10% HCl for 48 hours, washed and cleaned with deionized water, and dried up [11,12].

2.3. Laboratory Analysis

The surface water samples were analyzed for the following: Electrical conductivity (EC), pH, Dissolved Oxygen (DO), Total dissolved solids (TDS), Temperature, and color. Also anions and cations such as, Calcium (Ca), Sodium (Na), Potassium (K), Phosphate (PO_4^{3-}), Nitrate (NO_3^{2-}), Sulphate (SO_4^{2-}), Lead (Pb), Copper (Cu), Iron (Fe), Nickel (Ni), Manganese (Mn), Zinc (Zn) and Cadmium (Cd) were determined

2.4. Instrumentation and reagents

The heavy metals concentrations were determined by a double beam flame atomic absorption spectrometer (FAAS, GBC 906, Aus.). The Air or N_2O -acetylene (C_2H_2), the deuterium lamp was used by FAAS. The Avanta system was used for calculating data. In addition, the electrothermal atomic absorption spectrophotometer ET-AAS, GBC, Aus.) was used for the validation of heavy metals in surface water samples. The current and wavelength of the HCL lamp were adjusted for each element. Chemical modifiers such as $\text{Pd}(\text{NO}_3)_2$ and $\text{Mg}(\text{NO}_3)_2$ were used for increasing the ashing point. The electrical conductivity was assessed using the HANNA HI8733 EC METER in $\mu\text{S cm}^{-1}$ and the pH was assessed using JENWAY 3510 pH METER. The DO centralization of the surface water tests was set up using a JENWAY 9071 digital oxygen analyzer. The anion examination was done using multi-parameter bench photometer HI 82300 by HANNA instruments. TDS were done using Groline TDS meter by HANNA instruments.

Also, many anions and cations such as calcium, sodium, potassium, iron, copper, cadmium, nickel, manganese, zinc, and lead, in the surface water during the dry and wet seasons were analyzed using atomic absorption spectrophotometer [13]. All reagents with AAS grade such as; metal solution, inorganic solutions (HNO_3 , NaOH) were purchased from Sigma Aldrich (Germany). Metal standard solution (M) was diluted from the stock of 1000 mg L^{-1} solution in 2% nitric acid for further studies. The standard solutions were diluted by distilled water (DW) from Millipore (USA). Reagents utilized all through the research were of high-quality analytical grade, which was bought from BDH Chemical Ltd, UK, and Sigma-Aldrich Chemie GmbH, Germany. Detergents and deionized water were utilized to wash the dish sets and sample bottles. They were splashed for the time being with a solution of 10% HNO_3 in a 1% HCl solution, trailed by washing with deionized water. Additionally, the reagents that were utilized for the assurance of anion focuses with the Hanna Hi 83,200 Instrument were gotten from Hanna Instruments. The instrument (GBC 903) utilized for the assurance of the groupings of metallic elements in the samples has high sensitivity—commonly (more than 0.9 absorbances) with an exactness (less than 0.5% RSD) from ten-second integrations for 5 mg L^{-1} metal standard.

2.5. Data Analysis

The data were evaluated for their mean and standard deviation by SPSS software. The data obtained was subjected to pollution index models and contamination. Also, Spear-man's correlation coefficient, degree of contamination, Hierarchical Cluster Analysis (HCA), water quality index (WQI) analysis and, health risk assessment was carried out.

3. Results and Discussion

3.1. Physicochemical parameters of surface water

The physicochemical analysis of the surface water collected in the dry and rainy seasons is presented in Table 1. The obtained results were compared with WHO permissible limits.

Table 1. The mean levels of studied parameters linked with WHO in wet and dry season

Parameters	wet						dry						W.H.O
	Ogw ₁	Ogw ₂	Ogw ₃	Ogw ₄	Ogw ₅	Mean±Std	Ogd ₁	Ogd ₂	Ogd ₃	Ogd ₄	Ogd ₅	Mean±Std	
Temp. (°C)	24.32	25.43	25.48	25.71	25.53	25.29±0.55	28.37	27.99	29.01	28.36	28.31	28.40±0.38	20-30
DO (mg ⁻¹)	8.87	8.92	8.65	9.02	8.9	8.87±0.13	5.49	5.29	5.36	5.41	5.59	5.42±0.12	10.0
EC	197.55	200.21	199.11	199.36	196.85	194.74±1.37	99.02	100.57	101.61	100.96	101.24	100.68±1.0	2500
pH	5.24	5.57	5.82	5.49	5.74	5.57±0.22	5.33	5.02	5.29	5.79	5.44	5.37±0.28	6.50-8.50
TDS	122.07	123.03	123.34	119.36	123.07	122.17±1.74	64.32	63.47	62.63	63.71	64.91	63.80±0.86	500
Color	11.00	12.00	11.00	13	12	11.8±0.83	12.00	13.00	13.00	14.00	13.00	13±0.00	15
NO ₃ ⁻ (mg L ⁻¹)	22.4	21.32	22.94	21.32	21.54	21.9±0.73	21.33	21.41	22.31	20.59	21.32	21.39±0.61	50
PO ₄ ²⁻ (mg L ⁻¹)	59.93	60.24	61.32	60.97	61.23	60.74±0.61	59.97	60.39	60.12	59.99	60.89	60.27±0.38	1.0
SO ₄ ²⁻ (mg L ⁻¹)	0.57	0.52	0.51	0.58	0.52	0.54±0.03	0.42	0.47	0.44	0.41	0.45	0.43±0.02	250
Ca (mg L ⁻¹)	3.67	4.02	4.13	3.99	4.17	4.0±0.19	3.40	3.44	3.60	3.41	3.52	3.49±0.08	75
Na (mg L ⁻¹)	7.05	7.63	7.04	7.14	7.11	7.19±0.24	6.20	5.98	6.02	6.07	6.13	6.08±0.08	200
K (mg L ⁻¹)	5.88	5.39	5.47	5.71	5.69	5.63±0.19	5.09	5.12	5.42	5.15	5.17	5.19±0.13	20
Fe (mg L ⁻¹)	8.42	8.36	8.52	8.39	8.42	8.42±0.06	6.31	6.32	6.42	6.11	6.28	6.28±0.11	0.3
Cu (mg L ⁻¹)	0.06	0.07	0.07	0.06	0.07	0.07±0.01	0.08	0.09	0.08	0.07	0.09	0.08±0.01	2.00
Cd (mg L ⁻¹)	0.00	0.00	0.00	0.00	0.00	0.00±0.00	0.00	0.00	0.00	0.00	0.00	0.0±0.0	0.003
Ni (mg L ⁻¹)	0.00	0.00	0.00	0.00	0.00	0.00±0.00	0.00	0.00	0.00	0.00	0.00	0.0±0.0	0.02
Mn (mg L ⁻¹)	0.05	0.06	0.05	0.07	0.07	0.06±0.01	0.07	0.08	0.07	0.08	0.08	0.07±0.01	0.4
Zn (mg L ⁻¹)	2.22	2.16	2.39	2.35	2.33	2.29±0.09	1.11	1.31	1.09	1.13	1.13	1.15±0.09	3.00
Pb (mg L ⁻¹)	0.63	0.71	0.59	0.82	0.74	0.69±0.09	0.47	0.09	0.50	0.49	0.48	0.40±0.18	0.01

The temperature of water centers on its proposed usage. The temperature of surface water, conferring to the standards used falls within 20-30°C. From this study and displayed in Table 1 above, the temperature of the assessed river was higher during the dry season and this could be attributed to the hot weather during the dry season. It can be seen that the season has an effect on the temperature of the river body. Nevertheless, the dry season in the study revealed a minor upsurge in temperature which possibly will be due to the current weather condition of the environment at the location of study. Decline and expansion in temperature level are some of the prominent significant highlights of seasonal variation and weather change. The slight increase in dissolved oxygen [DO] and pH during the wet season can be concentrated in accordance with the affectation by

comparative anthropogenic exercises. Interrelated outcomes were seen for Nworie river [14]. The EC can critically affect the taste of water. The EC in this study falls between 100.68±1.0 - 194.74±1.37 $\mu\text{S cm}^{-1}$ in the dry and wet seasons. The values obtained were contained by the WHO standard for risk-free drinking water. The pH value in this study for the two seasons varied from 5.57±0.22 to 5.73±0.28 $\mu\text{S cm}^{-1}$ which shows a little acidity that was not in agreement with the standard pH (6.50-8.50) recorded by [11] guidelines for safe drinking water. The lower pH might be a result of daily anthropogenic activities on this river on daily basis by the community inhabitants. In the current study, TDS for wet and dry seasons goes from 122.17±1.74 mg L^{-1} and 63.80±0.86 mg L^{-1} . This may conceivably be a sign of typical pollution from the runoff of soils in the study area. Color

in essence corresponds to the appearance, taste, and also general drinkability of water. The color of the water samples at all the sampling locations was lower than the permissible limit which has $13.00 \pm 0.00 - 11.038$ PCU in the wet and dry season against 15 PCU used as the W.H.O standard. The nitrate in this present study for the wet season was all found to be below the standard of WHO standard for safe drinking water both for wet and dry seasons and they range from $8.72-2154$ mg L⁻¹ to $1.20-21.32$ mg L⁻¹. Sulfate values observed in the current study 0.54 ± 0.03 mg L⁻¹ in the wet season and 0.43 ± 0.02 mg L⁻¹ in the dry season were all below WHO standard for good drinking water and for domestic water use. Similar findings were observed in sulfate values obtained from the study carried out in the Okumpi river [11]. One of the huge and crucial nutrients responsible for the richness and

strength of fish ponds is phosphorous. Phosphate at a sensible sum is fitting for the development of plankton [16]. The phosphate level in both wet and dry seasons goes from 60.74 ± 0.61 to 60.27 ± 0.38 mg L⁻¹ in both seasons. The high phosphate levels obtained from this current study; likely could be as a result of the existence of blue-green growth on the water surface in the study area in both seasons. This research perhaps will conclude that phosphate grounded fertilizer may possibly have been applied on farmlands near the rivers. Nitrate in all the points is below the WHO standards. Calcium, potassium, and sodium as found from the current study in the wet and dry seasons are below the standard used for this current study. This result is in agreement with the outcome of the result obtained from the Obiaraedu River [17] and the Okumpi River in Imo State [11].

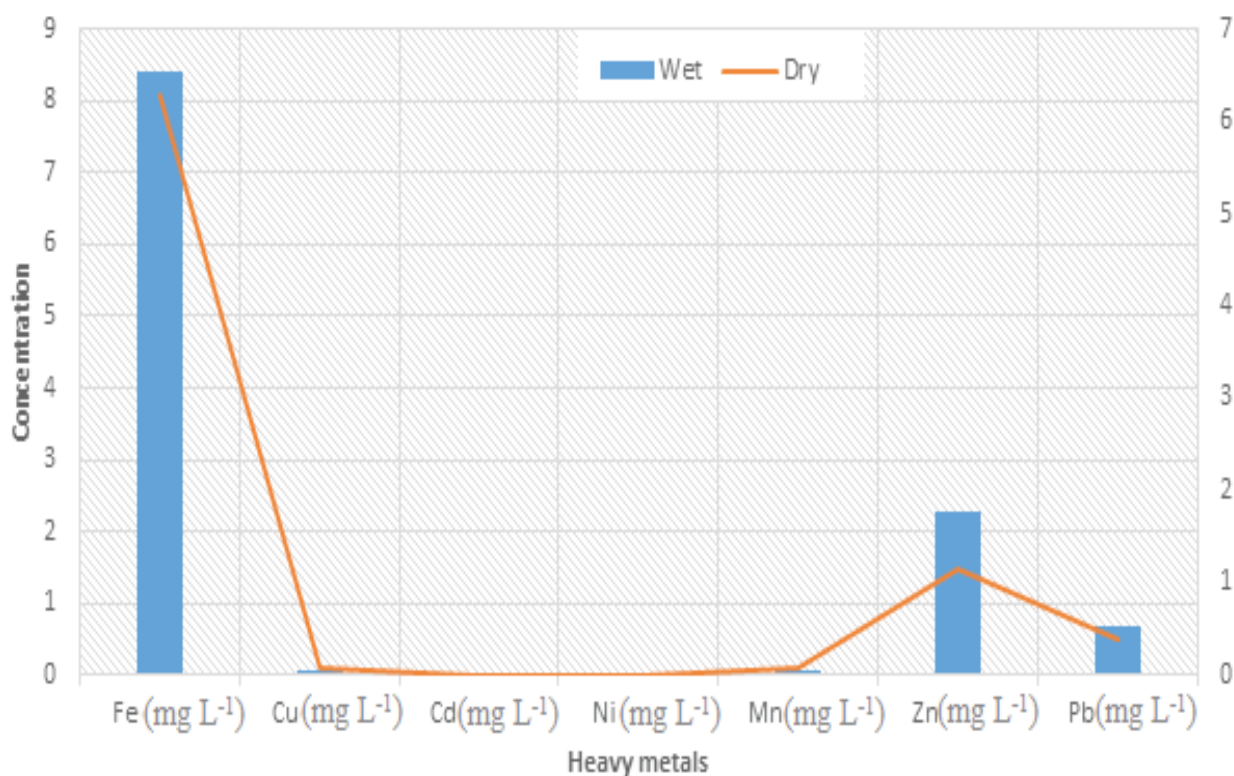


Fig. 2. Clustered column plots for the distribution of the heavy metal

Cadmium and nickel were not detected in the surface water from the Ogbajarajara River in both seasons, the plotted distribution of heavy metals are presented in Figures 2. Iron values observed in this current study ranges from 8.42 ± 0.06 to 6.28 ± 0.11 mg L⁻¹ in wet and dry season are higher than WHO standards of 0.3 mg L⁻¹. Iron detected in every one of the samples in the wet season may be as a result of the utilization of iron coagulants [18]. This higher concentration of Fe observed during the wet than the dry season might be because most mineral residues on the soil may have a high level of iron, subsequently runoff from residue may taint the water, particularly during the rainy season. Copper is an imperative supplement, also drinking water impurity [19]. Cu amount for both wet and dry seasons in this current study was all underneath WHO standard for drinking water and domestic uses and they went from 0.08 ± 0.01 to 0.07 ± 0.01 mg L⁻¹. Running river is probably going to display a low level of copper [19]. The low level of copper in this current study is in line with the result observed in the Nwangele River [5] and in River Nworie [14]. Equivalent discoveries were likewise seen in a study done on River Uramurukwa in Imo State [20] and Obiaredu River [17]. Manganese goes from 0.07 ± 0.01 to 0.06 ± 0.01 mg/L through the wet and dry season. With respect to WHO standard and NSDWQ for household and drinking water value for Mn, all points for the wet season showed a low level of Mn. At high concentrations, Mn can comprise an aggravation with a particular metallic taste and staining properties [16]. Zinc observed both in wet and dry season between 2.29 ± 0.09 – 1.15 ± 0.09 mg L⁻¹; were observed to be below the WHO standard for water quality against the scheduled level of 3.0 mg L⁻¹. Zinc uncovered an unwanted harsh taste to water [15]. Pollution of lead in a river may conceivably be an outcome of the disbanding of lead from the soil and earth's external layer. Lead is in participation a harmful and superfluous metal that has no healthful significance to living creatures. Lead levels in every one of the samples are observed to be high, going from 0.69 ± 0.09 to 0.40 ± 0.18 mg L⁻¹ in the wet and dry

season which are higher than the WHO standard at 0.01 mg L⁻¹. No amount of Pb is viewed as protected in drinking water. A related study was observed in a study of the river Uramurukwa in Imo State [20].

3.2. Correlation coefficient matrix

A substantial positive correlation ($r > 0.5$) was observed between some of the metals, and anions parameters. Table 2 shows the coefficient of relationship for all the metals and anions. The metals showed a negative association/relationship with copper and cadmium. Nevertheless, significant positive relations during the wet season were exhibited between NO₃⁻/Fe (0.888), PO₄²⁻/Ca (0.847), PO₄²⁻/Fe (0.544), PO₄²⁻/Zn (0.894), Ca/Cu (0.769) and Mn/Pb (0.934). Significant positive associations through the dry season were exhibited between NO₃⁻/Fe (0.888), PO₄²⁻/Ca (0.847), PO₄²⁻/Fe (0.544), PO₄²⁻/Zn (0.894), SO₄²⁻/K (0.746), Ca/Cu (0.769), Ca/Zn (0.524), Fe/Zn (0.691) and Mn/Pb (0.934). Once the correlation is seen positive, the establishment of tainting of the positively connected metals is indistinguishable while negative correlation suggests disparate/various bases of contamination. Notable pollution can be through the washing of engine cars, tricycles and, motorcycles at the river. Some of the relationship shown by the metals has been examined by [21].

3.3. Hierarchical Cluster Analysis (HCA)

Additionally, we performed Hierarchical Cluster Analysis (HCA) to identify groupings of physicochemical characteristics based on their Square Euclidian Distance (SED) [21]. The cluster plots for physicochemical parameters in the water in dry and wet seasons are presented in Figure 3. In the dry season, three groups were identified. In group 1, the combination included all parameters except for pH, Phosphate, and, EC in another group and then TDS in the third group. Similarly, in the wet season, the combination includes all parameters except for DO and temperature in group 2 while TDS and EC in group 3. The clustering of all metals in similar indicates that their source(s) are common. The HCA results agree with correlation analysis.

Table 2. Correlation coefficient matrix heavy metals and anions from surface water samples in wet/dry season (mg L⁻¹)

	NO ₃ ⁻	PO ₄ ²⁻	SO ₄ ²⁻	Ca	Na	K	Fe	Cu	Cd	Ni	Mn	Zn	Pb
Wet													
NO ₃ ⁻	1												
PO ₄ ²⁻	0.098	1											
SO ₄ ²⁻	-0.217	-0.402	1										
Ca	-0.168	0.847	-0.702	1									
Na	-0.586	-0.398	-0.277	0.115	1								
K	0.051	-0.260	0.746	-0.635	-0.642	1							
Fe	0.888	0.544	-0.384	0.256	-0.671	-0.083	1						
Cu	0.054	0.424	-0.986	0.769	0.365	-0.772	0.257	1					
Cd	0	0	0	0	0	0	0	0	1				
Ni	0	0	0	0	0	0	0	0	0	1			
Mn	-0.848	0.383	0.154	0.457	0.161	0.063	-0.540	-9.312	0	0	1		
Zn	0.338	0.894	-0.072	0.524	-0.721	0.064	0.691	0.047	0	0	0.181	1	
Pb	-0.900	0.155	0.424	0.203	0.235	0.134	-0.693	-0.271	0	0	0.934	0.040	1
Dry													
NO ₃ ⁻	1												
PO ₄ ²⁻	0.098	1											
SO ₄ ²⁻	-0.217	-0.402	1										
Ca	-0.168	0.847	-0.705	1									
Na	-0.586	-0.398	-0.277	0.115	1								
K	0.051	-0.260	0.746	-0.635	-0.642	1							
Fe	0.888	0.544	-0.384	0.256	-0.671	-0.083	1						
Cu	0.054	0.424	-0.986	0.769	0.365	-0.772	0.257	1					
Cd	0	0	0	0	0	0	0	0	1				
Ni	0	0	0	0	0	0	0	0	0	1			
Mn	-0.844	0.383	0.154	0.457	0.161	0.063	-0.540	-9.344	0	0	1		
Zn	0.338	0.894	-0.072	0.524	-0.721	0.064	0.691	0.047	0	0	0.181	1	
Pb	-0.900	0.155	0.424	0.203	0.239	0.134	-0.693	-0.271	0	0	0.934	0.040	1

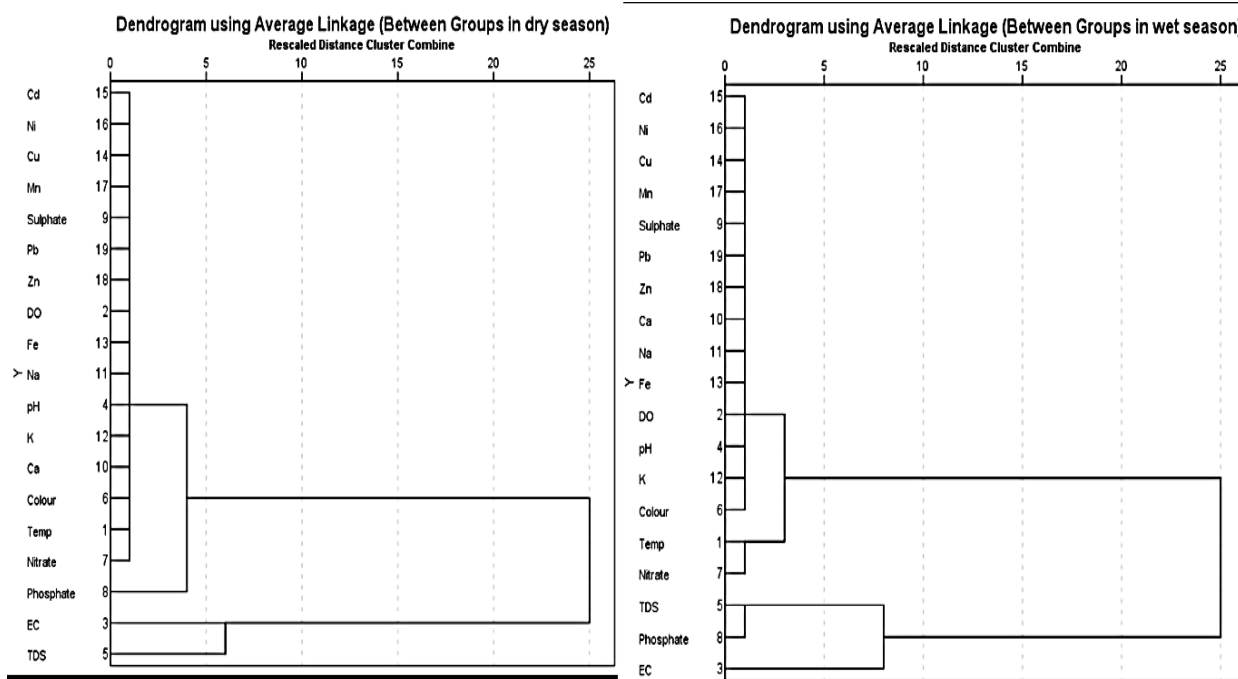


Fig. 3. Hierarchical cluster analysis for physicochemical properties in the dry and wet season

3.4. Chemometric Analysis

3.4.1. Contamination factor

The contamination factor was employed to check the rate of individual metal contamination in the water samples. Contamination factors were calculated with equation I.

$$Cf = \frac{c_{metal}}{C_{background}} \quad (\text{Eq. I})$$

Where Cf connote contamination factor, C metal address the grouping of heavy metal and $C_{background}$ means the foundation worth of metal. WHO suggestions for safe drinking water are taken as the foundation esteems for a water sample. Contamination factor ranking followed by Table 3.

3.4.2. Pollution load index (PLI)

The proposed pollution load record through Tomlinson for distinguishing pollution levels in soil was applied to the water tests to recognize the convergence of contamination of heavy metal in the different areas. The PLI appraises the metal fixation status and gives a thought of the different moves that can be made to control the issue [22]. Scientists have assessed the pollution load index utilizing equation II.

$$PLI = \sqrt[n]{C_{f1} \times C_{f2} \times C_{f3} \times \dots C_{fn}} \quad (\text{Eq. II})$$

A PLI value > 1 point toward an instantaneous intervention to ameliorate pollution; a PLI value < 1 specifies that extreme rectification procedures are not needed.

High contamination factor was recorded for lead

Table 3. Contamination factor ranking

Cf values	Contamination factor level
$C_f < 1$	Low contamination
$1 \leq C_f < 3$	Moderate contamination
$3 \leq C_f < 6$	Considerable contamination
$6 \leq C_f$	Very high contamination

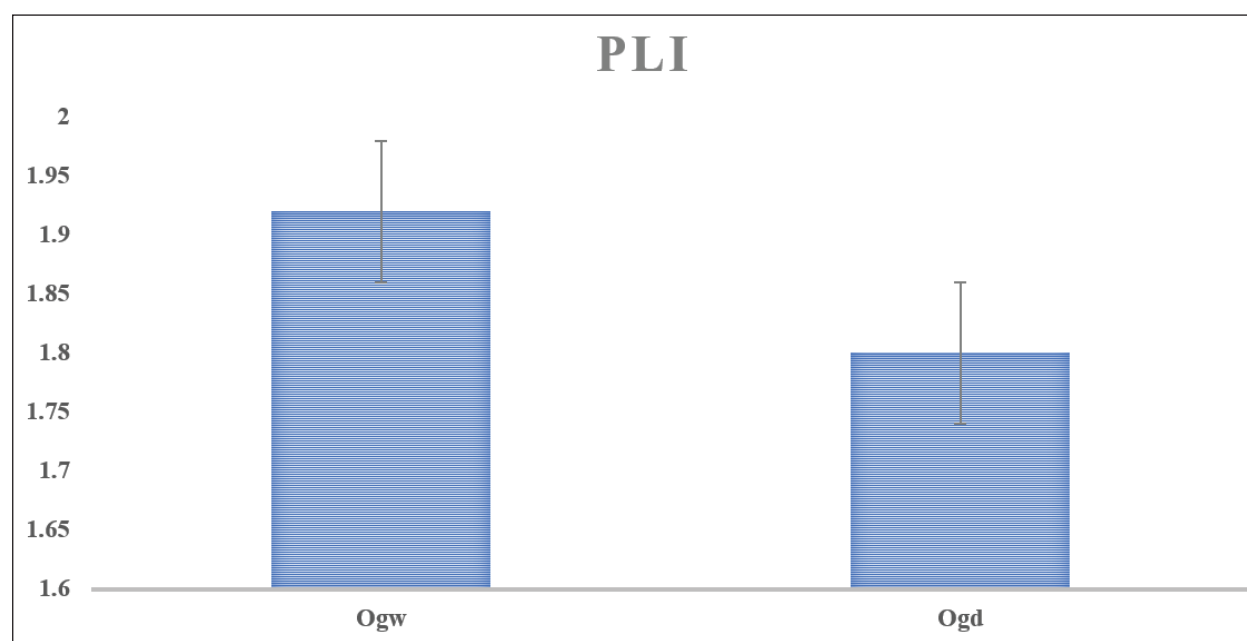
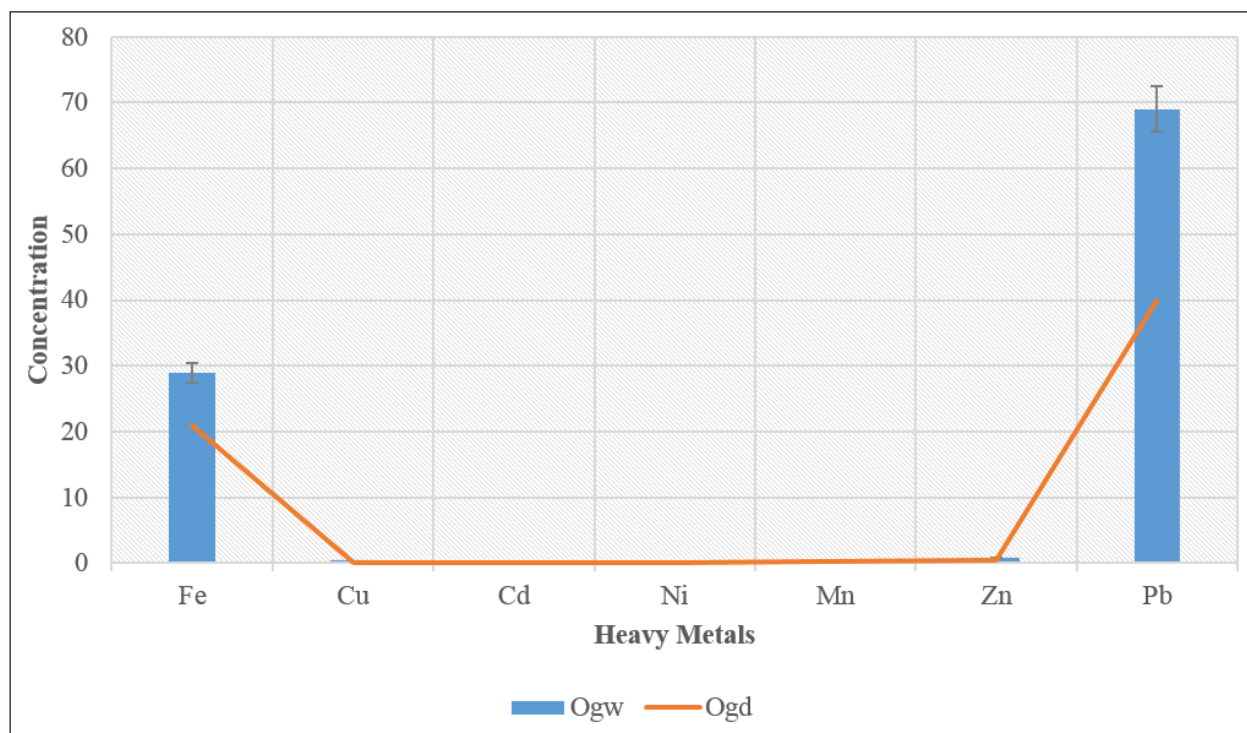


Fig. 4. Contamination factor and PLI for heavy metals and anions in the wet season

and iron in this present study both in wet and dry seasons. The contamination was higher during the wet seasons and this may be due to runoff during the wet season which comes directly from the farmlands surrounding the river. The contamination factor was recorded accordingly $Pb > Fe > n > Mn > Cu > Cd$ and Ni in both wet and dry seasons. The river has shown a high pollution load index of 1.192 in wet and 1.8 in the dry season as shown in Figure 4 above. However, there is a need to constantly evaluate the water source in this location.

3.4.3. Water quality index (WQI)

WQI is a number-arithmetic articulation used to change the enormous number of adjustable data into a solitary number, which implies the water quality level. The WQI is created from the accompanying formula presented to equation III [23].

$$W_i = \frac{w_i}{\sum_{i=1}^n w_i} \quad (\text{Eq. III})$$

Where: W_i is equal to the comparative weight, w_i is equal to the mass of every single parameter and n is confer to the parameters. Water quality evaluation may be developed conferring to equation VI [24, 25].

$$q_i = \frac{C_i}{S_i} \times 100 \quad (\text{Eq. IV})$$

Where q_i is the quality positioning, C_i is the concentration of every chemical boundary in each and every water sample in $mg\ L^{-1}$, and S_i is the WHO drinking water quality standard. To work out the WQI, the SI was set up for every chemical boundary, which is then used to decide the WQI utilizing Equation V and VI.

$$SI_i = W_i \times q_i \quad (\text{Eq. V})$$

$$WQI = \sum SI \quad (\text{Eq. VI})$$

SI_i is the sub-index of i th (mathematics Occurring at position [i] in the sequence) parameter, q_i is the rating dependent on the concentration of i th parameter and n is the number of parameters. The benchmark esteems were procured from World Health Organization (WHO) standard for drinking water, 2007. The accompanying point of arrangement of (WQI) and the nature of water WQI showed in Table 4 [27].

The examined samples from this study are severely polluted with physicochemical tracers given the value of 549 for wet and 328 for a dry season as reported in Figure 5 below, which makes the water unsuitable for drinking. Various activities around the sampling point might have contaminated the rivers in an intense way, while the wet season recorded more concentration from this present study.

Table 4. Water Quality Index Values

Cf Value	Water Quality
WQI < 50	Excellent water quality
50 < WQI ≤ 100	Good water quality
100 < WQI ≤ 200	Poor water quality
200 < WQI ≤ 300	Very poor water quality
WQI > 300	Unsuitable for drinking

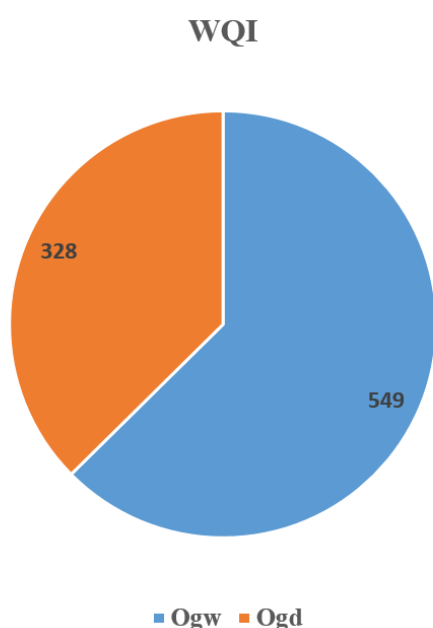


Fig. 5. WQI values of the sampling points in the wet season

3.5. Assessment of health risk after determination

3.5.1. Dermal and ingestion exposure, Hazard quotient (HQ), Hazard Indices (HI)

Health risk through human exposure to these metals contamination can be either by means of dermal ingestion, inhalation, or absorption, which are the normal contact passageways to the water. Thusly all the rivers studied in this research are constantly utilized by individuals generally for their domestic exercises and sporting exercises. The calculation of health risk was calculated using equations VII and VIII according to the USEPA risk estimation method [30-32].

$$Exp_{ing} = \frac{C_{WATER} \times IR \times EF \times ED}{BW \times AT} \quad (\text{Eq. VII})$$

$$Exp_{derm} = \frac{C_{water} \times SA \times KP \times ET \times EF \times ED \times CF}{BW \times AT} \quad (\text{Eq. VIII})$$

Exp_{ing} denotes the exposure dose through ingestion of water (mg kg^{-1} per day); Exp_{derm} addresses the exposure dose by means of dermal absorption (mg kg^{-1} per day); C_{water} : show the normal level of the assessed metals in water ($\mu\text{g L}^{-1}$); IR shows the ingestion level in this study (2.2 L per day for

adults; 1.8 L per day for children); EF shows the exposure equation frequency (365 days/year); ED shows the exposure duration (70 years for adults; and 6 years for children); BW show the normal body weight (70 kg for adults; 15 kg for children); AT shows the averaging time (365 days/year \times 70 years for a grown-up; 365 days per year \times 6 years for a children); SA shows the uncovered skin area (18,000 cm^2 for adults; 6600 cm^2 for children); Kp shows the dermal permeability coefficient in water, (cm/h), 0.001 for Cu, Mn, Fe and Cd, though 0.0006 for Zn; 0.0001 for Ni; and 0.004 for Pb; ET shows the exposure time (0.58 h per day for adults; 1 h per day for children) and CF shows the unit conversion factor (0.001 L cm^{-3}) [29]. Potential non-cancer-causing chances in line for exposure of heavy metals were set up by assessing the determined toxin exposures from every exposure path (ingestion and dermal) with the proposal dose [29] utilizing equation IX.

$$HQ_{ing/derm} = \frac{Exp_{ing/derm}}{RfD_{ing/derm}} \quad (\text{Eq. IX})$$

Where $RfD_{ing/derm}$ addresses the ingestion and dermal toxicity suggestion dose ($\text{mg kg}^{-1} \text{day}^{-1}$). The RfD_{derm} and RfD_{ing} esteem were gotten from the literature [30, 31]. An HQ under 1 is presumed to be safe and taken as substantial non-carcinogenic as equation X [29].

$$HI = \sum_{i=1}^n HQ_{ing/derm} \quad (\text{Eq. X})$$

Where $HI_{ing/derm}$ is hazard index through dermal contact or ingestion.

The dermal and ingestion exposure determined in Table 5 were utilized to decide the hazard quotient in Table 6. The hazard quotient (HQ) was resolved and both HQ_{derm} and HQ_{ing} in the two seasons for all the trace metals checked in the examination were lower one (1) as seen in Table 6 for adults and children. This shows there is basically no adversative health sway expected to be ordered by any of these metals when the

surface water is used. The HQ_{ing} and HQ_{derm} decreased in the request for lead > iron > zinc > manganese > copper > nickel > and cadmium, lead > manganese > iron > copper > zinc > nickel and cadmium, for the two children and adults in wet season, individually. HQ_{ing} and HQ_{derm} decreased in the request for nickel > lead > manganese > copper > zinc > iron and lead > zinc > nickel > copper > manganese > iron > for the both

children and adults in dry season, individually. It has been suggested that the calculated HQ results for metals > 1 for children ought not to be ignored [32], presumably in light of the fact that, children are limitlessly disposed to pollutants [33]. The significant source of non-cancer-causing health risk in the two ways were Pb and Ni. The assessed absolute HQ esteems were less than one as found in Table 6.

Table 5. Dermal and ingestion exposure (mg kg⁻¹ per day) for adults and children both in wet and dry season

Metals	Wet						Dry			
	RfD _{derm}	RfD _{ing}	EXP _{derm} (Adult)	EXP _{derm} (Children)	D _{ing} (Adult)	D _{ing} (Children)	EXP _{derm} (Adult)	EXP _{derm} (Children)	D _{ing} (Adult)	D _{ing} (Children)
Fe	140	700	1.25E-2	3.7E-3	2.26E0	1.01E0	9.36E-3	2.76E-3	1.97E0	7.53E-1
Cu	8	40	1.04E-4	3.08E-5	2.2E-2	8.0E-3	1.19E-4	3.52E-5	2.5E-2	9.0E-3
Cd	0.5	0.025	0.00	0.00	0.00	0.00	0.00	0.00	0.00	0.00
Ni	5.4	20	0.00	0.00	0.00	0.00	0.00	0.00	0.00	0.00
Mn	0.96	24	8.94E-5	2.64E-5	1.8E-2	7.0E-3	1.04E-4	3.08E-5	2.22E-2	8.0E-3
Zn	120	300	2.04E-3	6.04E-4	7.19E-1	2.74E-1	1.02E-3	3.03E-4	3.61E-1	1.38E-1
Pb	0.42	1.4	4.11E-3	1.21E-3	2.16E-1	8.2E-2	2.38E-3	7.04E-4	1.25E-1	4.8E-2

Table 6. Hazard quotient for potential non-carcinogenic risk (HQ) and cumulative hazard indices (HI) for each heavy metal present in wet and dry season for Adult and Children

Metals	Wet				Dry			
	HQ _{derm} (Adult)	HQ _{derm} (children)	HQ _{ing} (Adult)	HQ _{ing} (children)	HQ _{derm} (Adult)	HQ _{derm} (children)	HQ _{ing} (Adult)	HQ _{ing} (children)
Fe	1.78E-4	2.64E-5	3.22E-3	1.44E-3	6.68E-5	1.79E-5	2.71E-3	1.07E-3
Cu	1.3E-5	3.85E-6	5.5E-4	2.0E-4	1.48E-5	4.4E-6	6.25E-4	2.25E-4
Cd	0.00	0.00	0.00	0.00	0.00	0.00	0.00	0.00
Ni	0.00	0.00	0.00	0.00	0.00	0.00	0.00	0.00
Mn	1.02E-4	2.75E-5	7.5E-4	2.91E-4	1.08E-4	3.2E-5	9.25E-4	3.33E-4
Zn	1.7E-5	5.03E-6	2.39E-3	9.0E-4	8.5E-6	2.52E-6	1.2E-3	4.6E-4
Pb	9.78E-3	2.88E-3	1.52E-1	5.85E-2	5.66E-3	1.67E-3	8.92E-2	3.42E-2
HI	1.01E-2	2.94E3	1.61E-1	6.13E-2	5.85E-3	1.73E-3	9.46E-2	3.63EE-2

3.5.2. Chronic daily intake (CDI) and Carcinogenic risk (CR)

The carcinogenic risk (CR_{ing}) shows a gradual possibility that an individual will foster cancer during his lifetime inferable from disclosure under portrayed conditions were registered for the selected metals in this current study [30]. The chronic daily consumption of heavy metals through ingestion was computed using equation XI.

$$CDI = C_{water} \times \frac{DI}{BW} \quad (\text{Eq. XI})$$

Where C_{water} addresses the centralization of trace metal in water in (mg L^{-1}), DI infer the; normal everyday admission of water which is referred to as daily intake (2.2 L each day for adults; 1.8 L each day for children) and BW shows the entire body weight (70 kg for adults; 15 kg for children), correspondingly [34]. The cancer risk (CR) was calculated using the formula in equation XII.

$$CR_{ing} = \frac{D_{ing}}{SF_{ing}} \quad (\text{Eq. XII})$$

whereas SF_{ing} represent the cancer slop factor. The SF_{ing} for Pb is 8.5 mg kg^{-1} per day [26].

The CDI indices for heavy metals during the experimental time frame for the two ages were discovered to be in the request for $\text{Fe} > \text{Pb} > \text{Zn} > \text{Cu} > \text{Mn} > \text{Ni} > \text{Cd}$ in wet season; and $\text{Fe} > \text{Zn} > \text{Pb} > \text{Mn} > \text{Cu} > \text{Ni} > \text{Cd}$ in dry season as seen in Table 7. This proposes that the surface water expects less health dangers to the two adults and children by means of the pathways, except for Fe during the wet season for children which appears to be more than one. Table 8 present the carcinogenic risk of Pb for this present study for both adults and children in wet and dry season, for the reason that the value of carcinogenic slope factor for different metals couldn't be followed in literature, only lead was determined. Under extreme regulatory program the carcinogenic risk esteems within the range of 10^{-6} and 10^{-4} could present possible risk to an individual, subsequently, the outcomes in this present study showed that the level of Pb in the surface water could present a carcinogenic risk to both adults and children.

Table 7. Chronic risk assessment (CDI_{ing}) of heavy metals in adults and children

Metals	wet		dry	
	CDI (Adult)	CDI (children)	CDI (Adult)	CDI (children)
Fe	2.64E-1	1.01E-0	1.97E-1	7.53E-1
Cu	2.19E-3	8.4E-2	2.51E-3	9.6E-3
Cd	0.00	0.00	0.00	0.00
Ni	0.00	0.00	0.00	0.00
Mn	1.88E-3	5.0E-1	219E-3	8.E-3
Zn	7.19E-2	2.74E-1	3.6E-1	1.38E-1
Pb	2.16E-2	8.28E2	1.25E-2	4.8E-2

Table 8. Carcinogenic risk assessment (CR_{ing}) of Pb for wet and dry season for both adults and children

Metal	Wet		Dry	
	Adult	Children	Adult	Children
Pb	2.54E-3	9.74E-3	1.47E-3	5.64E-3

4. Conclusion

The current study has shown that some actual appearances of pollution from surface water from the study area during the wet and dry seasons are not in line with WHO guidelines. The heavy metals; and cations were analyzed in surface water by photometer spectrometry and flame atomic absorption spectrometry (F-AAS). The results for metal analysis were validated by electrothermal atomic absorption spectrometry (ET-AAS). The study has shown additionally that the pH of all the sampling points is acidic. Phosphate apparently is high in all the sampling points at the various season and this can be related to the high utilization of more phosphate grounded fertilizer on farmlands surrounding the Rivers. The current study has uncovered also that the surface waters are profoundly contaminated with Fe, Zn and Pb, also this current study has shown that the surface water isn't appropriate for drinking purposes as shown by the high water quality index (> 300).

5. Recommendation

With regard to the results of the present study, the succeeding references are made after pollution analysis.

- The water resources observed in the Nwangele Local Government area should be done routinely to survey pollution levels (instrumental analysis) to check the spread of water-related complexities, particularly in the study area.
- In a circumstance of uncertain water quality, treatment is recommended through filtration, boiling, and the utilization of added substances (alum, liming, chlorine), accordingly lessening the danger of water-related issues.

6. Acknowledgments

The authors sincerely appreciate the efforts of the laboratory attendants of the chemistry department of Imo State University and Anambra state university Uli.

7. References

- [1] R.G. Timothy, T. Makoto, K. Henk, J.G. Jason, M.A. Diana, Beneath the surface of global change: Impacts of climate change on groundwater, *J. Hydrol.*, 405 (2011) 532-560. <https://doi.org/10.1016/j.jhydrol.2011.05.002>
- [2] G. Dubnov-Raz, N.W. Constantini, H. Yariv, S. Nice, N. Shapira, Influence of water drinking on resting energy expenditure in overweight children, *Int. J. Obesity*, 35 (2011) 1295–1300. <https://doi.org/10.1038/ijo.2011.130>
- [3] P.U. Okorie, The challenges of declining freshwater resources, Paper presented at the world environment day conference held at Imo state University Owerri, Nigeria, 2017. <http://ijfac.unsri.ac.id/index.php/ijfac/article/view/156>
- [4] L. Gang, G.X. Sun, X. Ren, S. Luo, Y.G. Zhu, Urban soil and human health: a review, *Eur. J. Soil Sci.*, 69 (2018) 196-215. <https://doi.org/10.1111/ejss.12518>
- [5] J. Anudike, M. Duru, F. Uhegbu, Water quality assessment of Nwangele River in Imo State, Nigeria, *J. Ecobiotechnol.*, 11 (2019) 1-5. <https://doi.org/10.25081/jebt.2019.v11.3866>
- [6] E.A. Ubuoh, S.M.O. Akhionbare, S. Ogbuji, W.N. Akhionbare, Effectiveness of water quality index in assessing water resources, Characteristics in Izombe, Oguta Local government Area of Imo State, Nigeria. *I.J.A.B.R.*, 3 (2013) 31-35. [http://www.scienceandnature.org/IJABR_Vol3\(1\)2013.php](http://www.scienceandnature.org/IJABR_Vol3(1)2013.php)
- [7] S. Srivastava, V. Sharma, Ultra-portable, smartphone-based spectrometer for heavy metal concentration measurement in drinking water samples, *Appl. Water Sci.*, 11 (2021) 177. <https://doi.org/10.1007/s13201-021-01519-w>
- [8] A. Rotimi Ipeaiyeda, A. Ruth Ayoade, Flame atomic absorption spectrometric determination of heavy metals in aqueous solution and surface water preceded by co-precipitation procedure with copper(II) 8-hydroxyquinoline, *Appl. Water Sci.*, 7 (2017) 4449–4459. <https://doi.org/10.1007/s13201-017-0590-9>

- [9] S. T. Palisoc, R. I. M. Vitto, Highly sensitive determination of heavy metals in water prior to and after remediation using *Citrofortunella Microcarpa*, *Sci. Reports*, 11 (2021) 1394. <https://doi.org/10.1038/s41598-020-80672-9>
- [10] O. V. Rodinkov, A. Y. Pisarev, Sensitivity increase in headspace analysis of hydrocarbons in water by using online selective elimination of gas extractant, *Sep. J.*, 9 (2022) 15. <https://doi.org/10.3390/separations9010015>
- [11] S.C. Ihenetu, F.C. Ihenetu, G.I. Kalu, Determination of heavy metals and physicochemical parameters of crude oil polluted soil from Ohaji Egbema Local government in Imo State, *Open J. Yangtze Gas Oil*, 2 (2017) 161-167. <https://doi.org/10.4236/ojogas.2017.23012>
- [12] E.E. Christian, W.V. Andrew, J.E. Ngozi, pH variations and chemometric assessment of borehole water in Orji, Owerri Imo State, Nigeria, *J. Environ. Anal. Chem.*, 5 (2018) 1000238. <https://doi.org/10.4172/2380-2391.1000238>
- [13] WHO (World Health Organization), guidelines for drinking water quality (3rd ed.) Vol.1 Recommendation, Geneva, 515, 2007. https://www.who.int/water_sanitation_health/dwq/fulltext.pdf
- [14] M. Duru, K. Nwanekwu, Physicochemical and microbial status of Nworie River, Owerri, Imo State, Nigeria, *Asian J. Plant Sci. Res.*, 2 (2012) 433-436. <https://www.imedpub.com/articles/physicochemical-and-microbialstatus-of-nworie-river-owerri-imo-state-nigeria.pdf>
- [15] WHO (World Health Organization), guidelines for drinking water quality, 4th edition, incorporating the 1st addendum, 2017. https://www.who.int/water_sanitation_health/dwq/GDWQ2004web.pdf
- [16] E.I. Ugwu, N.E. Uzoma, E.L. Ikechukwu, Study on Physicochemical Parameters of Water Samples from Onuimo River Imo state, Nigeria, *South Asian J. Eng. Technol.*, 2 (2016) 1–8. <https://journals.eleyon.org/index.php/sajet>
- [17] S. C. Ihenetu, V. O. Njoku, A. Chinweuba, F. C. Ibe, and N. B. Ekeoma, A review: Effects of air, water and land dumpsite on human health and analytical methods for determination of pollutants, *Anal. Methods Environ. Chem. J.* 4 (2021) 80-106. <https://doi.org/10.24200/amecj.v4.i03.147>
- [18] D.W. Macdonald, E.O. Christopher, Pollution studies on Nigerian rivers: heavy metals in surface water of Warri River, Delta State, *J. Biodiversity Environ. Sci.*, 1 (2011) 7-12. <https://innspub.net/journal/journal-of-biodiversity-and-environmental-sciences-jbes/>
- [19] B.A. Amadi, P.C. Chikezie, H.C. Okeoma, Physicochemical characteristics of Nworie river and its effect on liver function on rats, *J. Nigeria Environ. Sci.*, 3 (2006) 183-187. <https://nijest.com/about-nijest/>
- [20] A.W. Verla, E.N. Verla, C.E. Amaobi, C.E. Enyoh, Water pollution scenario at river uramurukwa flowing through Owerri metropolis, Imo state, Nigeria, *Int. J. Environ. Pollut. Res.*, 6 (2018) 38-49. <https://www.eajournals.org/journals/international-journal-of-environment-and-pollution-research-ijepr/>
- [21] E.N Verla, A.W Verla, C.E Enyoh, Finding a relationship between physicochemical characteristics and ionic composition of River Nworie, Imo State, Nigeria, *PeerJ Anal. Chem.*, 2 (2020) e5. <https://doi.org/10.7717/peerj-achem.5>
- [22] S. Naruka, M.S. Sharma, Water quality assessment of Rajsamand Lake, Rajasthan, India, *Int. Res. J. Environ. Sci.*, 6 (2017) 22-28. <https://portal.issn.org/resource/ISSN/2319-1414>
- [23] C.E. Duru, I.P. Okoro, C.E. Enyoh, Quality assessment of borehole water within Orji mechanic village using pollution and contamination models, *Int. J. Chem., Mater. Environ. Res.*, 4 (2017) 123-130. <https://portal.issn.org/resource/ISSN/2410-5945>

- [24] F.C. Ibe, A.I. Opara, B.O. Ibe, C.E. Amaobi, Application of assessment models for pollution and health risk from effluent discharge into a tropical stream: case study of Inyishi River, Southeastern Nigeria, *Environ. Monit. Assess.*, 19 (2019) 191-753. <https://doi.org/10.1007/s10661-019-7936-8>
- [25] A.A. Bordalo, R. Teixeira, W. J. Wiebe, Water quality index applied to an international shared river basin: the case of Douro River, *Environ. Manage.*, 38 (2006) 910-920. <https://doi.org/10.1007/s00267-004-0037-6>.
- [26] EPA (Environmental Protection Agency), Risk assessment guidance for superfund, vol. 1, human health evaluation manual, part A, Report EPA/540/1-89/002, Washington, DC., 1989. <https://www.epa.gov/sites/default/files/2015-09/documents/ragsa.pdf>
- [27] S.Y. Li, Q.F. Zhang, Spatial characterization of dissolved trace elements and trace metals in the upper Han River (China) using multivariate statistical techniques, *J. Hazard. Mater.*, 176 (2010) 579–588. <https://doi.org/10.1016/j.jhazmat.2009.11.069>
- [28] A.O. Eludoyin, O.T. Oyeku, Heavy metal contamination of groundwater resources in a Nigerian urban settlement, *African J. Environ. Sci. Technol.*, 4 (2010) 201-214. <https://doi.org/10.1007/s00128-008-9497-3>.
- [29] EPA (Environmental Protection Agency), Water monitoring and assessment, Retrieved October 14, 2009. <http://water.epa.gov/type/rsl/monitoring/vms510.cfm>
- [30] B. Wu, D.Y. Zhao, H.Y. Jia, Y. Zhang, X.X. Zhang, S. P. Cheng, Preliminary risk assessment of trace metal pollution in surface water from Yangtze River in Nanjing Section, China, *Bull. Environ. Contam. Toxicol.*, 82 (2009) 405–409. <https://doi.org/10.1007/s00128-008-9497-3>.
- [31] J. Iqbal, M.H. Shah, Health risk assessment of metals in surface water from freshwater source lakes Pakistan, *Human Ecolol. Risk Asses. Int. J.*, 19 (2013) 1530–1543. <https://doi.org/10.1080/10807039.2012.716681>
- [32] S. Giandomenico, N. Cardellicchio, L. Spada, C. Annicchiarico, A. Di Leo, Metals and PCB levels in some edible marine organisms from the Ionian Sea: dietary intake evaluation and risk for consumers, *Environ. Sci. Pollut. Res.*, 23 (2016) 12596–12612. <https://doi.org/10.1007/s11356-015-5280-2>.
- [33] S. Sudsandee, K. Tantrakarnapa, P. Tharnpoophasiam, Y. Limpanont, R. Mingkhwan, S. Worakhunpiset, Evaluating health risks posed by heavy metals to humans consuming blood cockles (*Anadara granosa*) from the Upper Gulf of Thailand, *Environ. Sci. Pollut. Res.*, 24 (2017) 14605–14615. <https://doi.org/10.1007/s11356-017-9014-5>
- [34] L. Yonglong, S. Song, R. Wang, Impacts of soil and water pollution on food safety and health risks in China, *Int. J. Environ.*, 77 (2015) 5-15. <https://doi.org/10.1016/j.envint.2014.12.010>.



A new analytical method based on Co-Mo nanoparticles supported by carbon nanotubes for removal of mercury vapor from the air by the amalgamation of solid-phase air removal

Danial Soleymani-ghoozhdi ^a, Rouhollah Parvari ^a, Yunes Jahani ^b, Morteza Mehdipour-Raboury ^a and Ali Faghihi-Zarandi ^{a,*}

^a Department of Occupational Health and Safety at Work, Kerman University of Medical Sciences, Kerman, Iran

^b Department of Biostatistics and Epidemiology, School of Public Health, Kerman University of Medical Sciences, Kerman, Iran

ARTICLE INFO:

Received 5 Dec 2021

Revised form 10 Feb 2022

Accepted 26 Feb 2022

Available online 28 Mar 2022

Keywords:

Mercury removal,
Air,
Adsorption,
Cobalt and molybdenum nanoparticles,
Multiwalled Carbon nanotube,
Amalgamation solid-phase air removal

ABSTRACT

Heavy metals are a major cause of environmental pollution, and mercury is a well-known toxicant that is extremely harmful to the environment and human health. In this study, new carbon nanotubes coated with cobalt and molybdenum nanoparticles (Co-Mo/MWCNT) were used for Hg⁰ removal from the air by the amalgamation of solid-phase air removal method (ASPAR). In the bench-scale setup, the mercury vapor in air composition was produced by the mercury vapor generation system (HgGS) and restored in a polyethylene airbag (5 Li). In optimized conditions, the mercury vapor in the airbag passed through Co-Mo/MWCNT and was absorbed on it. Then, the mercury was completely desorbed from Co-Mo/MWCNT by increasing temperature up to 220 °C and online determined by cold vapor atomic absorption spectrometry (CV-AAS). The recovery and capacity of Co-Mo/MWCNT were obtained at 98% and 191.3 mg g⁻¹, respectively. The Repeatability of the method was 32 times. The mercury vapors absorbed on Co-Mo/MWCNT adsorbent could be maintained at 7 days at the refrigerator temperature. The Co-Mo/MWCNT as a sorbent has many advantages such as; high capacity, renewable, good repeatability and chemical adsorption (amalgamation) of mercury removal from the air. The method was successfully validated by a mercury preconcentrator analyzer (MCA) and spiking of real samples.

1. Introduction

Heavy metals are a major cause of environmental pollution, and mercury (Hg) is a well-known toxicant that is extremely harmful to the environment and human health because of its persistence, bioaccumulation, and neurological toxicity [1, 2]. Hg can affect many organs and cause a variety of symptoms in the body, although it targets the nervous system, it may also have serious

toxicological effects on the kidney. In addition to the nervous and kidney system, other systems such as the cardiovascular system can also be damaged by exposure to mercury [3, 4]. Mercury has been used in various products and processes due to its unique properties. It is utilized in industrial processes that produce chlorine, sodium hydroxide (Chlor-alkali plants), the vinyl chloride monomer for polyvinyl chloride (PVC) production, and polyurethane elastomers. Mercury is also released from coal-fired power plants and cement production [5, 6]. Therefore, Hg emissions have attracted worldwide attention. Minamata Convention on mercury, which

*Corresponding Author: [Ali Faghihi-Zarandi](mailto:Ali.Faghihi-Zarandi@kmu.ac.ir)

Email: Alifaghihi60@yahoo.com

<https://doi.org/10.24200/amecj.v5.i01.163>

aims is to protect human health and the environment from anthropogenic emissions and releases of mercury and mercury compounds, entered into force on 16 August 2017 [7, 8]. Recently, the different methods have been introduced for the sampling and analysis of mercury. NIOSH 6009 and OSHA 140 are the recommended methods for the sampling of mercury. In these methods, sample preparation depends on the applied nitric acid and hydrochloric acid which can be hazardous to the environment and human health [9, 10]. Emissions from different sources, mercury release in different forms, including elemental mercury (Hg^0), oxidized mercury (Hg^{2+}), and particulate bound mercury (Hg^p) [11, 12]. Among of various states of mercury, Hg^0 is difficult to remove due to its stability, long persistence time, high volatility and insolubility in water [13, 14]. Therefore, effective Hg^0 control technologies are immediately needed. Several control technologies for Hg^0 , including catalytic oxidation [15], photocatalytic oxidation [16], photochemical removal [17], wet oxidation [18], and adsorption method [19] have been developed. Among the various Hg^0 removal methods, the adsorption technique has been widely studied because of its simplicity, economical, and good removing efficiency [20, 21]. In recent years, novel carbon-based materials, such as graphene and graphene oxide, carbon nanotubes and nanofibers, carbon spheres, and metal-organic frameworks, have been applied for Hg^0 removal. Carbon nanotubes (CNTs) are one type of one-dimensional nanomaterials, which have been used for Hg^0 removal from water and air due to their unique physicochemical properties. Carbon-based materials Because of their large surface area, flexible surface chemistry, and variety diversity, are the most widely studied adsorbents for Hg^0 removal from flue gases and air [21–23]. Because of its high removal efficiency, the activated carbon (AC) based adsorption process is considered one of the most effective technologies for mercury removal, but high operation costs and adsorbent loss have impeded its further development [22, 23]. Therefore, developing more cost-effective carbon-based sorbents for Hg^0

removal has significance [21]. In recent years, novel carbon-based materials, such as bio-chars [24], graphene and graphene oxide [25, 26], carbon nanotubes and nanofibers [27, 28], metal-organic frameworks [29], have been applied for Hg^0 removal by analytical methods. Carbon nanotubes (CNTs) are one type of one-dimensional nanomaterials which have been used for Hg^0 removal from water and air due to their unique physicochemical properties [30–32]. Also, to improve the performance of Hg^0 adsorption, some modification methods have been studied which mainly improve the surface pore structure of adsorbents and/or increase the active sites on the surface of adsorbents [33]. Metal or metal oxide loaded on the surface of CNTs and other carbon-based materials were a type of catalyst with both high adsorption and catalytic capability. Consequently, these types of catalysts can be an effective material for Hg^0 removal from the air. Shen et al. reported that the surface area (BET) of activated carbon (AC) was decreased after loading of Mn or Co on AC, but the on the other hand, the metal oxide functionalized on the AC surface can promote Hg^0 catalytic oxidation [34]. Ma et al used the analytical method based on Fe-Ce decorated multi-walled carbon nanotube (MWCNT) for removal of Hg^0 from flue gas. The results showed that Fe-Ce/MWCNT had good Hg^0 removal performance [32]. Liu et al Suggested the adsorption of Co/TiO₂ for Hg^0 . The results showed that the high oxidation activities for Hg^0 was obtained by this catalyst [35]. Molybdenum (Mo) is commonly added as a promoter to vanadium-based catalysts in Hg^0 oxidation, but its catalytic oxidation activity is poor [36].

In this work, Hg^0 was removed from the air by using Co-Mo/MWCNTs. Brunauer–Emmett–Teller (BET) analysis, X-ray diffraction (XRD), scanning electron microscopy (SEM) and transmission electron microscopy (TEM) were employed to analyze the characteristics of the samples. Experimental parameters affecting the Hg^0 removal process from the air such as temperature and flow rate were investigated and optimized. Also, comparisons between the proposed method and previous methods were obtained.

2. Experimental

2.1. Materials and Chemical reagents

Mercury standard was used in the mercury vapor generation system (HgGS). It was prepared by dilution of 1 ppm (1000 mg L⁻¹) Hg (II) standard solution (CAS Number.: 7487-94-7) which was purchased from Fluka, Germany. Deionized water (DW) was prepared by water purification system from RIPI. The stannous chloride (SnCl₂, CAS Number: 7772-99-8) and the NaBH₄ (CAS Number: 6940-66-2) analytical grade were purchased from Merck and Sigma (Germany) which was diluted with DW. The SnCl₂ or the NaBH₄ as reducing agents was used by dissolving in HCl and NaOH/DW, respectively. The reducing agents was added to 100 mL deionized water (DW) and mixed well. All the laboratory glassware (Sigma) and PVC plastics were cleaned by nitric acid (10% v/v) for at least 2 days and then washed for many times with DW. Cobalt (II) nitrate hexahydrate (Co (NO₃)₂.6 H₂O; CAS Number: 10026-22-9) and Molybdenum powder (10 μm, ≥99.95%, CAS Number: 7439-98-7) were purchased from Sigma Aldrich (Germany). The MWCNTs and Co/Mo-MWCNTs adsorbents was synthesized and prepared from nano center of RIPI. In this study, the Co-Mo/MWCNTs adsorbent was used for mercury removal from air.

2.2. Apparatus

The mercury standard (Hg⁰) was generated by the mercury vapor generation system (HgGS) in chamber. The bench scale included of HgGS for HgH₂, chamber, PVC bags, the quartz tubes as a column, the heater accessory (220 AC Voltage, 35-450 °C), the digital flow meter control (50-500 ml min Ar/air), Pure air accessory, O₂ and water digital detectors, the digital temperature control, the MC-3000 as trace mercury analyser (Germany), and the CV-AAS for determining the mercury concentration. The pure air pushed with flowrate of 50-250 ml min⁻¹ to chamber and mixed with mercury vapour at 100 °C. The air lines (tubes) and PVC bags were covered with heating jackets. The quartz tubes with outer diameter of 0.35 inch,

inner diameter of 0.2 inch and length of 4.0 inch was used as a column for the Co-Mo/MWCNTs adsorbent. The Hg⁰ determined by a cold vapor atomic absorption spectrometer (CV-AAS, GBC Plus 932, AUS). A mercury hollow-cathode lamp with a current of 8 mA, the wavelength of 253.7 nm based on a spectral band width (0.5 nm) was used. Argon (99.99%) was used as a carrier gas for mixer of CV-AAS and glass separator. The SKC air sampling pump (USA), 50 to 2000 ml min⁻¹ was used.

2.3. Co and Mo Catalyst preparation

The sol-gel method has been extensively used in the preparation of supported metal catalysts because it typically results in highly homogeneous materials with high degree of metal dispersion. In this sense, catalysts were supported on silica sol-gel with the metal to 50 percent based on silica added. To obtain metallic catalyst supported on high-surface area silica by the sol-gel method, the polymerization of an alkoxy-silane such as tetrathoxysilane (TEOS), also known as tetraethyl orthosilicate, is carried out in the presence of the appropriate metal precursors. In our case, catalyst nanoparticles were prepared from high purity salts of the transition metals: Co (NO₃)₂.6H₂O and (NH₄)₆Mo₇O₄. 4H₂O, from Baker Co. To accelerate the polymerization, an increase in pH can be brought about by addition of a base, which causes a rapid hydrolysis followed by polymerization. Simultaneously with this polymerization process, the metallic ions (Co and Mo) precipitate, thus forming a homogeneous and well-dispersed mixture (Fig.1).

2.4. Co-Mo/MWCNTs synthesis

As Figure 1, After placing the catalyst inside a quartz tube, a continuous nitrogen flow rate of 1 L min⁻¹ was passed through the reactor for removing the oxygen. Subsequently, the reduction process was accomplished within at 600 °C. The reduction process was kept for 30 minutes in an atmosphere of 90 % v/v of N₂ and 10 % v/v of H₂. Next, the temperature was increased up to 700 °C for the nucleation and growing of CNTs [37-39].

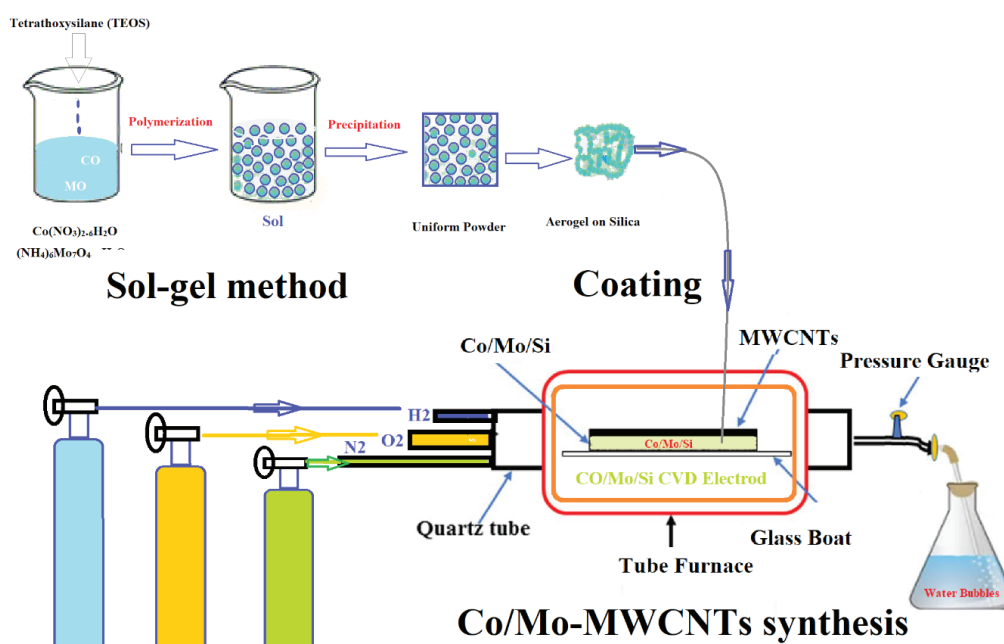


Fig.1. Synthesis of Co-Mo/MWCNTs by Sol gel method and CVD procedure

2.5. Characterization

The high-resolution images were obtained using a high-resolution transmission electron microscope JEOL JEM-2010, operated at 200 kV and a scanning electron microscopy (SEM) JEOL JSM 5300 operated at 5 kV. Complementary RAMAN spectroscopy was performed. The Co-Mo/MWCNTs samples were deposited onto a sample holder with an adhesive carbon foil and sputtered with Au before imaging. The morphology of Co-Mo/MWCNTs was obtained by a transmission electron microscopy (TEM, Zeiss, Germany). For the TEM analysis, the samples were dispersed in C_2H_5OH and a drop was used. The chemical analysis for the determination of Co and Mo concentration in synthesized samples was performed using F-AAS.

2.6. General Procedure

The mercury vapor removal was performed using a bench-scale setup (Fig. 2). First, 40 mg of Co-Mo/MWCNTs nanoadsorbent was put onto the quartz tubes. Then, the end of the adsorbent were tied by fire-proof linen. The pure air was mixed with mercury vapor in chamber containing $0.1-10 \mu\text{g Hg}^0$ per liter air (21% O_2 , 0.2% H_2O) at 25°C .

By the procedure, $0.1-10 \mu\text{g}$ of Hg^0 was generated by the mercury vapor generation system (HgGS) and restored in a PVC bag. The value of mercury in PVC bag was validated using MC analyzer. Due to procedure, the mercury standard solution ($1-2 \text{ mL min}^{-1}$), HCl (5% v/v, 5 mL min^{-1}), and $SnCl_2$ as reducing agent (2.5 mL min^{-1}) were mixed with pure air in mixer and pass through a peristaltic pumps. Elemental mercury vapor was generated in the reaction loop, and pumped into a 5 L polyethylene (PE) bag, as a bulk container. Finally, the mercury concentration was obtained $0.1-10 \mu\text{g Hg}^0$ per liter air in the polyethylene bag (5 L) was mixed with 21 % O_2 and 0.2 % H_2O vapor at 25°C ($10-100 \times \text{TLV OSHA}$). Then The mixture Hg^0 and pure air passed through 40 mg of the Co-Mo/MWCNTs adsorbents, at optimized air flow rate 250 ml min . After amalgamation/adsorption process, the elemental mercury was released from the Co-Mo/MWCNTs adsorbents by a thermal desorption accessory at 220°C , under Ar flow rate and transferred to the absorption cell of CV-AAS (Fig.2). Finally, Hg^0 concentration was determined by CV-AAS. The conditions were presented in Table 1.

3. Results and Discussion

3.1. Co-Mo/MWCNTs Raman Spectra

Figure 3a shows the Raman spectra for CNTs-Co, in which the ratio ID/IG is 0.26, relating a high purity material. On the other hand, with Mo the quality is decreased in a high level (Figure 3b), mainly with Mo (ID/IG ~ 0.59). This is due to the solubility of C in Mo. In order to obtain a better quality, in this case the CVD process must be performed to high temperatures (~900°C). In our experiments, for comparison purposes, the temperature was always the same for the different metal-catalyst (~700°C). According

to previous reports, the increase of the D band intensity (characteristic peak at ~1350 cm⁻¹) with decreasing multiwalled carbon nanotubes (MWCNT) content, is a direct result of the addition of carbonaceous by-products. In the same sense, a decrease in the G' band intensity (characteristic peak at ~2700 cm⁻¹) is observed as the MWCNT mass fraction decreases. The G' band on Figures a reflects the well-structured carbon walls in the samples with Co catalyst, while the Figure 3b (CNTs-Mo), indicate a less ordered structures, due to the carbonaceous byproducts.

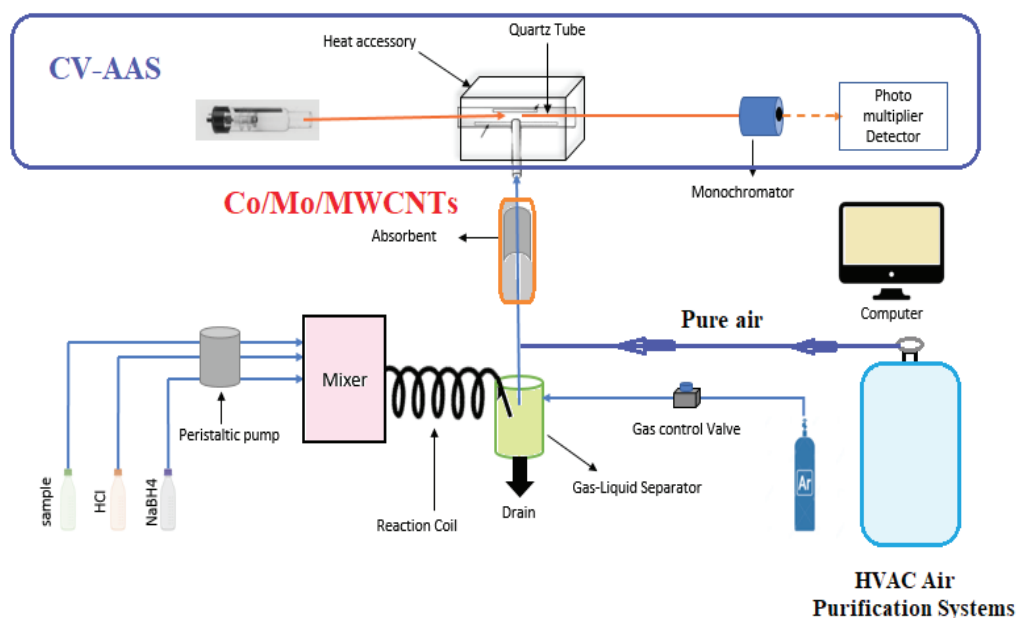


Fig.2. The procedure for removal mercury vapor from air based on Co-Mo/MWCNTs by the ASPAR procedure

Table1. Method conditions for mercury vapor removal with the Co-Mo/MWCNTs

Chamber Conditions	Value
Hg ⁰ values	0.1–10 µg per liter
O ₂ (g)	21%
H ₂ O (g)	0.2%
PVC bag	5 L
Ar flow rate	0.2 L min ⁻¹
Air flowrate	0.25 L min ⁻¹
Heat	220 °C
Removal efficiency with air	More than 95%
Absorption capacity	191.3 mg g ⁻¹ (2% Co and 2% Mo)
Adsorbent amount	40 mg

3.2. SEM imaging

The morphology and structural features of Co-Mo/MWCNTs and MWCNTs were shown by the SEM images. As shown in Figures 4a and 4b, the morphology of MWCNTs and the Co-Mo/MWCNTs

were shown in the nanoscale range between 30–80 nm. Co and Mo were seen in MWCNTs as the brilliant spots. The elemental analysis (EDX) of Co-Mo/MWCNTs was shown in Table 2.

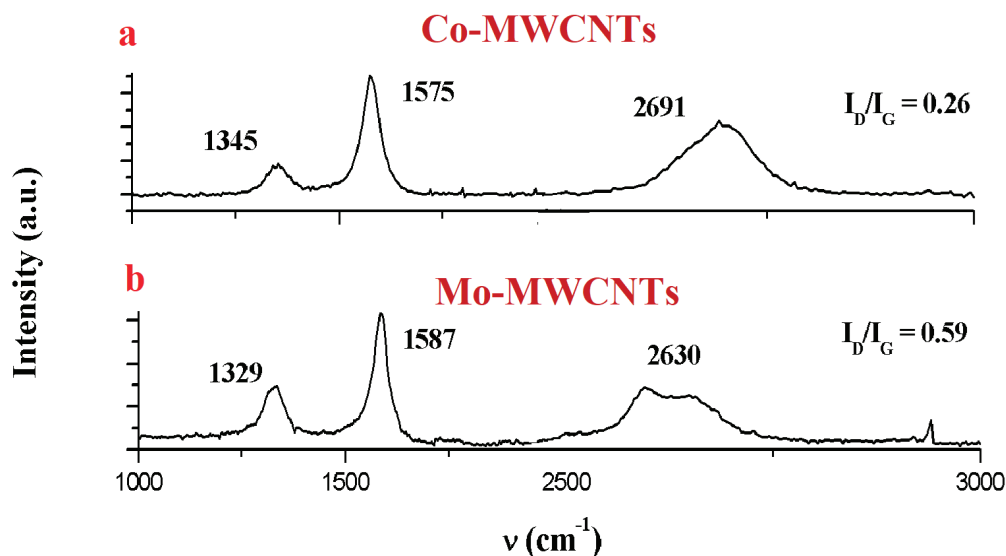


Fig.3. Raman spectra of CNTs samples using a) Co-MWCNTs and b) Mo-MWCNTs

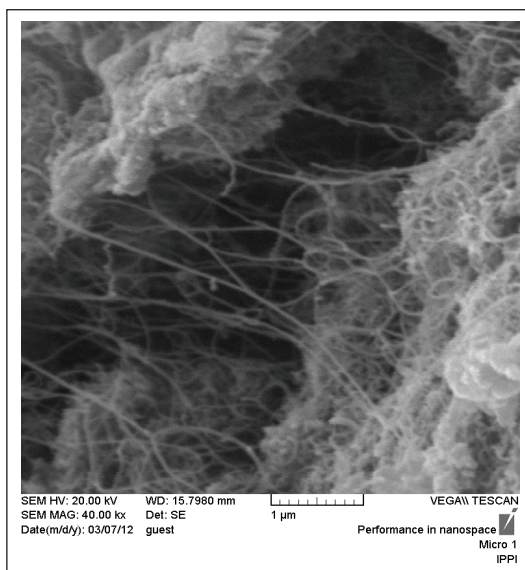


Fig.4a. SEM image of MWCNTs

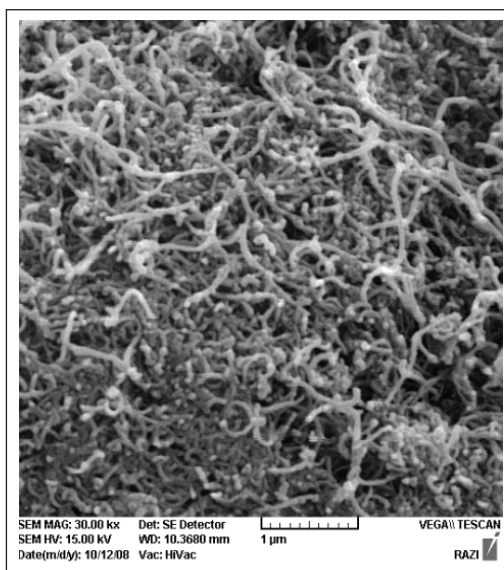


Fig.4b. SEM image of Co-Mo/MWCNTs

Table 2. EDX analysis for elemental values for the Co-Mo/MWCNTs

Elements	% Values
Carbon	67.5
N	17.2
Co	2.6
Mo	2.8
H	4.3
O	5.6

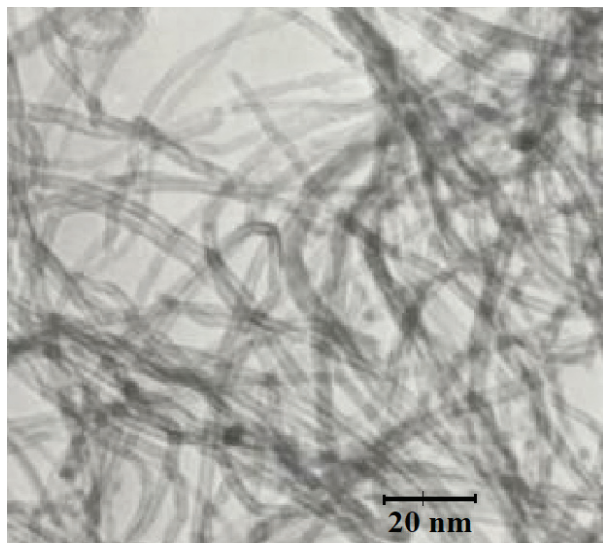


Fig. 5a. TEM image of MWCNTs



Fig. 5b. TEM image of Co-Mo/MWCNTs

3.3. TEM imaging

The TEM of MWCNTs showed in [Figure 5a](#). Also. The TEM of Co-Mo/MWCNTs adsorbent can be seen that Co and Mo nanoparticles (brilliant points) were incorporated into the MWCNTs, both on the external and internal surface of MWCNTs, with no effect on the porous structure of MWCNTs ([Fig. 5b](#)). The Co and Mo particles in MWCNTs distributed with the average size of 35 nm (20-50 nm).

3.4. XRD analysis

The immobilized Co and Mo on MWCNTs were characterized by XRD spectroscopy. In [Figure](#)

[6](#). A many peaks can be observed from Co-Mo/MWCNTs, which was ascribed to the highly crystalline structure of carbon nanotubes. The diffraction peaks at 26° and 41° are related to (002) and (100) planes of hexagonal graphite. There are, however, no characteristic peaks of Co and Mo in the XRD pattern of Co/Mo-MWCNTs. This indicates that Co and Mo are uniform dispersed on the MWCNTs, and no effect on XRD spectrum of MWCNTs. The Textural properties of samples for Co-Mo/MWCNTs and MWCNTs adsorbents synthesized with the CO-MO/MWCNTs ([Table 3](#))

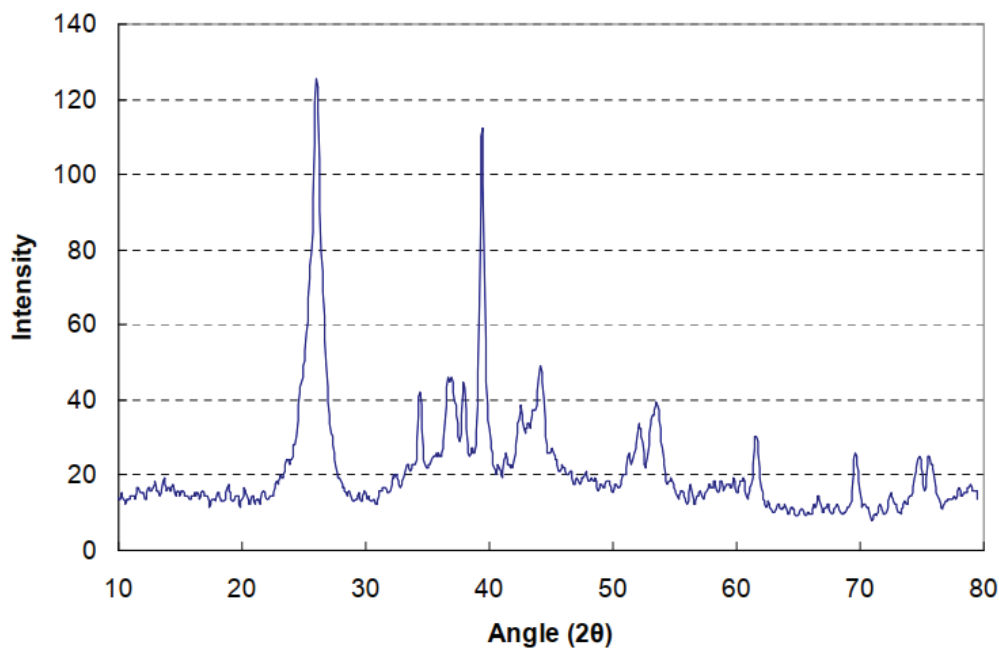


Fig. 6. The XRD analysis for CO/MO-MWCNTs

Table 3. Textural properties of samples synthesized with the Co-Mo/MWCNTs

Material	S_{BET} (m ² g ⁻¹) ^a	V (cm ³ g ⁻¹) ^b	a(nm) ^c	d(nm) ^d	W (nm) ^e
MWCNTs	288.84	0.52	5.1	3.85	1.55
CO-MO/MWCNTs	145.16	0.34	4.9	3.8	1.62

^a BET specific surface area, ^b the pore volume, ^c Unit cell parameter obtained from XRD diffractograms,

^d the pore diameter (nm), ^e Wall thickness(nm)

3.5. Optimization of parameters for removal mercury

In this work, a novel method was used for the removal of mercury vapor (Hg⁰) from air by using of the Co-Mo/MWCNTs adsorbent. The chamber was designed to generate a gas containing amounts of mercury vapor based on O₂ and H₂O vapor. For efficient removal of Hg⁰, the conditions of proposed method were optimized.

3.5.1. Effect of O₂ and H₂O

The general procedure was performed with O₂ and H₂O vapor for Hg⁰ removal by Co-Mo/MWCNTs adsorbent. In presence of O₂ and H₂O vapor, the percentages of mercury removal decreased about 4-8%. Due to oxidation of the Co-Mo/MWCNTs, the surface activity of the adsorbent decreased. The results showed, the quantitative recoveries of Hg⁰ were obtained at the moisture contents of 0.05-0.22%. By increasing of water vapor content, slightly decreased the recovery values. By increasing the O₂, the surface morphology of the Co-Mo/MWCNTs adsorbent was changed due to the oxidation of Co and Mo nanoparticles. So, the removal efficiency of adsorbent a slightly decreased at 25°C (5%). On the other hand, the oxidation process accelerates in high temperature and reduce the surface area (BET) and the adsorption capacity. At 35-55 °C, the removal efficiency was decreased from 5% to 25% in present of O₂ value.

3.5.2. Effects of Co-Mo/MWCNTs amount and flow rate

The effect of the Co-Mo/MWCNTs amount on the mercury removal from air was evaluated (Fig. 7). It was evaluated with different amounts of Co-Mo/MWCNTs adsorbent in

the range of 1 to 50 mg. Due to results, the adsorption of Hg⁰ was increased more than 25 mg of adsorbent. So, the high recovery for removal of mercury vapor in air were achieved more than 95% by 40 mg of Co-Mo/MWCNTs adsorbent. Also, the MWCNTs adsorbent had low recovery about 10-14%. Due to high surface area and metal sites of Co and Mo, the high absorption capacity was achieved for the Co-Mo/MWCNTs adsorbent by amalgamation process (Co-Hg; Mo-Hg).

The mercury vapor was generated in chamber and mixed with pure air (21% O₂; 0.2% of H₂O, 0.1-10 µg L⁻¹). The flow rate is a critical role in removal recovery of mercury, which was directly affected on interaction and adsorption process. The flow rate must be tuned to enable a high recovery for mercury removal from air. So, the effect of flow rates was evaluated in ranges of 50-500 mL min⁻¹ (25°C). The results showed us, the best removal efficiency was occurred at flow rates of 50-300 mL min⁻¹ (25°C). However, it was observed that the absorption process started to decrease at more than 300 mL

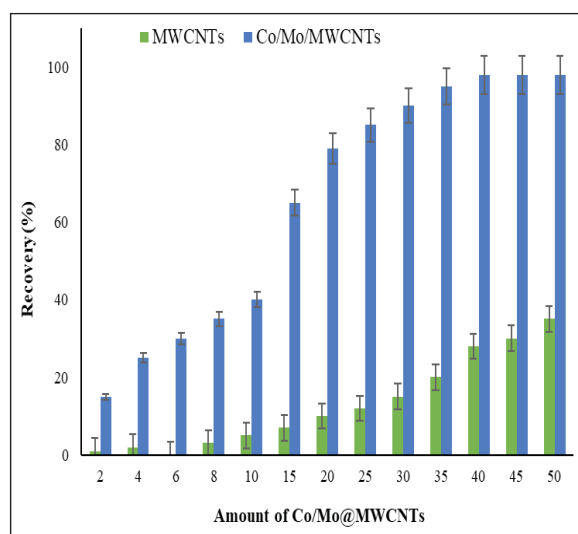


Fig. 7. The effect of sorbent mass for Hg⁰ removal

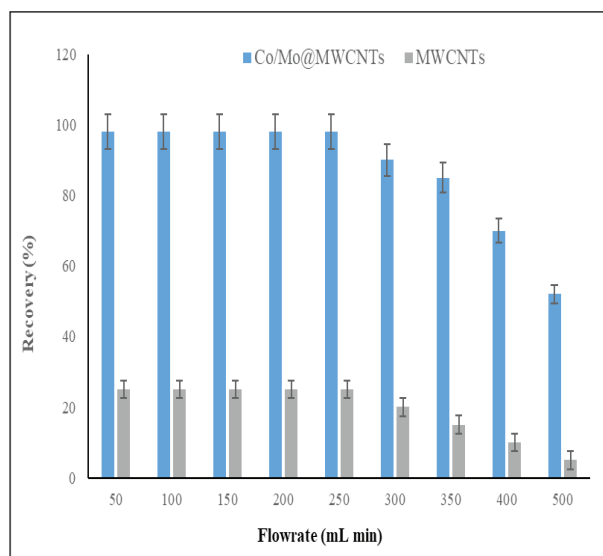


Fig. 8. The effect of flowrate for Hg⁰ removal

min⁻¹. Therefore, the flowrate of 250 mL min⁻¹ was selected as optimum flowrate for mercury removal by the Co-Mo/MWCNTs adsorbent (Fig. 8).

3.5.3. Effect of temperature

The main role for the adsorption and desorption of Hg⁰ by the Co-Mo/MWCNTs and MWCNTs adsorbents is temperature. So, the effect of temperature for the adsorption and desorption of mercury from Co-Mo/MWCNTs adsorbents were examined in the range of 25–60°C and 50–400°C, respectively (21% O₂, 0.2% H₂O; 0.1–10 µg L⁻¹ Hg⁰). As Figure 9, the mercury vapor removed from air at temperatures up to 30 °C. In higher temperatures

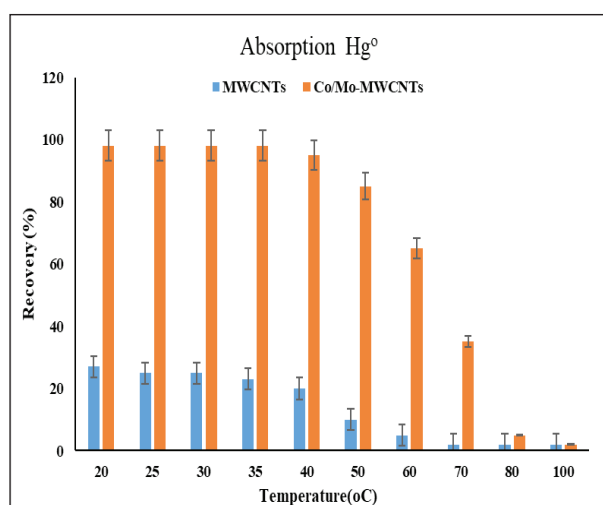


Fig. 9. Effect of temperature on absorption mercury

the Hg⁰ adsorption was decreased. Moreover, the desorption of Hg⁰ from the Co-Mo/MWCNTs and MWCNTs adsorbents were obtained at 190–250 °C. Therefore, the Co-Mo/MWCNTs can be removed the mercury from air by the amalgamation interactions at 220 °C (Fig. 10).

3.5.4. Adsorption capacity

In-addition the adsorption capacities of mercury vapor by the Co-Mo-MWCNTs and MWCNTs adsorbents were evaluated (21% O₂, 0.2% H₂O; 0.1–10 µg L⁻¹ Hg⁰). The mercury vapor was generated and passed through the Co-Mo/MWCNTs and MWCNTs adsorbents (40 mg) at the optimized conditions. The maximum adsorption capacities of the Co-Mo/MWCNTs and MWCNTs adsorbents for mercury removal from air were obtained 191.3 mg g⁻¹ and 22.4 mg g⁻¹, respectively. This mechanism was related to the interaction of mercury with Mo and Co which was supported on MWCNTs due to amalgamation process. The physical adsorption of MWCNTs (about 20%) and chemical adsorption by the amalgamation processes (more than 80%) caused to increase the removal efficiency of mercury from air. In chamber, 40 mg of the Co-Mo/MWCNTs and MWCNTs adsorbents were placed on PVC bag and mercury vapor generated/ flowed in column by 250 mL min⁻¹. Then the mercury concentration in stock PVC bag was determined by MC-3000. In dynamic system, the adsorption

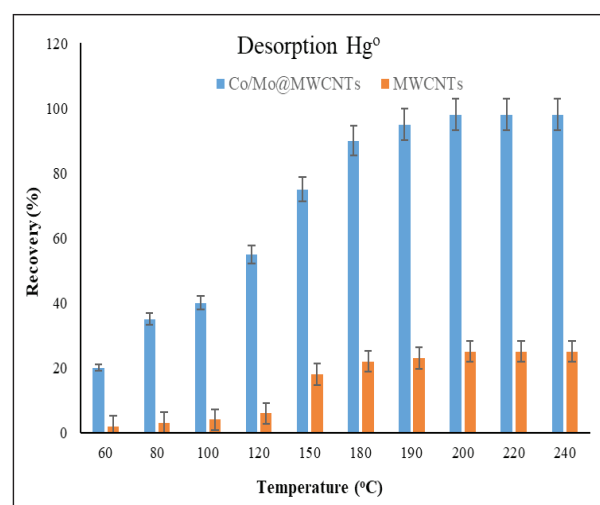


Fig. 10. Effect of temperature on desorption mercury

capacities of the Co-Mo/MWCNTs and MWCNTs for mercury removal were found 132.7 mg g⁻¹ and 8.4 mg g⁻¹, respectively which was lower than static system. The reusability of the Co-Mo/MWCNTs adsorbent for mercury removal was decreased after 32 times absorption/desorption process.

3.5.5. Method Validation

The ASPAR method was used for the removal of Hg⁰ from the air. The method was validated based on the Co-Mo/MWCNTs and MWCNTs adsorbent by spiking real samples in presence of air (21% O₂, 0.2% H₂O; 0.1-10 µg L⁻¹ Hg⁰). Due to absorption and desorption process the concentration of mercury was determined by CV-AAS at optimized conditions. Also, the validation of the methodology was followed by MC3000

analyzer. There is no standard reference material (SRM) for mercury vapor from air, So, the method validation for Hg⁰ removal found by spiking of the standard mercury solutions which was confirmed the accuracy and precision of the ASPAR method. The mixture of mercury in pure air (21% O₂, 0.2% H₂O, 0.1-10 µg), was moved from chamber to the PVC bags and then moved into the Co-Mo/MWCNTs and MWCNTs adsorbents. Many spiked samples based on various concentration of Hg⁰ were used in presence of air (Table 4). The procedure was found for real samples in presence of air composition which was validated based on spiking samples and compared to MC3000 analyzer (Table 5). The results showed a simple, low cost, high recovery and favorite repeatability for mercury removal from air.

Table 4. Validation of the ASPAR method based on Co-Mo/MWCNTs by spiking of mercury vapour (µg L⁻¹ air)

Sample	**HgGS	Added	*Found	Recovery (%)
Air 1	0.102± 0.005	-----	0.108± 0.006	-----
		0.1	0.210± 0.011	102
Air 2	0.532± 0.026	-----	0.528± 0.025	-----
		0.5	1.021± 0.044	98.6
Air 3	1.076± 0.062	-----	1.009± 0.066	-----
		1.0	1.984± 0.096	97.5
Air 4	3.035± 0.145	-----	2.965± 0.152	-----
		3.0	5.882± 0.274	97.2
Air 5	5.578± 0.238	-----	5.397± 0.255	-----
		5.0	10.226± 0.513	96.6
Air 6	10.124± 0.453	-----	9.965± 0.493	-----
		10	20.051± 0.937	100.9

*Mean of three determinations ± confidence interval (P = 0.95, n = 3)

** Mercury in HgGS determined by CV-AAS (n=10)

Table 5. Validation of the ASPAR method based on Co-Mo/MWCNTs by spiking of real sample and compared to MCA (µg L⁻¹ air)

Sample	**MCA(µg)	Added (µg)	*Found (µg)	Recovery (%)
Air I	0.402± 0.018	-----	0.392± 0.022	97.5
		0.5	0.882± 0.042	98.0
Air II	0.957± 0.053	-----	0.962± 0.063	100.5
		1.0	1.938± 0.096	97.6
Air III	2.882± 0.144	-----	2.756± 0.154	95.6
		2.5	5.198± 0.268	97.7
Air VI	5.264± 0.246	-----	5.361± 0.253	101.8
		5.0	10.188± 0.483	96.5
Air V	8.016± 0.412	-----	7.914± 0.388	98.7
		10	17.865± 0.832	99.5

*Mean of three determinations ± confidence interval (P = 0.95, n = 3)

**Mercury determined by MC3000

3.5.6. Discussion

By the ASPAR method, the mercury removal from air was achieved based on Co-Mo/MWCNTs adsorbent and compared to other published methods (Table 6). Ma et al were investigated on Hg⁰ removal by multi-walled carbon nanotubes supported Fe-Ce mixed oxides nanoparticles (Fe-CeO_x/MWCNTs). The Fe₍₂₎ Ce_(0.5) O_x/MWCNTs catalyst showed the best catalytic activity, its Hg⁰ removal efficiency reached as high as 88.9% at 240 °C [32]. Also, the removal of Hg⁰ was studied based on Mn-Mo/CNT by Zhao et al. The optimum temperature and MnO₂ content for removal of Hg⁰ was 250 °C and 5 wt%. Also, experimental of mercury oxidized by Mn-Mo/CNT indicated that SO₂ could increase mercury oxidation by this catalyst and that the optimum temperature for mercury oxidized by Mn-Mo/CNT decreased to 150 °C [27]. According to the study of Wu et al, the removal efficiency of Hg⁰ based on Ce-Mn/TiO₂ was investigated by N₂, 6% O₂ and 500–2000 ppm of SO₂. The average removal efficiency of Ce-Mn/TiO₂ was obtained about 80% which was lower than Co-Mo/MWCNTs (more than 95%). Furthermore, the results showed the reusability of Ce-Mn/TiO₂ was achieved for 10 times (adsorption/desorption cycles) which was

lower than the Co-Mo/MWCNTs adsorbent with 32 times [2]. Ma et al showed the Hg⁰ removal from flue gas with Ag-Fe₃O₄@rGO composite. The Hg⁰ was efficiently removed higher than 92% at 100 °C, which was lower than Co-Mo/MWCNTs [26]. Yang et al was studied on Hg⁰ removal from air based on Fe_{3-x}Mn_xO₄/CNF. The results showed that at the optimal temperature (150–200 °C), the removal efficiency for Hg⁰ was attained above 90 % [28]. Xu et al showed that ultrasound-assisted impregnation promoted Hg⁰ removal with Cu-Ce/RSU. the optimal Cu/Ce molar ratio, loading value and reaction temperature were 1/5, 0.18 mol L⁻¹ and 150 °C, respectively. Also, the highest Hg⁰ removal efficiency obtained was 95.26%. As compared to Co-Mo/MWCNTs, the removal efficiency of Cu-Ce/RSU was lower value [24]. In another study, Xu et al synthesized MnO_x/graphene composites for the removal of Hg⁰ in flue gas. MnO_x/graphene sorbents with 30% graphene showed that the Hg⁰ removal efficiency was achieved more than 90% at 150 °C (4% O₂). Furthermore, MnO_x/graphene showed an good regenerative ability [25]. Liu et al. prepared Co/TiO₂ catalysts for Hg⁰ removal. results showed that the optimal loading of Co was 7.5%. The Hg⁰ removal efficiency was reached more than 90% at the temperature range 120–330 °C [35].

Table 6. Comparing of ASPAR method for the mercury removal from air based on Co-Mo/MWCNTs with other published methods

Adsorbent	Mechanism/method	Sample	Adsorption capacity	Removal Efficiency	Ref.
Mn-Mo/CNT	chemisorption	Flue gas	--	80%	[27]
Ag-CNT	Amalgamation	Flue gases	9.3 mg g ⁻¹	---	[40]
Silver nano particles/MGBs	Amalgamation/SPGE	Air/Artificial Air	91.8 mg g ⁻¹	98%	[41]
NPd@MSN	amalgamation/adsorption	Air	149.4 mg g ⁻¹	95%	[42]
Mn/MCM-22	catalytic oxidation and chemisorption	Flue gas	300 mg g ⁻¹	92%	[43]
Cu-Zn/SBA-15	Adsorption	Natural Gas	12.75 mg g ⁻¹	100%	[44]
Co-Mo/MWCNTs	Amalgamation	Air	191.3 mg g ⁻¹	98%	This study

4. Conclusions

In this research, a novel Co-Mo/MWCNTs adsorbent was used for mercury removal from air by the ASPAR method and finally mercury was measured by CV-AAS. First the mercury vapor generated by HgGS (0.1-10 $\mu\text{g L}^{-1}$ air), mixed with pure air (21% of O_2 and 0.2% of H_2O) and moved to column which was filled with the Co-Mo/MWCNTs adsorbent. The mechanism of absorption was obtained by amalgamation Co and Mo. The best thermal desorption was occurred at 220 $^\circ\text{C}$. Due to results, the mean recovery, the reusing and adsorption capacity were obtained 98.8%, 32, 191.3 mg g^{-1} , respectively. The range of adsorption efficiencies for ten air samples with 40 mg of the Co-Mo/MWCNTs adsorbent was achieved between 94.6-102.4 in optimized conditions. The O_2 content may be affected by oxidation of Co or Mo and can reduce the mercury adsorption by the adsorbent by about 5-10%. The ASPAR method was validated by spiking samples and MC3000 analyzer.

5. Acknowledgements

The authors thanks from department of occupational health and safety at work and department of biostatistics and epidemiology, Kerman University of Medical Sciences (KUMS), Kerman, Iran.

6. References

- [1] H. Wang, S. Wang, Y. Duan, Y.-n. Li, Y. Xue, Z. Ying, Activated carbon for capturing Hg in flue gas under O_2/CO_2 combustion conditions. Part 1: Experimental and kinetic study, *Energy Fuels*, 32 (2018) 1900-1906. <https://doi.org/10.1021/acs.energyfuels.7b03380>.
- [2] X. Wu, Y. Duan, N. Li, P. Hu, T. Yao, J. Meng, S. Ren, H. Wei, Regenerable Ce-Mn/ TiO_2 catalytic sorbent for mercury removal with high resistance to SO_2 , *Energy Fuels*, 33 (2019) 8835-8842. <https://doi.org/10.1021/acs.energyfuels.9b00978>.
- [3] G. Genchi, M.S. Sinicropi, A. Carocci, G. Lauria, A. Catalano, Mercury exposure and heart diseases, *Int. J. Environ. Res. Public Health*, 14 (2017) 74. <https://doi.org/10.3390/ijerph14010074>.
- [4] S.E. Orr, C.C. Bridges, Chronic kidney disease and exposure to nephrotoxic metals, *Int. J. Mol. Sci.*, 18 (2017) 1039. <https://doi.org/10.3390/ijms18051039>.
- [5] E.G. Pacyna, J.M. Pacyna, F. Steenhuisen, S. Wilson, Global anthropogenic mercury emission inventory for 2000, *Atmos. Environ.*, 40 (2006) 4048-4063. <https://doi.org/10.1016/j.atmosenv.2006.03.041>.
- [6] C. Winder, N.H. Stacey, Occupational toxicology, 2ed, CRCpress, 2004. <https://www.routledge.com/Occupational-Toxicology/Winder-Stacey/p/book/9780367394554>
- [7] M. Sakamoto, N. Tatsuta, K. Izumo, P.T. Phan, L.D. Vu, M. Yamamoto, M. Nakamura, K. Nakai, K. Murata, Health impacts and biomarkers of prenatal exposure to methylmercury: Lessons from Minamata, Japan, *Toxins*, 6 (2018). <https://doi.org/10.3390/toxins6030045>.
- [8] UNEP, Minamata convention on mercury, United Nations environment programme Geneva, Switzerland, 2013. <https://www.unep.org/resources/report/minamata-convention-mercury>.
- [9] R. Andrews, P.F. O'Connor, NIOSH manual of analytical methods (NMAM), 2020. <https://www.cdc.gov/niosh/nmam/default.html>.
- [10] A. Ebrahimi, A. Salarifar, Air pollution Analysis: Nickel paste on Multi-walled carbon nanotubes as a novel adsorbent for the mercury removal from air, *Anal. methods. Environ. chem. J.*, 2 (2019) 79-88. <https://doi.org/10.24200/amecj.v2.i03.70>.
- [11] Y. Liu, Y. Li, H. Xu, J. Xu, Oxidation removal of gaseous Hg^0 using enhanced-Fenton system in a bubble column reactor, *Fuel*, 246 (2019) 358-364. <https://doi.org/10.1016/j.fuel.2019.03.018>.
- [12] S. Zhang, M. Díaz-Somoano, Y. Zhao, J. Yang, J. Zhang, Research on the mechanism of elemental mercury removal over Mn-Based SCR catalysts by a developed Hg-TPD method, *Energy Fuels*, 33 (2019) 2467-2476. <https://doi.org/10.1021/acs.energyfuels.8b04424>.

- [13] H. Zeng, F. Jin, J. Guo, Removal of elemental mercury from coal combustion flue gas by chloride-impregnated activated carbon, *Fuel*, 83 (2004) 143-146. [https://doi.org/10.1016/S0016-2361\(03\)00235-7](https://doi.org/10.1016/S0016-2361(03)00235-7).
- [14] B. Zhang, P. Xu, Y. Qiu, Q. Yu, J. Ma, H. Wu, G. Luo, M. Xu, H. Yao, Increasing oxygen functional groups of activated carbon with non-thermal plasma to enhance mercury removal efficiency for flue gases, *Chem. Eng. J.*, 263 (2015) 1-8. <https://doi.org/10.1016/j.cej.2014.10.090>.
- [15] H. Li, S. Wu, C.Y. Wu, J. Wang, L. Li, K. Shih, SCR atmosphere induced reduction of oxidized mercury over CuO-CeO₂/TiO₂ catalyst, *Environ. Sci. Technol.*, 49 (2015) 7373-7379. <https://doi.org/10.1021/acs.est.5b01104>.
- [16] J. Wu, C. Li, X. Zhao, Q. Wu, X. Qi, X. Chen, T. Hu, Y. Cao, Photocatalytic oxidation of gas-phase Hg⁰ by CuO/TiO₂, *App. Catal. B*, 176-177 (2015) 559-569. <https://doi.org/10.1016/j.apcatb.2015.04.044>.
- [17] Y. Liu, J. Zhang, J. Pan, Photochemical oxidation removal of Hg⁰ from flue gas Containing SO₂/NO by an ultraviolet irradiation/hydrogen peroxide (UV/H₂O₂) process, *Energy Fuels*, 28 (2014) 2135-2143. <https://doi.org/10.1021/ef401697y>.
- [18] Y. Liu, Y. Wang, Gaseous elemental mercury removal using VUV and heat coactivation of Oxone/H₂O/O₂ in a VUV-spraying reactor, *Fuel*, 243 (2019) 352-361. <https://doi.org/10.1016/j.fuel.2019.01.130>.
- [19] D. Liu, W. Zhou, J. Wu, Kinetic behavior of elemental mercury sorption on cerium- and lanthanum-based composite oxides, *Surf. Rev. Lett.*, 26 (2019) 1-9. <http://dx.doi.org/10.1142/S0218625X1850141X>.
- [20] G. Li, Q. Wu, S. Wang, Z. Li, H. Liang, Y. Tang, M. Zhao, L. Chen, K. Liu, F. Wang, The influence of flue gas components and activated carbon injection on mercury capture of municipal solid waste incineration in China, *Chem. Eng. J.*, 326 (2017) 561-569. <https://doi.org/10.1016/j.cej.2017.05.099>.
- [21] H. Yang, Z. Xu, M. Fan, A.E. Bland, R.R. Judkins, Adsorbents for capturing mercury in coal-fired boiler flue gas, *J. Hazard. Mater.*, 146 (2007) 1-11. <https://doi.org/10.1016/j.jhazmat.2007.04.113>.
- [22] Z. Tan, L. Sun, J. Xiang, H. Zeng, Z. Liu, S. Hu, J. Qiu, Gas-phase elemental mercury removal by novel carbon-based sorbents, *Carbon*, 50 (2012) 362-371. <https://doi.org/10.1016/j.carbon.2011.08.036>.
- [23] Y. Zheng, A.D. Jensen, C. Windelin, F. Jensen, Dynamic measurement of mercury adsorption and oxidation on activated carbon in simulated cement kiln flue gas, *Fuel*, 93 (2012) 649-657. <https://doi.org/10.1016/j.fuel.2011.09.053>.
- [24] W. Xu, Y.G. Adewuyi, Y. Liu, Y. Wang, Removal of elemental mercury from flue gas using CuOx and CeO₂ modified rice straw chars enhanced by ultrasound, *Fuel Proc. Technol.*, 170 (2018) 21-31. <https://doi.org/10.1016/j.fuproc.2017.10.017>.
- [25] H. Xu, Z. Qu, C. Zong, W. Huang, F. Quan, N. Yan, MnOx/graphene for the catalytic oxidation and adsorption of elemental mercury, *Environ. Sci. Technol.*, 49 (2015) 6823-6830. <https://doi.org/10.1021/es505978n>.
- [26] Y. Ma, B. Mu, X. Zhang, H. Xu, Z. Qu, L. Gao, B. Li, J. Tian, Ag-Fe₃O₄@rGO ternary magnetic adsorbent for gaseous elemental mercury removal from coal-fired flue gas, *Fuel*, 239 (2019) 579-586. <https://doi.org/10.1016/j.fuel.2018.11.065>.
- [27] B. Zhao, X. Liu, Z. Zhou, H. Shao, M. Xu, Catalytic oxidation of elemental mercury by Mn-Mo/CNT at low temperature, *Chem. Eng. J.*, 284 (2016) 1233-1241. <https://doi.org/10.1016/j.cej.2015.09.090>.
- [28] J. Yang, Y. Zhao, S. Liang, S. Zhang, S. Ma, H. Li, J. Zhang, C. Zheng, Magnetic iron-manganese binary oxide supported on carbon nanofiber (Fe_{3-x}MnxO₄/CNF) for efficient removal of Hg⁰ from coal combustion flue

- gas, *Chem. Eng. J.*, 334 (2018) 216-224. <https://doi.org/10.1016/j.cej.2017.10.004>.
- [29] X. Zhang, B. Shen, S. Zhu, H. Xu, L. Tian, UiO-66 and its Br-modified derivatives for elemental mercury removal, *J. Hazard. Mater.*, 320 (2016) 556-563. <https://doi.org/10.1016/j.jhazmat.2016.08.039>.
- [30] B. Tawabini, A. A. M. Khaled, Removal of mercury from water by multi-walled carbon nanotubes, *Water Sci. Technol.*, 61 (2010) 591-598. <https://doi.org/10.2166/wst.2010.897>.
- [31] F. Golbabaie, A. Ebrahimi, H. Shir Khanloo, A. Koohepaie, A. Faghihi-Zarandi, Single-walled carbon nanotubes (SWCNTs), as a novel sorbent for determination of mercury in air, *Glob. J. Health Sci.*, 8 (2015) 273. <https://doi.org/10.5539/gjhs.v8n7p273>.
- [32] Y. Ma, D. Zhang, H. Sun, J. Wu, P. Liang, H. Zhang, Fe-Ce mixed oxides supported on carbon nanotubes for simultaneous removal of NO and Hg⁰ in flue gas, *Ind. Eng. Chem. Res.*, 57 (2018) 3187-3194. <https://doi.org/10.1021/acs.iecr.8b00015>.
- [33] W. Xu, A. Hussain, Y. Liu, A review on modification methods of adsorbents for elemental mercury from flue gas, *Chem. Eng. J.*, 346 (2018) 692-711. <https://doi.org/10.1016/j.cej.2018.03.049>.
- [34] Z. Shen, J. Ma, Z. Mei, J. Zhang, Metal chlorides loaded on activated carbon to capture elemental mercury, *J. Environ. Sci.*, 22 (2010) 1814-1819. [https://doi.org/10.1016/S1001-0742\(09\)60324-7](https://doi.org/10.1016/S1001-0742(09)60324-7).
- [35] Y. Liu, Y. Wang, H. Wang, Z. Wu, Catalytic oxidation of gas-phase mercury over Co/TiO₂ catalysts prepared by sol-gel method, *Catal. Commun.*, 12 (2011) 1291-1294. <http://dx.doi.org/10.1016/j.catcom.2011.04.017>.
- [36] S. Zhao, Z. Li, Z. Qu, N. Yan, W. Huang, W. Chen, H. Xu, Co-benefit of Ag and Mo for the catalytic oxidation of elemental mercury, *Fuel*, 158 (2015) 891-897. <https://doi.org/10.1016/j.fuel.2015.05.034>.
- [37] L.C. Klein, Sol-Gel Processing of Silicates, *Annu. Rev. Mater. Sci.*, 15 (1985) 227-248. <https://doi.org/10.1146/annurev.ms.15.080185.001303>.
- [38] L.M. Hoyos-Palacio, A.G. García, J. F. Pérez-Robles, J. González, H.V. Martínez-Tejada, Catalytic effect of Fe, Ni, Co and Mo on the CNTs production, *IOP Con. Ser. Mater. Sci. Eng.*, 59 (2014) 012005. <https://doi.org/10.1088/1757-899X/59/1/012005>.
- [39] V.M. Irurzun, Y. Tan, D.E. Resasco, Sol-Gel synthesis and characterization of Co-Mo/Silica catalysts for single-walled carbon nanotube production, *Chem. Mater.*, 21 (2009) 2238-2246. <https://doi.org/10.1021/cm900250k>.
- [40] G. Luo, H. Yao, M. Xu, X. Cui, W. Chen, R. Gupta, Z. Xu, Carbon nanotube-silver composite for mercury capture and analysis, *Energy Fuels*, 24 (2010) 419-426. <https://doi.org/10.1021/ef900777v>.
- [41] H. Shir Khanloo, M. Osanloo, M. Ghazaghi, H. Hassani, Validation of a new and cost-effective method for mercury vapor removal based on silver nanoparticles coating on micro glassy balls, *Atmos. Pollut. Res.*, 8 (2017) 359-365. <https://doi.org/10.1016/j.apr.2016.10.004>.
- [42] H. Shir Khanloo, F. Golbabaie, A. Vahid, A. Faghihi Zarandi, A novel nano-palladium embedded on the mesoporous silica nanoparticles for mercury vapor removal from air by the gas field separation consolidation process, *Appl. Nanosci.*, (2022). <https://doi.org/10.1007/s13204-022-02366-0>.
- [43] Y. Ma, T. Xu, X. Zhang, Z. Fei, H. Zhang, H. Xu, Y. Ma, Manganese bridge of mercury and oxygen for elemental mercury capture from industrial flue gas in layered Mn/MCM-22 zeolite, *Fuel*, 283 (2021) 118973. <https://doi.org/10.1016/j.fuel.2020.118973>.
- [44] H. Zhang, J. Wang, T. Liu, M. Zhang, L. Hao, T. Phouthavong, P. Liang, Cu-Zn oxides nanoparticles supported on SBA-15 zeolite as a novel adsorbent for simultaneous removal of H₂S and Hg⁰ in natural gas, *Chem. Eng. J.*, 426 (2021) 131286. <https://doi.org/10.1016/j.cej.2021.131286>.



Management and removal of nitrate contamination of water samples based on modified natural nanozeolite before determination by the UV-Vis spectrophotometry

Bahareh Azemi Motlagh^a, Ali Mohammadi^{a,*} and Mehdi Ardjmand^{b,c}

^a Department of Natural Resource and Environment, Science and Research Branch, Islamic Azad University, Tehran, Iran

^b Chemical Engineering Department, South Tehran Branch, Islamic Azad University, Tehran, Iran

^c Nanotechnology Research Center, South Tehran Branch, Islamic Azad University, Tehran, Iran

ARTICLE INFO:

Received 20 Nov 2021

Revised form 17 Jan 2022

Accepted 23 Feb 2022

Available online 28 Mar 2022

Keywords:

Removal,
Nitrate,
Adsorption,
Water samples,
Nanozeolite,
UV-Vis spectrophotometry

ABSTRACT

Nitrate is a hazardous substance for human health, the removal of which is an important environmental priority. Therefore, in this study, first, the sources of nitrate pollution of water were investigated, then the structure, role, and application of nanozeolites for the removal of nitrate ions were studied by the analytical method. Also, the presentation of management solutions, identification of polluting industrial sectors, different methods of removal and fabrication of ZSM-5/Fe/Ni nanosorbents, and the determination of optimal conditions for nitrate removal were investigated by experimental design software and graphical analysis of effective parameters. The results of graphical analysis of laboratory method showed us, the highest nitrate removal efficiency at a residence time of 150 minutes, pH 3, 4 g L⁻¹ adsorbent, and 40 mg L⁻¹ nitrate were achieved (%RE:91.5-97.4). Experimental results indicate the high efficiency, absorption capacity, and effectiveness of ZSM-5/Fe/Ni adsorbents for nitrate removal in waters. Finally, the absorbance values or nitrate concentrations between 20-120 mg L⁻¹ were measured by the UV-Vis spectrophotometry. The maximum absorption capacity of ZSM-5/Fe/Ni adsorbents for nitrate was obtained 136.7 mg g⁻¹. The developed method based on a novel ZSM-5/Fe/Ni adsorbents has many advantages such as simple, low cost, high efficiency, and favorite recovery of more than 90% for removal nitrate in water samples by nanotechnologies as compared to other reported methods.

1. Introduction

Nitrate and nitrite compounds are important factors in groundwater pollution. Due to the lack of nitrification of municipal, industrial and agricultural wastewater, its average amount is increasing. Therefore, various methods such as adsorption, ion exchange, reverse osmosis, chemical, and biological methods are used [1-3]. Banu et al Have

identified the chitosan beads (CS) technique as an efficient biosorbent for the removal of toxic anions from aqueous solutions. In this study, zirconium encapsulated quaternary chitosan beads (Zr@CSQ) were prepared and used to remove nitrate and phosphate ions from the prepared water. Zr@CSQ beads were identified by a sequence of analytical techniques, including XRD, SEM, EDAX, BET, FTIR, and TGA-DSC analysis. Various kinetic models and known Langmuir, Freundlich, and Dubinin-Radushkovich (D-R) isotherm models have been used to define the isotherm [4]. Revilla

*Corresponding Author: [Ali Mohammadi](mailto:Ali.Mohammadi@srbiau.ac.ir)

Email: ali.mohammadi@srbiau.ac.ir

<https://doi.org/10.24200/amecj.v5.i01.165>

et al Studied the removal of nitrate from aqueous solutions using adsorption-activated biochar from municipal solid waste (MSWAB). Initially, municipal solid waste (MSW), another important source of environmental pollution, was used as a raw material for biochar production, which was activated using potassium hydroxide to produce MSWAB. MSWAB activation increased the level from 2.5 to 6.5 m²/g. Then, the effect of initial nitrate concentration (A), pH (B), and adsorbent dose (C) on nitrate removal was evaluated using a 2K factorial experimental design. The results showed that the initial nitrate concentration, pH, and bilateral interactions of AB and AC have a significant effect on nitrate removal [5]. Liyun Yang et al reported a new modified steel slag for nitrate removal from water. Steel slag (SS) has been used to remove nitrate pollution from the liquid phase. They prepared and activated SS by mixing steel with aluminum hydroxide and deionized water at 800 ° C. The physicochemical properties of steel scrap before and after modification were also investigated to compare the effect of their surface properties on nitrate adsorption behavior, contact time, adsorbent dose effects, and pH effects on it. The results showed that nitrate uptake was significantly increased due to the increase in the specific surface area of the modified waste compared to the unmodified type. They reported the optimal parameters for nitrate removal with this adsorbent: 20 mg L⁻¹ nitrate concentration, 1 g per 100 mL adsorbent, and 180 min residence time in Freundlich adsorption isotherm [6]. In another study, Caterji et al Investigated the uptake of nitrate on bisulfate-modified chitosan seeds. The results showed that cross-link and capacity modification increased uptake compared to conventional chitosan seeds. The maximum absorption capacity relative to the crosslink is 0.4. The maximum modified NaHSO₄ concentration capacity was reported to be 0.1 mM. The maximum nitrate uptake was 104 mg g⁻¹ at pH 5. It also corresponds to the Freundlich isotherm model [7]. Betangar et al used nano-alumina to remove nitrate from water. Their study studied the parameters of contact

time, pH, and nitrate concentration with a pseudo-second-order kinetic model. The highest nitrate removal was observed at a concentration of 4 mg/g, a temperature of 23-27°C, and a pH of 4.4. The Langmuir isotherm model was used to study nitrate uptake. This study showed that nano-adsorbent nanoalumina is useful and effective for the removal of nitrate from aqueous solutions [8]. Morado et al removed nitrate in water with zero-capacity iron and copper/iron nanoparticles. Zero-capacity iron and copper/iron particles in this study were fabricated by reducing sodium bromide at room temperature and atmospheric pressure. The results showed an increase in the rate of nitrate reduction by copper/iron particles so that the residence time of nitrate removal was reduced from 150 minutes to 60 minutes [9]. Hanache et al Developed an anion exchange ZSM-5 nanocatalyst modified with a cationic surfactant. This study showed that the larger the surface area of this nanocatalyst and the smaller the particle size, the higher its adsorption and properties. This modified nanocatalyst has been shown to have a high adsorption capacity and is modified by surfactants. The adsorption kinetics of this system is consistent with the Pseudo-Second isotherm model [10]. Due to the effectiveness of the adsorption method to remove nitrate and the existence of many sources of zeolites in our country, which can act as a suitable substrate for adsorption due to their high porosity and high specific surface area. In this study, the management strategies of nitrate ion removal by interviewing several experts and also the removal of this ion through adsorption by ZSM-5 nano zeolite functionalized with iron and nickel metals will be investigated. Also, in this study, the management methods of ion removal were reviewed and discussed through interviews with active experts in the water and wastewater industry. Several analytical methods such as high-performance liquid chromatography [11] and spectrophotometric [12] have been used for nitrate analysis in waters. The Association of analytical chemists announced that the spectrophotometric method is the favorite determination of Nitrite and Nitrate in waters [13]. The 3D image of nitrate ion

was shown in Figure 1.

Moreover, the metals such as Al, Sn, Zn, Fe, and Ni are effective agents for remediation of contaminated groundwater. Hence the present study was tested based on iron functionalized on ZSM-5 nanozeolite for removal nitrate in waters due to its availability, inexpensiveness, non-toxicity, high efficiency, and rapid reaction in the decomposition of contaminants. In addition, nitrate concentration was determined by the UV-Vis spectrophotometry and the optimal conditions based on effective factors for nitrate removal, including pH, contact time, and adsorbent dosage were evaluated.

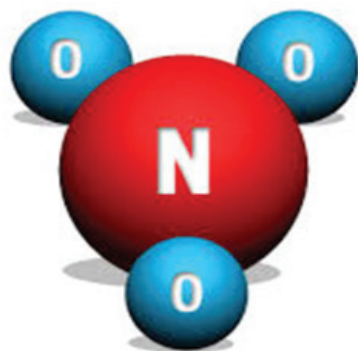


Fig.1. The 3D image of nitrate ion

2. Experimental

2.1. Material

The ZSM-5 nanozeolite powder (from the Zeolites family) was purchased from Sigma Aldrich with a crystal size of 0.5 μm and a pore size of 5.5 \AA . Ferric chloride (FeCl_3), sodium hydroxide (NaOH), potassium nitrate (KNO_3), hydrochloric acid (HCl), and %98 sulfuric acids (H_2SO_4) were also obtained from Merck Germany.

2.2. Characterization

X-ray diffraction (XRD, STADI-P, the USA) was used to investigate ferrous (Fe) metals in the nanozeolite structure functionalized with these metals. Brunauer-Emmett-Teller (BET) surface area analysis (Belsorb apparatus, Japan) was used to determine the SSA of nanozeolite particles. The concentration of nitrate was measured with Spectrophotometer UV-Vis Hach model Dr2800 was used.

2.3. Preparation of ZSM-5/Fe/Ni nanosorbent

To Preparation the functionalized ZSM-5 nanozeolite, the first 2.5 g of ZSM-5 nanozeolite powder was placed in the furnace at a temperature of 500°C for 4 hours and calcined. Then, 0.5 g of ferric chloride (FeCl_3) powder was dissolved in distilled water twice for one hour, added to the calcined ZSM-5 nanozeolite powder and mixed for another 30 minutes, and filtered with a filter paper. The resulting powder was rinsed three times with distilled water and placed in an oven at a temperature of 80°C for 2 hours. Next, the powder was separated from the filter paper and re-calcined at a temperature of 500°C for 4 hours. To produce ZSM-5/Fe/Ni nanozeolite powder, ZSM-5 was first doped with Fe as previously mentioned, and then 0.5 g of nickel sulfate (Ni_2SO_4) powder was dissolved in deionized water for one hour. Next, the calcined ZSM-5/Fe nanozeolite powder was added and stirred for 30 minutes. Afterward, the solution was filtered and the powder was washed three times with distilled water and placed in an oven at a temperature of 80°C for 2 hours. The resulting powder was re-filtered and placed in the furnace at a temperature of 500°C for 4 hours [14].

2.4. Preparation of solutions and procedure

To prepare a standard concentrated potassium nitrate solution, 7 g of anhydrous KNO_3 was dried at 100°C for an hour. After cooling, 1.805 g of KNO_3 was dissolved in a volumetric flask and diluted to 250 ml, thus preparing a standard solution of 1000 mg L^{-1} or 1 mg mL^{-1} . HCl and NaOH solutions were prepared to set the pH values. Then, nitrate solutions with concentrations of 20, 40, 60, 80, 100, and 120 mg per liter were prepared from the standard solution of potassium nitrate 1000 mg L^{-1} [15]. In this research, the experimental design table was first provided using the effective variables of pH, contact time, and stirring speed in the intervals defined to RSM and the central composite design (CCD) by Design Expert.7 software. Then, the value of each parameter was provided according to the experimental design table and finally, the absorbance values or nitrate concentrations in

water samples were measured by the UV-Vis spectrophotometry. A UV-Vis spectrophotometer (Thermo Fisher, GENESYS, 140/150 Vis/UV-Vis Spectrophotometers) was used to collect absorbance data from 190 to 1100 nm. Due to the comparatively low concentrations and absorbance of NO_2^- , all the samples were measured in a 2-4 cm quartz cuvette. DW was used as the reference. The spectral resolution was set as 1-2 nm. A higher resolution (0.3–1 nm) yields similar results. The results were analyzed by experimental design

software, and the optimal values of pH, contact time, and stirring speed were determined.

3. Results and Discussion

3.1. XRD characterization

The XRD spectrum for the ZSM-5/Fe/Ni nanozeolite confirms the presence of iron and nickel particles doped with silicate particles (Fig.2a-2c). The XRD spectrum for the ZSM-5 nanozeolite confirms the silicate particles (Fig.2a) and iron in ZSM-5/Fe (Fig.2b) and iron and nickel in ZSM-5/Fe/Ni (Fig.2c)

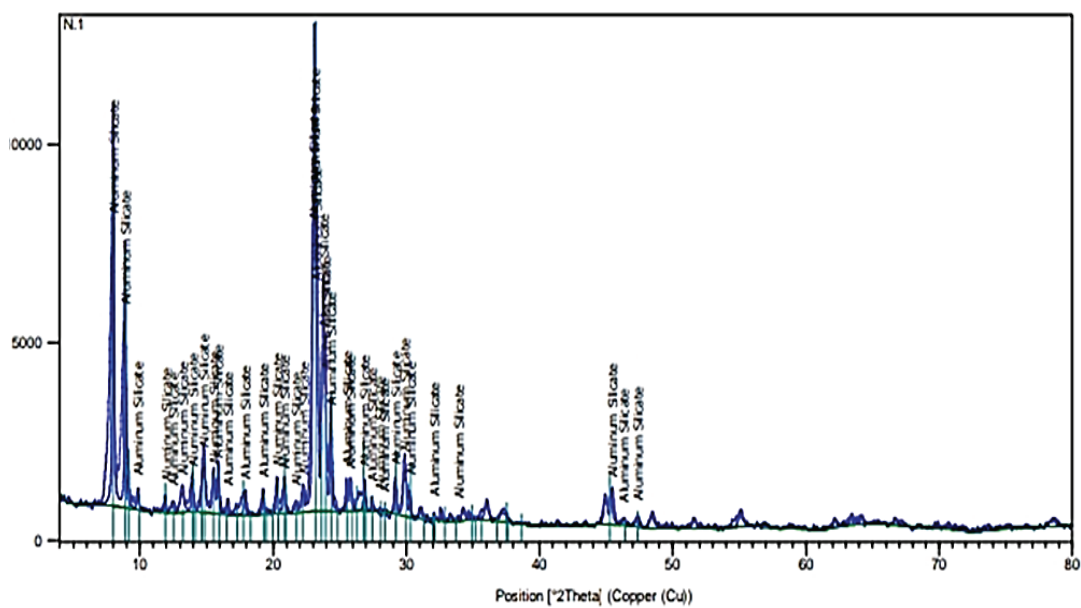


Fig.2a. The XRD spectrum for ZSM-5

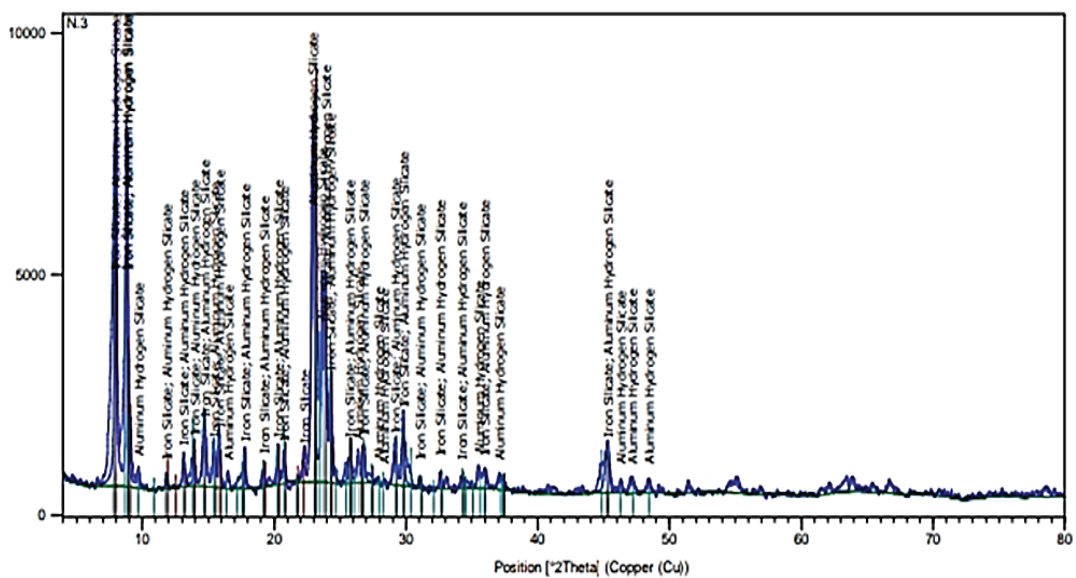


Fig. 2b. The XRD spectrum for ZSM-5/Fe

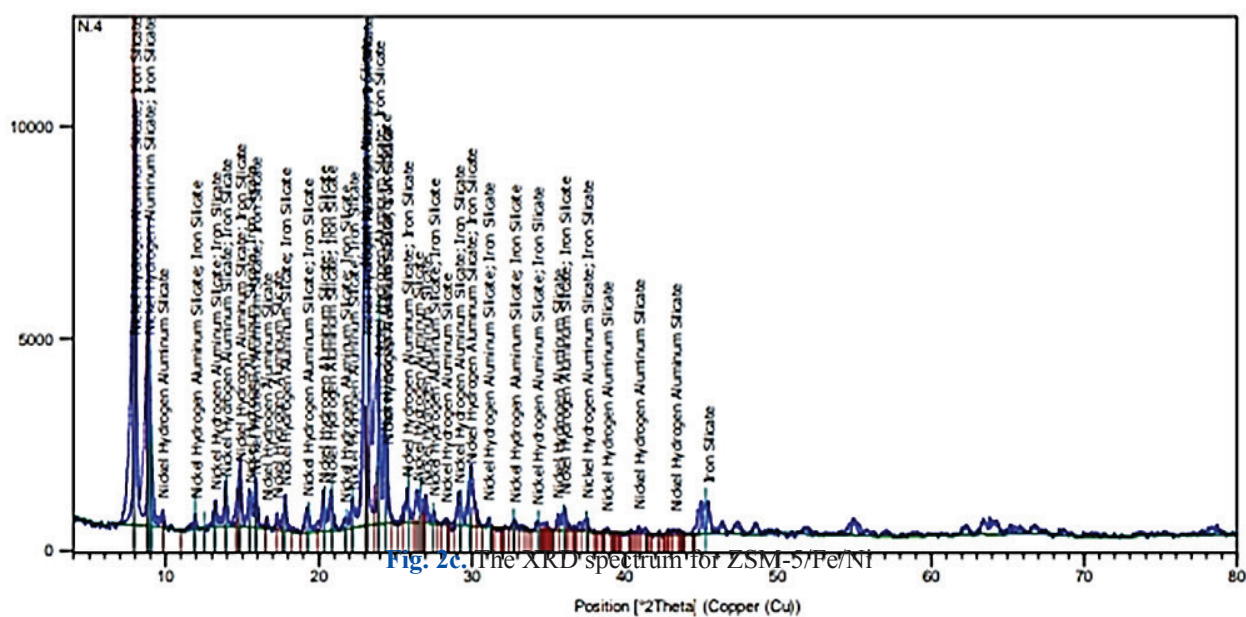
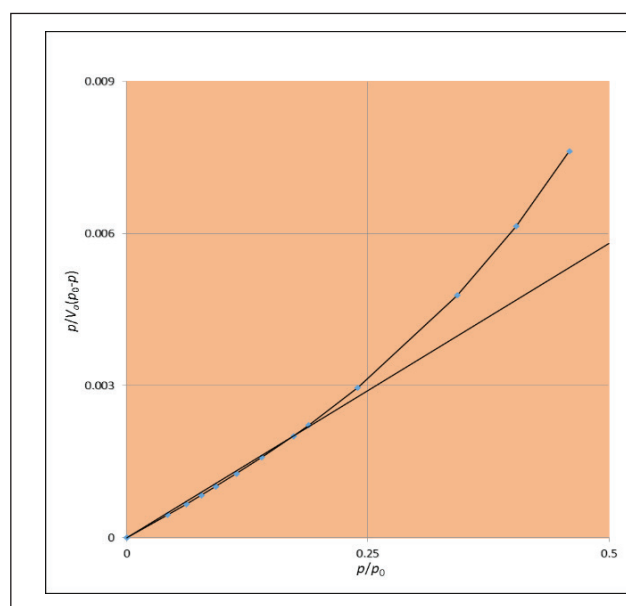


Fig. 2c. The XRD spectrum for ZSM-5/Fe/Ni

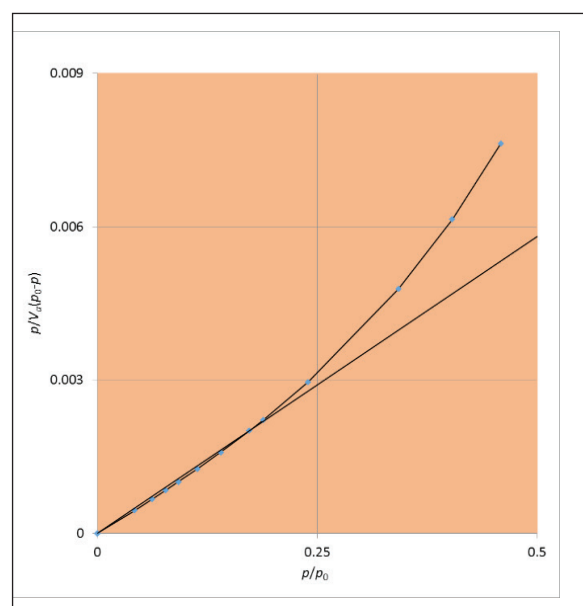
3.2. BET characterization

By comparing the BET parameter as in Figure 3 and Table 1. In each of the four BET analysis curves of the nanozeolite, the highest SSA was

related to the zeolite functionalized with Fe and Ni metal (ZSM-5/Fe/Ni, which was determined to be $418.76 \text{ m}^2 \text{ g}^{-1}$).



ZSM-5



ZSM-5/Fe/Ni

Fig. 3. BET curves of the prepared nanosorbent.

Table 1. The specific surface area of the prepared nanozeolite

Row	Nanocatalysts	BET	Unit
1	ZSM-5	374/66	m ² g ⁻¹
2	ZSM-5/Fe/Ni	418/76	m ² g ⁻¹

3.3. Optimization and experimental design

In this research, the experimental design using RSM in combination with the CCD method was performed to investigate the effects of influential variables of pH (range: 2-8) (A), contact time (30-180 minutes) (B), and adsorbent dosage (1-5 g L⁻¹) (C) on nitrate removal efficiency. Due to the extensive use of research on (A), (B), and (C) parameters for the nitrate removal process, these parameters as effective factors were used for optimizing nitrate removal [16-17]. The RSM method is a mathematical and statistical method used for the analysis and empirical modeling of problems where a given answer is influenced by several variables and the RSM can be calculated to determine the optimal conditions. One advantage of this method is to reduce the number of empirical tests which was performed to obtain statistically valid results. In addition, the RSM method can also analyze the interactions between variables. By optimizing parameters, the result can report more comprehensive and accurate data by performing the least number of experiments [18-19]. In this study, Table 2 showed the range of independent variables and design levels of the experiments examined. The results of the complete design of the test and the exact responses of the tests used are also listed in Table 3.

According to the results of the data analysis in Table 4, a quadratic function model can fit well to the empirical results. The fit of this model was evaluated by Analysis of Variance (ANOVA),

normal probability plot, and residual analysis. The quadratic function for nitrate removal efficiency is expressed as follows:

$$\begin{aligned} \% \text{ Removal Nitrate} = & 51.29 - (10.17 \times A) + (4.13 \times B) - (3.51 \times C) + (11.69 \times D) + (5.16 \times A \times B) + (3.69 \times A \times C) - (0.056 \times A \times D) + (2.84 \times B \times C) + 5.59 \times B \times D - (2.43 \times C \times D) + (0.47 \times A^2) + (0.83 \times B^2) + (2.81 \times C^2) - (1.28 \times D^2) \end{aligned}$$

In Table 4, the ANOVA analysis showed the importance of each parameter in response to nitrate removal by P and F values. The smaller the P-value, the higher its impact factor and its contribution to the response variable. The P values less than 0.05 indicate that the model expressions are significant. The P values of more than 0.1 indicate that the model terms are insignificant. Accordingly, the seven terms of (AC), (BD), and (C²) are significant parameters of the model and have the greatest effect on nitrate removal efficiency. The P values of the other terms were greater than 0.05, which means that their effect on the response model was not statistically significant.

Figure 4 shows the residual curve in terms of the predicted response for the response of nitrate removal efficiency. This Figure shows that all empirical data are uniformly distributed around the mean response variable. This indicates that the proposed model is sufficient and there has

Table 2. Factors and levels for CCD study

Level	pH	Temperature	Time
-α	-22.4874	-4.31981	-13.7046
-1	3	5	1
+1	8	50	72
+α	472.487	59.3198	86.7046

Table 3. Experimental range and values of different variables studied.

standard	Run	Block	pH	Time (Min)	Nitrate (mg L ⁻¹)	Absorbent (g L ⁻¹)	%Removal Nitrate(mg L ⁻¹)
5	1	Block 1	7	60	40	4	46.62
7	2	Block 1	3	150	100	4	78.11
11	3	Block 1	5	105	70	3	51.42
8	4	Block 1	3	60	40	2	68.27
12	5	Block 1	5	105	70	3	51.19
1	6	Block 1	7	150	100	2	43.28
10	7	Block 1	5	105	70	3	49.41
3	8	Block 1	7	60	100	4	39.56
9	9	Block 1	5	105	70	3	54.12
6	10	Block 1	3	60	100	2	58.34
2	11	Block 1	7	150	40	2	30.47
4	12	Block 1	3	150	40	4	91.51
14	13	Block 2	8	105	70	3	29.19
17	14	Block 2	5	105	20	3	60.73
20	15	Block 2	5	105	70	5	57.16
22	16	Block 2	5	105	70	3	50.92
21	17	Block 2	5	105	70	3	51.69
15	18	Block 2	5	30	70	3	37.48
18	19	Block 2	5	105	120	3	45.33
13	20	Block 2	2	105	70	3	67.11
19	21	Block 2	5	105	70	1	18.81
16	22	Block 2	5	180	70	3	58.25

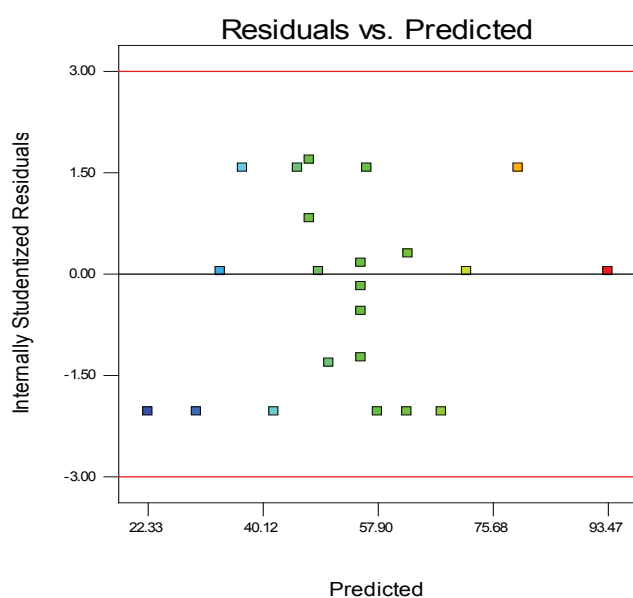
**Fig. 4.** The residual value curve in terms of the predicted response

Table 4. Experimental design and actual results of nitrate removal efficiency.

Source	Sum of Squares	dF	Mean Square	F Value	p-value Prob > F
Block	346.13	1	369.12		
Model	5119.11	13	331.08	18.81	0.0007 <i>significant</i>
A-pH	714.14	1	713.46	35.61	0.0007
B-Time	121.42	1	121.29	6.59	0.0354
C-gr nitrate	176.02	1	176.14	11.41	0.0181
D-gr adsorbent	809.74	1	783.41	42.12	0.0005
AB	94.18	1	95.13	4.26	0.0576
AC	105.00	1	106.63	5.09	0.0413
AD	0.011	1	0.011	6.417E-004	0.9563
BC	73.61	1	66.57	3.94	0.0791
BD	107.46	1	103.34	7.16	0.0465
CD	62.52	1	58.49	2.83	0.1017
A ²	3.93	1	3.83	0.62	0.6173
B ²	13.17	1	13.41	0.51	0.4019
C ²	157.63	1	162.83	7.68	0.0238
D ²	43.08	1	47.19	2.36	0.1609
Residual	105.38	5	19.04		
Lack of Fit	83.59	3	40.56	8.17	0.0381 <i>significant</i>
Pure Error	18.53	3	4.69		
Cor Total	5568.06	23			

been no deviation from the hypotheses made. As can be seen in Table 5, the difference between the adjusted R² and the predicted R² is less than 0.2 and the precision of the model is 19.461 (which is greater than 4), indicating the used model is accurate.

Figure 5 shows a comparison between the actual response values obtained from the empirical

results and the predicted response values obtained from the quadratic function model equation. It is observed that the model describes the empirical results and data fairly accurately, meaning that it has been successful in comparing the correlations between the three variables. In addition, there is a sufficient correlation with the linear regression coinciding with the R-value of about 0.94612.

Table 5. Model equation statistical parameters for ANOVA model for nitrate removal efficiency

Type of variables	Value
Std. Dev.	3.79
R-Squared	0.94612
Mean	51.14
Adj R-Square	0.9056
C.V. %	7.18
Pred R-Squared	-3.0346
PRESS	25147.62
Adeq Precision	19.461

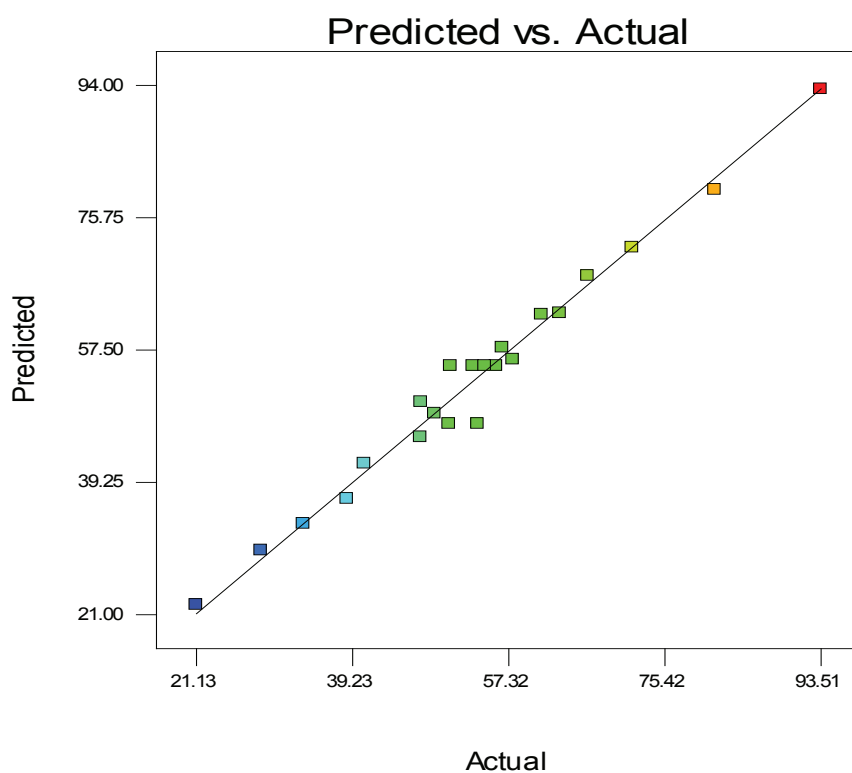
**Fig. 5.** Comparison between predicted and actual empirical values of nitrate removal efficiency.

Figure 6 shows the three-dimensional interaction curves of contact time, pH, adsorbent dosage, and initial nitrate concentration for nitrate removal efficiency. The highest nitrate removal efficiency was reported at the contact time of 150 min, pH

value of 3, an adsorbent dosage of 4 g L^{-1} and an initial concentration of 40 mg L^{-1} . Analysis of the diagrams in Figure 6 revealed higher nitrate removal efficiency at lower pH values and longer contact times.

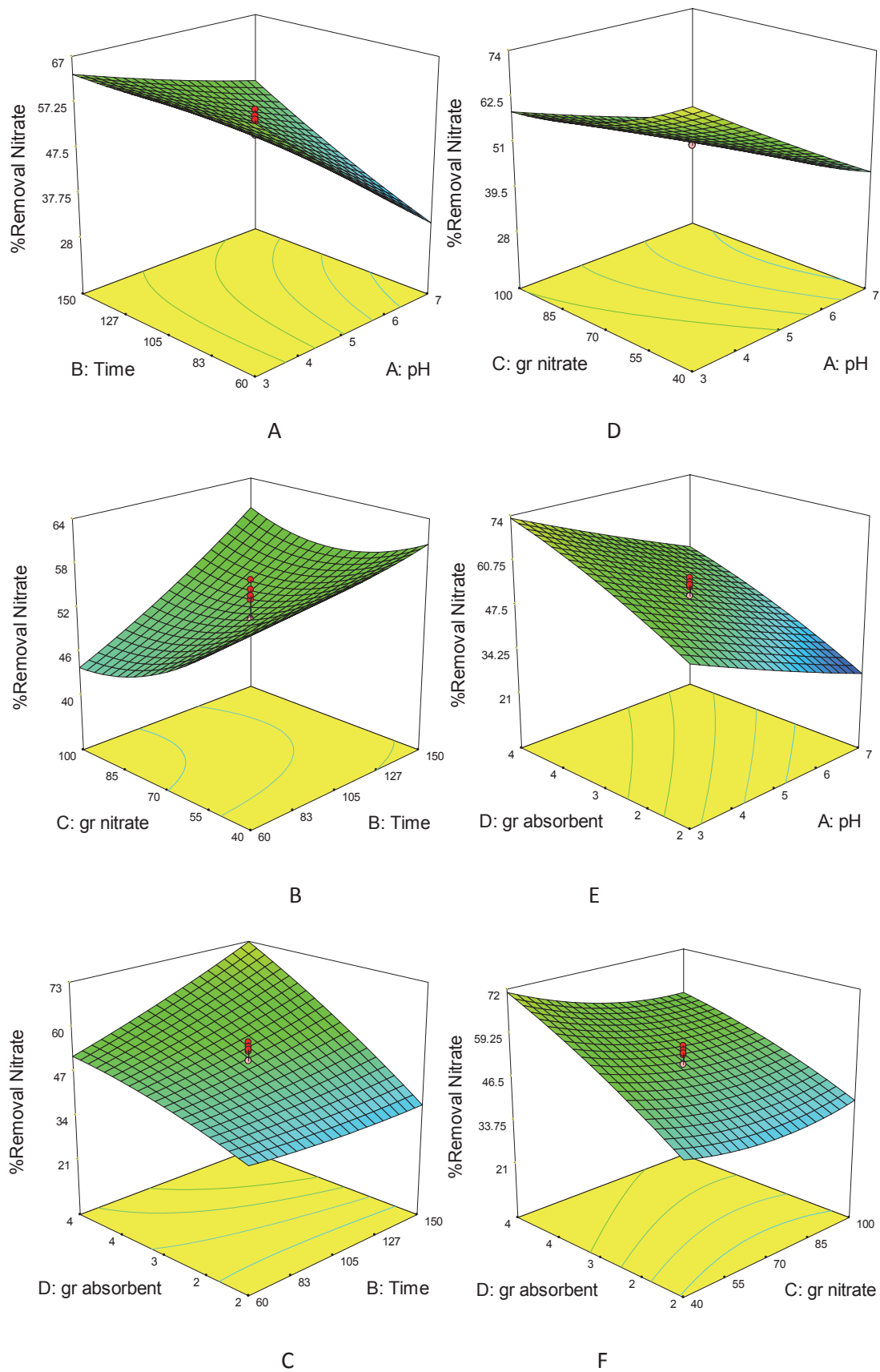


Fig. 6. 3D response surface method curves of nitrate removal efficiency

4. Management

According to the interviews conducted with active experts in the water and wastewater industry, the following items can be suggested as management strategies to remove and monitor nitrate ions from the source. According to the survey and statistical analysis of the interviewees, the highest amount of suggestions was related to the use of new technologies and nanosorbents (%85). Also, this procedure can be suggested as a management strategy to remove and monitor nitrate ions from the source. According to the survey and statistical analysis (Fig. 7 and Table 6), the highest number of suggestions was related to using new technologies and nanosorbents (%85).

*Identification of nitrate pollution-producing industries through sampling and testing

*Continuous instantaneous monitoring of effluents of different industries

*Establishment of nitrification unit in the effluent reservoirs of petrochemical industries and use of expert experts to manage it

*Transfer of effluent to the central treatment plant of industrial sites for re-treatment

*Designing the capacity of the central treatment plant in proportion to the amount of input and pollution of petrochemical units in the region to apply the conditions of complete nitrification

*Perform frequent inspections of various industries

*Prevent the activity of polluting industries

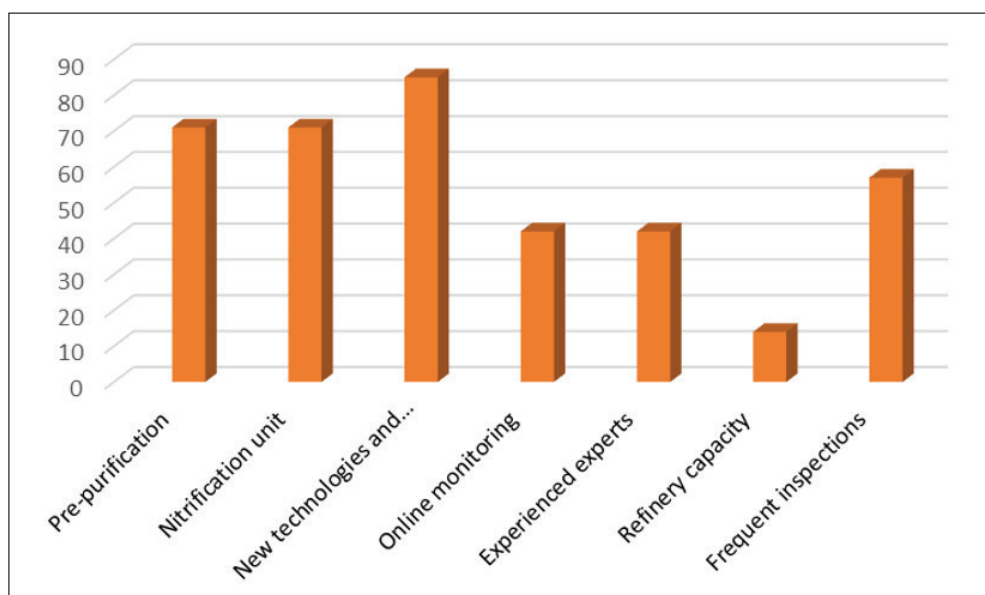


Fig.7. The percentage of importance of the proposed solutions of the interviewees to remove nitrate

Table 6. Percentage of the importance of the proposed solutions of the interviewees to remove nitrate

Cases	Percentage
Pre-purification	71
Nitrification unit	71
New technologies and nanosorbent materials	85
Online monitoring	42
Experienced experts	42
Refinery capacity	14
Frequent inspections	57

5. Conclusions

This study showed that the use of chemical fertilizers, lack of control of wastewater, including municipal, industrial, especially wastewater from food production plants and animal waste, and the entry of treatment plant effluents without applying the nitrification process are important sources of mixing nitrate with groundwater. It can be controlled by the following management methods. It can be eliminated by various executive methods such as adsorption, ion exchange, reverse osmosis, chemical and biological methods such as thermal hydrolysis, solar photocatalysis, and microbial fuel cells. According to the results of the analysis of three-dimensional diagrams, the highest nitrate removal efficiency (91.51%) was reported at a residence time of 150 minutes, pH 3 and 4 g L⁻¹ of sorbent, and 40 mg L⁻¹ nitrate which indicates the high efficiency and effectiveness of this nanosorbent in nitrate removal. Therefore, nanosorbent (ZSM-5 /Fe/ Ni) can be introduced as a promising adsorbent to remove nitrate from effluents. As compared to other studies, this nanosorbent is cheaper due to its abundance in the soils of our country, and in most cases, has a higher efficiency than others in removing nitrate. Another advantage of the proposed method is to use of the experimental design method with Design Expert.7 software, which will reduce the number of experiments performed by statistical and software methods. By procedure, the use of materials and nanosorbents was greatly reduced. The main difference and advantage of ZSM-5 /Fe/ Ni nanosorbents with other adsorbents is completely green and environmentally friendly. Another advantage of the present study is the management methods for removing this ion through interviews and the presentation of management solutions.

6. Suggestions

Due to the widespread use of nanozeolites as adsorbents for nitrate, nitrite, and heavy metals from aqueous media in various articles, it can be used in future research for the removal of heavy metals in waters.

7. Acknowledgments

The authors would like to thank and appreciate Dr. Mostafa Hassani.

8. References

- [1] T. Meftah, M. M. Zerafat, Nitrate removal from drinking water using organo-silane modified natural nano-zeolite, *Int. J. Nanosci. Nanotechnol.*, 12 (2016) 223-232. http://www.ijnnonline.net/article_22931.html
- [2] B. Kamarehie, E. Aghaali, SA. Musavi, SY. Hashemi, A. Jafari, Nitrate removal from aqueous solutions using granular activated carbon modified with Iron nanoparticles, *Int. J. Eng., Transactions A: Basics*, 31 (2018) 554-563. <https://doi.org/10.5829/ije.2018.31.04a.06>
- [3] M. Mazarji, B. Aminzadeh, M. Baghdadi, A. Bhatnagar, Removal of nitrate from aqueous solution using modified granular activated carbon, *J. Mol. Liq.*, 233 (2017) 139-148. <https://doi.org/10.1016/j.molliq.2017.03.004>
- [4] P. Revilla, M. Detras, V. Migo, C. Alfafara, Nitrate removal from aqueous solution by adsorption using municipal solid waste-derived activated biochar, *IOP Conference Series: Mater. Sci. Eng.*, 778 (2020) 012135. <https://doi.org/10.1088/1757-899X/778/1/012135>.
- [5] H.A.T. Banu, P. Karthikeyan, S. Meenakshi, Removal of nitrate and phosphate ions from aqueous solution using zirconium encapsulated chitosan quaternized beads: Preparation, characterization and mechanistic performance, *Results Surf. Interfaces*, 3 (2021) 100010. <https://doi.org/10.1016/j.rsurfi.2021.100010>
- [6] L. Yang, M. Yang, P. Xu, X. Zhao, Characteristics of nitrate removal from aqueous solution by modified steel slag, *Water*, 9 (2017) 757-774. <https://doi.org/10.3390/w9100757>
- [7] S. Chatterjee, D. Lee, S. Lee, M.S. Woo, Nitrate removal from aqueous solutions by cross-linked chitosan beads conditioned

- with sodium bisulfate, *J. Hazard. Mater.*, 166 (2009) 508-513. <https://doi/10.1016/j.jhazmat.2008.11.045>
- [8] A. Bhatnagar, E. Kumar, M. Sillanpää, Nitrate removal from water by nano-alumina: characterization and sorption studies, *Chem. Eng. J.*, 163 (2010) 317–323. <https://doi/10.1016/j.cej.2010.08.008>
- [9] G. Muradova, S. Gadjeva, L. Di Palma, Nitrates removal by bimetallic nanoparticles in water, *Chem. Eng. Trans.*, 47 (2016) 205-210. <https://doi/10.3303/CET1647035>
- [10] L.E. Hanache, L. Sundermann, B. Lebeau, J. Toufaily, T. Hamieh, T.J. Daou, Surfactant-modified MFI-type nanozeolites: Super-adsorbents for nitrate removal from contaminated water, *Micropor. Mesopor. Mater.*, 283 (2019) 1–13. <https://doi/10.1016/j.micromeso.2019.03.049>
- [11] A. Najdenkoska, Development of HPLC method for analysis of nitrite and nitrate in vegetable, *J. Agricultural Food Environ. Sci.*, 67 (2016), 33-39. <https://core.ac.uk/download/pdf/287304048.pdf>
- [12] V. Kmecl, T. Knap, D. Žnidarčič, Evaluation of the nitrate and nitrite content of vegetables commonly grown in Slovenia, *Italian J. Agronomy*, 12 (2017). 79-84. <https://doi.org/10.4081/ija.2017.801>
- [13] Association of official analytical chemists, guidelines for single laboratory validation of chemical methods for dietary supplements and botanicals, Association of official analytical chemists international, Maryland, 2002. <https://pdf4pro.com/view/aoac-guidelines-for-single-laboratory-5b9252.html>
- [14] M. Hassani, M. Zeeb, A. Monzavi, Z. Khodadadi, M. Kalae, Adsorption of nitrate from aqueous solution with ZSM-5/Fe nanosorbent based on optimizing of the isotherms conditions before determination by UV-Vis Spectrophotometry, *Anal. Methods Environ. Chem. J.*, 4 (2021) 49-63. <https://doi.org/10.24200/amecj.v4.i04.154>
- [15] M. Hassani, M. Zeeb, A. Monzavi, Z. Khodadadi, M. Kalae, Response surface modeling and optimization of microbial fuel cells with surface-modified graphite anode electrode by ZSM-5 nanocatalyst functionalized, *Chem. Methodol.*, 6 (2021) 253-268. <https://doi.org/10.22034/CHEMM.2022.324312.1425>
- [16] J. Rodríguez-Maroto, F. García-Herruzo, A. García-Rubio, C. Gómez-Lahoz, C. Vereda-Alonso, Kinetics of the chemical reduction of nitrate by zero-valent iron, *Chemosphere*, 74 (2009) 804-809. <https://doi/10.1016/j.chemosphere.2008.10.020>
- [17] S. Sepehri, M. Heidarpour, J. Abedi-Koupai, Nitrate removal from aqueous solution using natural zeolite-supported zero-valent iron nanoparticles, *Soil Water Res.*, 9 (2014) 224–232. <https://doi.org/10.17221/11/2014-SWR>
- [18] B.W. Chieng, N. A. Ibrahim, Department of optimization of tensile strength of poly(Lactic Acid)/graphene nanocomposites using response surface methodology, *Polymer-Plastics Technol. Eng.*, 51 (2012) 791–799. <https://doi/10.1080/03602559.2012.663043>.
- [19] Q. Zhang, G. Liu, L. Wang, X. Zhang, G. Li, Controllable decomposition of methanol for active fuel cooling technology, *Energy Fuels*, 28 (2014) 4431–4439. <http://doi.org/10.1021/ef500668q>.



Measurement of heavy metals in soil, plants and water samples based on multi-walled carbon nanotube modified with Bis(triethoxysilylpropyl)tetrasulfide by flame atomic absorption spectrophotometry

Mohammad Reza Rezaei Kahkha^a, Ahmad Salarifar^{b,*}, Batool Rezaei Kahkha^a

^a Department of Health Engineering, Zabol University of Medical Sciences, Zabol, Iran.

^b Environmental Engineering Department, Faculty of Natural Resources, Islamic Azad University, Bandar Abbas Branch, Iran

ARTICLE INFO:

Received 17 Nov 2021

Revised form 23 Jan 2022

Accepted 12 Feb 2022

Available online 28 Mar 2022

Keywords:

Heavy Metals,
Environment sample,
Bis(triethoxysilylpropyl)tetrasulfide,
Uniform dispersive -micro-solid phase extraction,
Flame atomic absorption spectrophotometer

ABSTRACT

Heavy metals (HMs) are considered as the major environmental pollutants that accumulated in soil and plant. Consumption of such contaminated plants by humans and animals would ultimately harm the health of communities. This study aims to evaluate the amount of copper(Co), cadmium(Cd), and lead(Pb) in soil and cultivated plants that are irrigated by the city of Zabol's wastewater. Also, the heavy metals determined in 20 mL of Zabol's water based on Bis(triethoxysilylpropyl)tetrasulfide ($S_4[C_3H_6Si(OEt)_3]_2$, TEOSiP-TS) modified on MWCNTs as an adsorbent by the uniform dispersive -micro-solid phase extraction (UD- μ -SPE) at optimized pH. In this study, 52 samples including wheat, corn grain, and wild spinach, as well as agricultural soil were selected randomly from three village stations. The concentrations of heavy metals in plants, soils, and water samples were measured using a flame atomic absorption spectrometer (F-AAS). The one-way ANOVA test was applied to compare the mean value of heavy metals at the three mentioned stations. The results indicate that the amount of lead at all three stations and in all types of plants exceeds the permissible range. The amount of copper in plant species and water is lower than the permitted range, while it is higher in agricultural soil. By optimizing parameters, the linear range (LR) and the detection limit (LOD) of Cu, Cd, and Pb were obtained $1.5-1000 \mu\text{g L}^{-1}$, $1-200 \mu\text{g L}^{-1}$, $5-1500 \mu\text{g L}^{-1}$ and $0.5 \mu\text{g L}^{-1}$, $0.25 \mu\text{g L}^{-1}$, $1.5 \mu\text{g L}^{-1}$, respectively in water samples ($RSD\% < 2$). This study indicates that irrigation of agricultural fields using wastewater causes the accumulation of heavy metals in soil and plants.

1. Introduction

Heavy metals(HMs) as hazardous elements, caused by human activities in different sections of industry, agriculture, and business. It has been discharged for years into the ecosystem and has polluted water, soil, and agricultural farms. Also,

heavy metals have endangered the health of humans and other creatures [1]. Heavy metals enter the environment on a large scale through natural and human-made resources. The releasing amount of heavy metals to the environment is considerable [2]. The first influencing element of metal pollution in an ecosystem is the existence of heavy metals in the biomass of polluted areas which endangers human health. One of the most fundamental issues,

*Corresponding Author: [Ahmad Salarifar](mailto:Ahmad.Salarifar)

Email: salarifar562@gmail.com

<https://doi.org/10.24200/amecj.v5.i01.167>

in terms of heavy metals, is that body does not metabolize them [3]. This would cause several diseases and complications in the body. In general, neurological disorders (Parkinson's, Alzheimer's, depression, schizophrenia), various cancers, nutrient deficiency, and hormones imbalance are the results of heavy metals amass in the human body [4]. Some analytical techniques were used for the measurement of HMs in environmental samples such as atomic absorption spectrophotometry [5,6], laser-induced breakdown spectroscopy [7], X-ray fluorescence spectroscopy [8], and electrochemical methods [9]. Among these techniques, atomic absorption spectrophotometry has a very advantages such as simplicity, effectiveness, reliability, and low detection limit [10]. Zabol's urban wastewater is used in some villages to irrigate agricultural farms at the time of drought. In this study, to evaluate the amount of heavy metals lead, copper, and cadmium in agricultural soil and cultivated plants, such as wheat, corn, and a species of wild spinach, which are irrigated with wastewater, three stations were selected in which the irrigation of agricultural fields with wastewater is common. After wheat sampling and given that most of the planted wheat used to feed livestock in late winter or early spring is immature, the root of the plant was separated and all methods of sample preparation were applied to analyze the plant, without considering other parts of it. A similar approach was applied to grain corn. Wild spinach is a volunteer plant in wheat fields, and as it is used widely in the Sistan region for the purpose of cooking a type of local food during fall and winter, it was sampled from mentioned stations in order to evaluate the heavy metals accumulation. Recently, many adsorbents such as graphene/graphene oxide [11], CNT [12], activated carbon [13], and silica pours [14] were used for extraction HMs in water samples. Also functionalized nanocarbon structures were also reported for extraction heavy metals in water, plant and soil samples [15]. In addition, the different technology such as, liquid-liquid extraction [16], dispersive ionic liquid-liquid extraction [17], dispersive micro solid-phase extraction [18], and

magnetic solid phase extraction were presented for water samples. In this study, the plants and soil samples were analyzed with F-AAS after sample digestion procedure and water samples determined after sample preparation method based on TEOSiP-TS@MWCNTs adsorbent by the UD- μ -SPE procedure.

2. Materials and Methods

2.1. Sampling and reagents

This research is conducted to evaluate the number of heavy metals such as lead, copper, and cadmium in three different types of plants, i.e. wheat, corn, and spinach, as well as in agricultural soil of selected fields. Given that use of wastewater in irrigation is performed in only three stations of Zabol in the east of Iran, and taking the extent of farmland areas, in total 52 samples were selected from all stations. Samples were randomly collected in June 2020 and February 2021. The water sample was prepared from Zabol by a clean glassy tube (100 mL) which was acidified with HNO₃ (2%) and filtered by Whatman filter Sigma, Germany (200 nm) by ASTM method for sampling of waters. The calibration of copper(Co), cadmium(Cd), and lead(Pb) in soil, cultivated plants, and water solution was prepared daily by appropriate Co(II), Cd(II), and Pb(II) stock solution (1000 mg L⁻¹) in Deionized water (DW, Millipore, USA) which was purchased from Sigma, Germany. The acid solutions such as HCl, H₂SO₄, and HNO₃ were purchased from Sigma, Germany. The bis(triethoxysilylpropyl)tetrasulfide (S₄[C₃H₆Si(OEt)₃]₂, TEOSiP-TS, CAS N:40372-72-3) was purchased from Merck, Germany.

2.2. Synthesis of Adsorbent

The modification of the Bis(triethoxysilylpropyl) tetrasulfide (S₄[C₃H₆Si(OEt)₃]₂, TEOSiP-TS) on the surface of MWCNTs nanostructure has shown in Figure 1. By the acid treatment methods (HNO₃ & H₂SO₄), the carboxylic acid-functionalized MWCNTs (MWCNTs-COOH) were synthesized based on previously reported papers [19]. By reducing the COOH to the OH groups, MWCNTs@

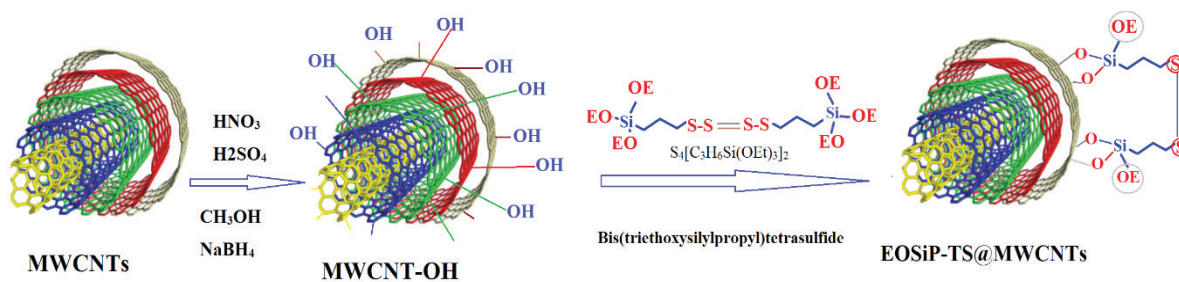


Fig. 1. Synthesis of EOSiP-TS@MWCNTs adsorbent by the Bis(triethoxysilylpropyl)tetrasulfide

OH created. By stirring, 5 g of MWCNTs-COOH mixed with 0.5 g of NaBH_4 and CH_3OH in a 100 mL flask condenser. Then, the mixture was refluxed for 3 h and then it was cooled in room temperature after 2 h. Finally, the MWCNTs-OH nanomaterials were filtered with a Whatman filter and washed many times with the methanol/DW. For the synthesis of the EOSiP-TS@MWCNTs adsorbent, 2 g of MWCNTs-OH were added to a solution of Bis(triethoxysilylpropyl)tetrasulfide (TEOSiP-TS) in presence of toluene in a 100 ml round-bottom flask equipped with magnetic stirring, and then the mixture was heated at 80°C for 3.5 h by Ar gas. Finally, the TEOSiP-TS @ MWCNTs product was filtered with a Whatman filter.

2.3. Sample preparation

Soil samples were collected from the depth of 2 cm. Polyethylene sampling containers were initially washed with detergent powder and then kept in a container containing 5% nitric acid for a certain period (acid washing). Then, it was rinsed with ionized water. Plant samples were collected inside polyethylene bags, then transferred to the laboratory, and after that completely washed with three-time distilled water to eliminate potential pollutions.

Afterward, the samples were dried up at room temperature. Dried samples were milled and completely crushed and then passed through a sieve with a pore diameter of approximately 0.5 mm. The milled plant samples were placed inside clean glass containers and were dried again at 65°C

for 24 hours. For digestion of plant sample, 2g of milled dried samples were placed inside a round-bottom flask, and then concentrated perchloric acid (4ml), concentrated sulphuric acid (2ml), and concentrated nitric acid (20ml) were added, respectively. The above solution was heated to boil carefully under a hood and over a heater to reduce its volume. In the next step, 20ml water was added to dissolve the sediments, and heated up again to reduce their volume. Afterward, the solution was filtered and its volume was reduced to 250ml. Soil samples were completely oven-dried for 24 hours in the laboratory at 70°C . In the next stage, they were sieved and milled to obtain a completely smooth powder. 0.5 g of the above sample was prepared to be injected into the device, using the complete digestion method [20-22]. After digestion, all samples were analyzed with F-AAS.

2.4. Analytical measurement

Flame atomic absorption spectroscopy (F-AAS, Agilent 55B-AA) was used to measure all elements in the sample. To obtain the required sensitivity in measurements, air/acetylene flame was applied. In order to ensure the accuracy of evaluation, each measurement was performed three times on each sample, and standard deviation and mean of data were obtained. One-way analysis of variance was used to compare the average heavy metals content in various types of selected plants at those three stations. The instrumental conditions for the determination of Cu, Pb, and Cd by F-AAS have explained in Table 1.

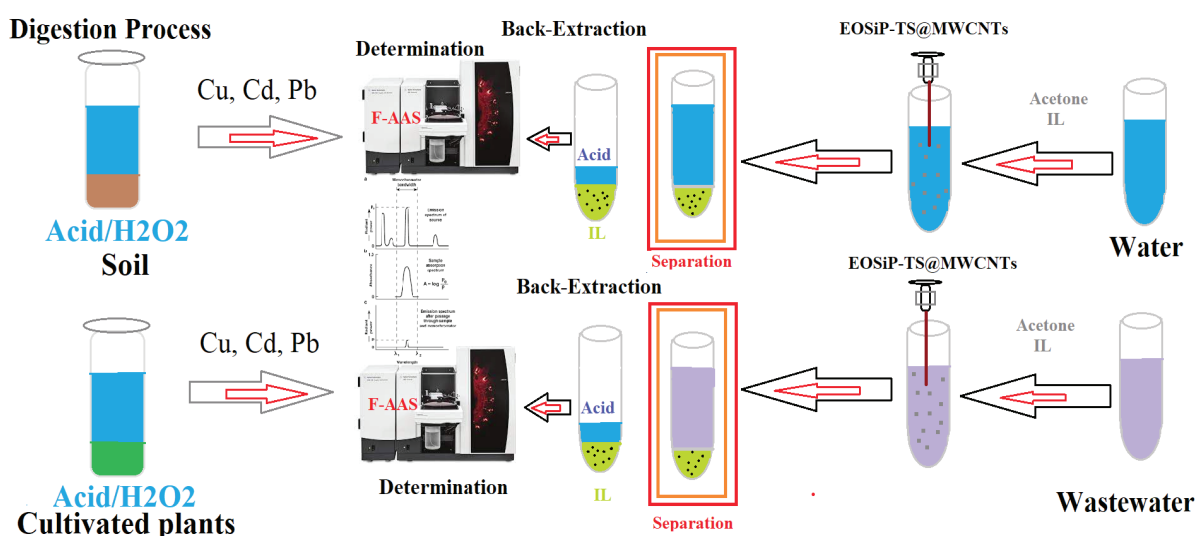
Table 1. The instrument conditions for determination Cu, Pb, and Cd ions by F-AAS

Metal	Lamp current	Fuel	Wavelength (nm)	Slit Width (nm)	Working Range ($\mu\text{g/mL}$)
Copper	4.0	Air- acetylene	324.7	0.5	0.03-10
			327.4	0.2	0.1-24
			217.9	0.2	0.2-60
Lead	5.0	Air- acetylene	217.0	1.0	0.1–30
			283.3	0.5	0.5–50
			261.4	0.5	5–800
Cadmium	4.0	Air- acetylene	228.8	0.5	0.02–3
			326.1	0.5	20-1000

2.5. General Procedure

The plant and soil samples were digested with acid solutions and after dilution with DW, the Cu, Pb, and Cd ions were determined with F-AAS. On the other hand, by the UD- μ -SPE method, 20 mL of water samples were used for the separation and extraction of the Cu, Pb, and Cd ions at pH 6-6.5. In this procedure, 20 mg of EOSiP-TS@MWCNTs adsorbent dispersed to a mixture of ionic liquid ([HMIM][PF₆], 50 mg) and acetone (250 μL). The mixture was rapidly injected into 20 mL of water and standard solution (5-200 $\mu\text{g L}^{-1}$) at pH \approx 6. After ultrasonic for 5.0 min, the Cu, Pb, and Cd ions were chemically adsorbed by four sulfur groups of EOSiP-TS@MWCNTs ([Cu, Cd, Pb]⁺²→[: S-S-

EOSiP]). By procedure, the Cu⁺², Cd²⁺, Pb⁺² ions were extracted by coordination of dative bond of sulfur at pH= 6.5. At high pH of more than 7.5, Cu⁺², Cd²⁺, Pb⁺² ions converted to Cu(OH)₂, Pb(OH)₂, Cd(OH)₂ and precipitated (Recovery of extraction: 65%, 57%, 36%). Finally, the Cu⁺², Cd²⁺, Pb⁺² ions were extracted from waters by a dative bond of S-S and trapped on the IL phase. Then, the IL/ EOSiP-TS@MWCNTs phase was collected by centrifuging for 5 min at 3500 rpm and settled down in the bottom of the conical tube. After back extraction of Cu⁺², Cd²⁺, Pb⁺² ions, the resulting solution was determined by FAAS after dilution up to 1 mL with DW (Fig. 2).

**Fig. 2.** General procedure for determination Ions in the plant, soil, and, water sample

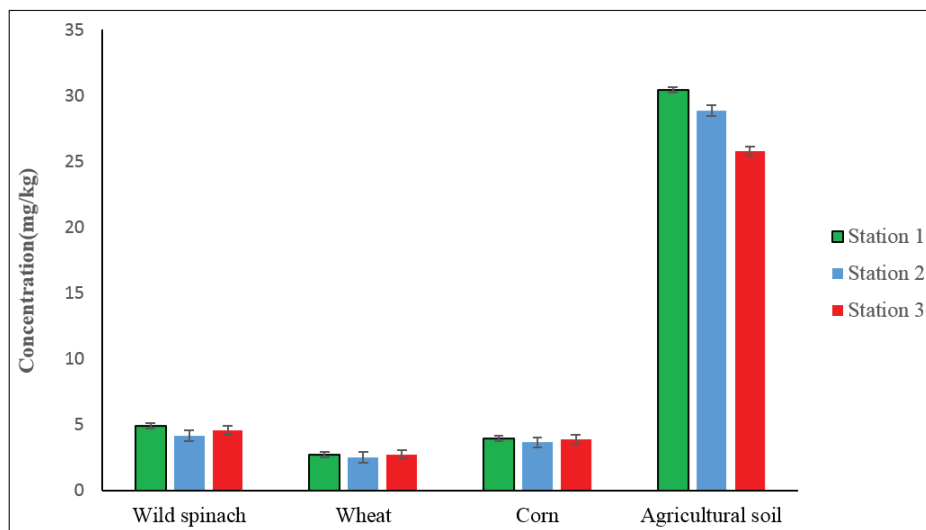


Fig. 3. The concentration of lead in plants and soil in selected stations.

3. Results and Discussion

3.1. Evaluation of Lead in plant and soil

Figure 3 represents that the amount of lead in wild spinach in three stations is above the permissible level for human consumption (2 mg kg^{-1}). While; it is within the normal range for plants ($0.1\text{-}10 \text{ mg kg}^{-1}$). In addition, the concentration of this metal in agricultural soil of all areas is above its permissible range (10 mg kg^{-1}). The statistical analysis was done using SPSS 19 and ANOVA. The findings showed that there is a significant difference between lead concentration in selected areas ($P 7.13 > 4.1$), where the confidence level is 95% and the significance level is less than 0.05.

3.2. Evaluation of Cadmium in plant and soil

Figure 4 indicates that the concentration of cadmium in wild spinach at all three stations is close to the borderline of the permissible range. By increasing in irrigation of wastewater, the cadmium concentration in the plant increased a little. The level of cadmium in wheat and grain corn is lower than the detection limit of the atomic absorption spectrophotometer and therefore not mentioned in Figure 4. The agricultural soil has high level of cadmium. The ANOVA analysis of results indicated that at a confidence level of 95% and a significance level of lower than 0.05, ($P 2.26 > 4.1$), there is a significant difference between mean concentrations of cadmium in the selected regions.

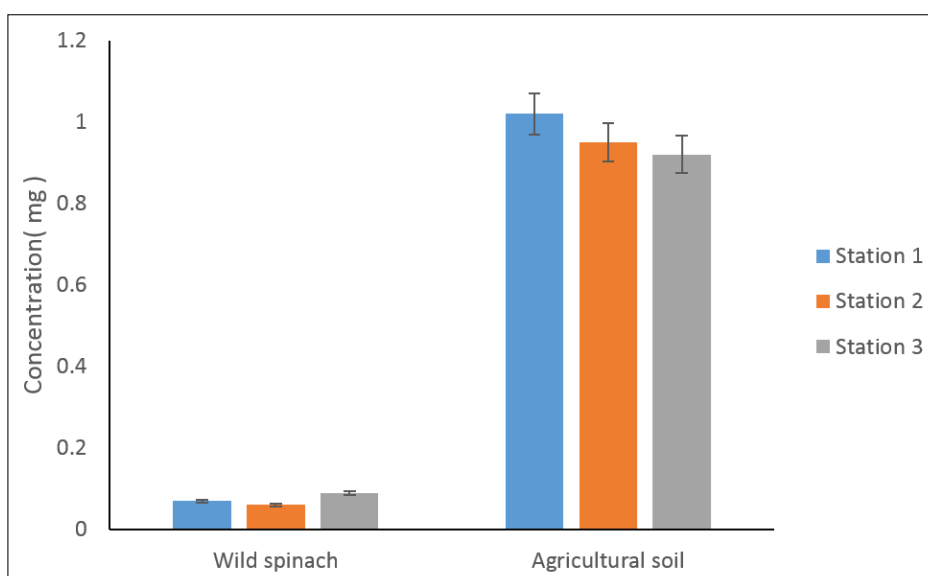


Fig. 4. The amount of cadmium in plant and soil in selected stations

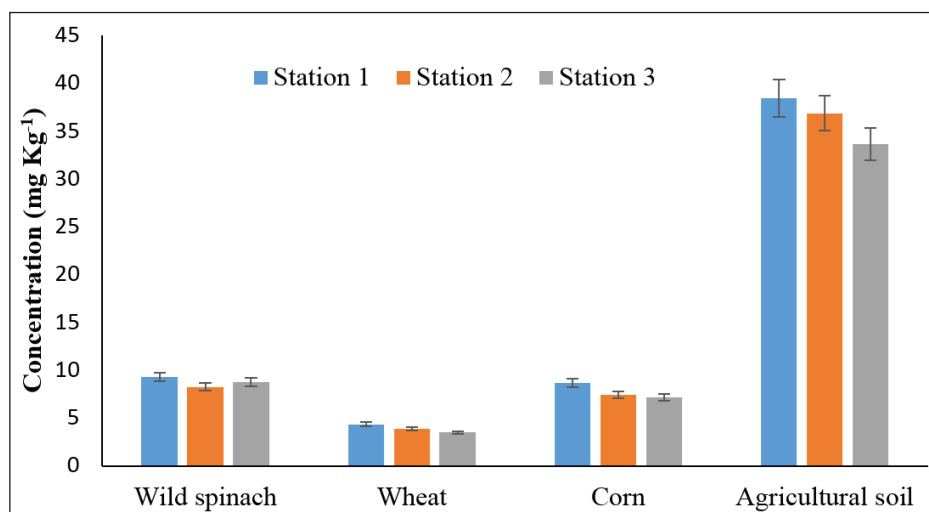


Fig. 5. The amount of copper in plants and soil in selected stations

3.3. Evaluation of copper in plant and soil

Figure 5 showed that the amount of copper in plant samples is lower than its permissible level (20 mg Kg^{-1}) but, in soil samples at all three stations is higher than its permissible range. The findings of ANOVA, at confidence level of 95% and significance level of lower than 0.05 ($P_{12.43} > 4.1$), indicate that the difference of means in copper measured at mentioned stations is significant.

3.4. Optimization process

3.4.1. Digestion reagent and time

1.0 g of plants and soil samples put on the beaker and digested with 10 mL of $\text{HNO}_3/\text{H}_2\text{SO}_4$ solutions and 2 mL of H_2O_2 . The mixture is placed on a heater magnet for 60 min under the hood condition, then 12 mL of extra reagents $\text{HNO}_3/\text{H}_2\text{SO}_4/\text{H}_2\text{O}_2$ solutions are added to samples and heated for 60 min at 90°C . The results showed us the favorite time for digestion process is 2 h. The solutions of digested samples (plants and soil) were determined by F-AAS after dilution with DW.

3.4.2. The effect of the amount of adsorbent

The favorite extraction of Cu, Cd, and Pb ions based on the EOSiP-TS@MWCNTs adsorbent was obtained in water samples. By the UD- μ -SPE procedure, the amount of the EOSiP-TS@MWCNTs was studied for $1.5\text{-}1000 \mu\text{g L}^{-1}$, $1\text{-}200 \mu\text{g L}^{-1}$, $5\text{-}1500 \mu\text{g L}^{-1}$ concentrations of Cu, Cd, and

Pb ions, respectively. Therefore, the amount of the EOSiP-TS@MWCNTs adsorbent between 5-50 mg was evaluated for the Cu, Cd, and Pb extraction in 20 mL of water samples before being determined by the F-AAS. The high extraction for the Cu, Cd, and Pb ions was achieved at 20 mg, 18 mg and 15 mg of the EOSiP-TS@MWCNTs adsorbent in standard and water samples. Therefore, 20 mg of the EOSiP-TS@MWCNTs adsorbent was used at pH 6-6.5 (Fig. 6).

3.4.3. The effect of pH

For extraction of Cu, Cd, and Pb ions in water samples, the pH samples were studied from 2 to 11 for 20 mg of adsorbent. So, the different pH sample was evaluated for ions extraction in water and standard samples. The results showed, the high recovery based on the EOSiP-TS@MWCNTs adsorbent for the Cu, Cd, and Pb ions was obtained at pH of 5.5-6.5, 6-7, and 6-6.5, respectively. So, pH 6 was selected for the Cu, Cd, and Pb extraction in water samples (Fig. 7). Also, the recoveries were decreased at less than pH 5.5 and more than pH 7. So, the pH of 6.0 was used as optimum pH for the Cu, Cd, and Pb extraction in water samples (Fig.7). The mechanism for the Cu, Cd, and Pb extraction based on the EOSiP-TS@MWCNTs adsorbent was obtained by the dative bond of sulfur groups (MWCNTs-S:-S:) at pH 6.0. Also, the Cu, Cd, and Pb ions participated at a pH of more than 8 ($\text{M}(\text{OH})_2$).

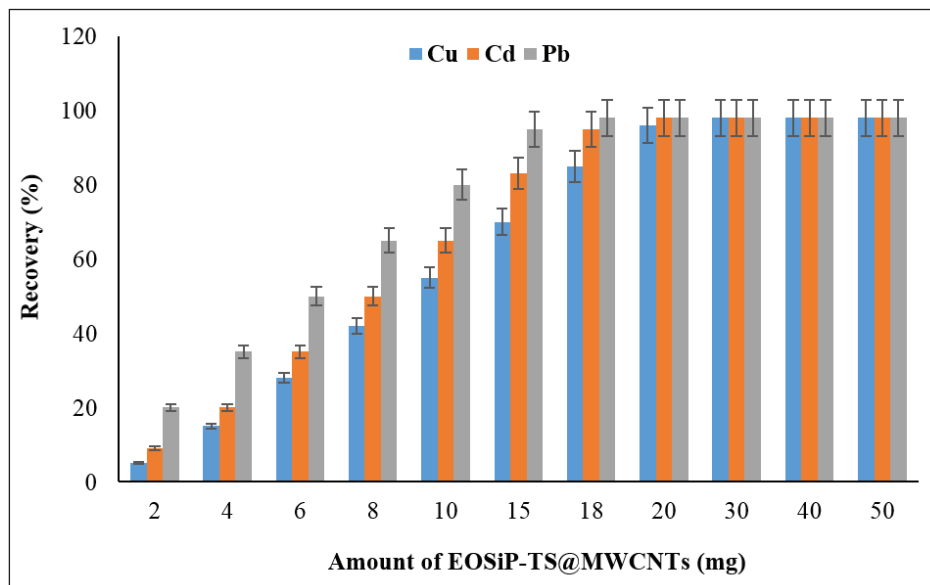


Fig.6. Effect of EOSiP-TS@MWCNTs adsorbent for extraction of Cu, Cd, and Pb ions in water samples by the UD- μ -SPE procedure

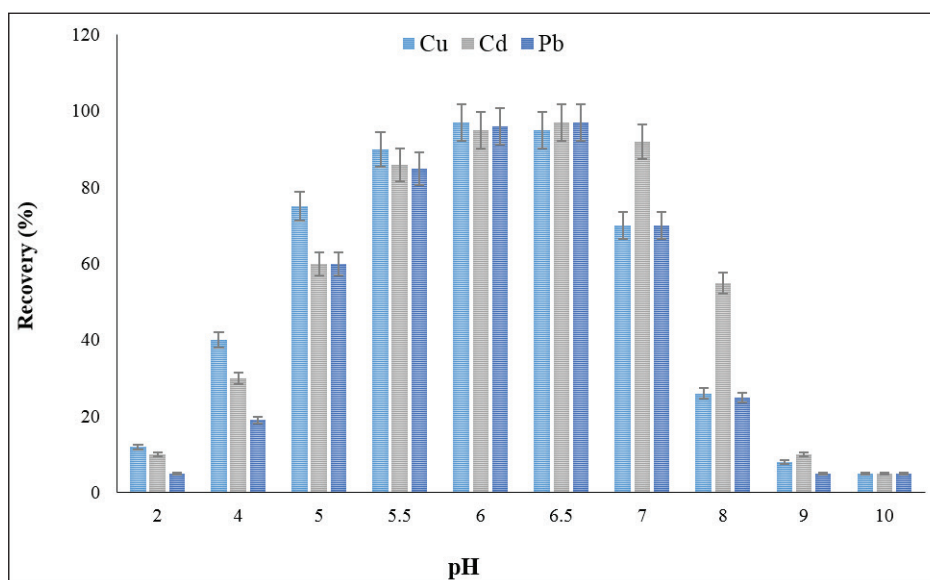


Fig.7. Effect of pH on extraction of Cu, Cd, and Pb ions in water samples by the UD- μ -SPE procedure

3.4.4. The effect of sample volume

Due to the Figure, the extraction of the Cu, Cd, and Pb ions was studied for various volumes of water samples. So, the different volumes between 5-50 mL were evaluated for a concentration of 1.5-1000 $\mu\text{g L}^{-1}$, 1-200 $\mu\text{g L}^{-1}$, 5-1500 $\mu\text{g L}^{-1}$, respectively. The efficient recovery was observed at less than 25 mL, 30 mL and 20 mL for extraction of the Cu, Cd, and Pb ions in water samples, respectively at pH 6.0. So, 20 mL of water samples were used as optimum sample volume for extraction of the Cu,

Cd, and Pb ions in water samples by the EOSiP-TS@MWCNTs adsorbent (Fig. 8).

3.4.5. Interference of ions and absorption capacity

The effect of some ions such as Co^{2+} , Ni^{2+} , Zn^{2+} , V^{3+} , Ag^+ , Mn^{2+} , Na^+ , Li^+ , K^+ , Mg^{2+} , Ca^{2+} , S^{2-} , CO_3^{2-} , NO_3^- , F^- , Cl^- and I^- for extraction of the Cu, Cd, and Pb ions in water samples were evaluated by the UD- μ -SPE procedure. For evaluating, the different interfering ions with various concentrations (2-10

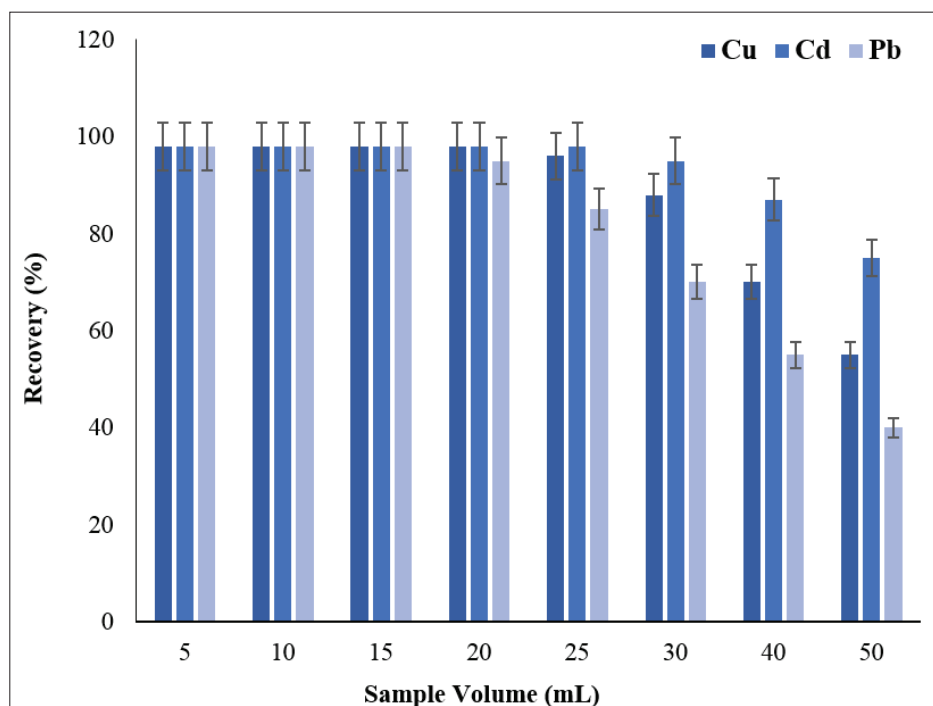


Fig.8. Effect of sample volume on extraction of Cu, Cd, and Pb ions in water samples by the UD- μ -SPE procedure

mg L⁻¹) were examined for 20 mL of water samples. The main concomitant ions in water samples were used and the Cu, Cd, and Pb ions concentrations in the liquid phase were determined by the F-AAS. The results showed that the interference ions cannot decrease the extraction recovery of the Cu, Cd, and Pb ions in water samples by the EOSiP-TS@MWCNTs adsorbent (Table 2). The absorption capacities of the EOSiP-TS@

MWCNTs adsorbent are related to the size, chemical adsorption, and surface area for the Cu, Cd, and Pb ions extraction in water samples. In a closed tube, 20 mg of the EOSiP-TS@MWCNTs adsorbent were mixed to 100 mg L⁻¹ of the standard solution of the Cu, Cd, and Pb ions in 100 mL of water sample at pH 6.0. After 40 minutes, the Cu, Cd, and Pb ions were chemically adsorbed by the sulfur group of the

Table 2. The effect of the interference of ions for extraction of the Cu, Cd, and Pb ions in water and digested plant/soil samples by the UD- μ -SPE procedure

Interference of Elements	Mean ratio (C _{IE} /C _{Pb,Cd,Cu})	Recovery Pb (%)	Recovery Cd (%)	Recovery Cu (%)
Zn ²⁺	600, 650, 750	97.3	98.4	96.8
V ³⁺	600, 650, 800	97.2	97.9	98.5
Co ²⁺	400, 400, 600	98.3	97.5	98.6
Na ⁺ , K ⁺ , Li ⁺ , Mg ²⁺ , Ca ²⁺	800, 850, 1000	98.7	99.2	98.1
F ⁻ , Cl ⁻ , I ⁻	900, 1000, 1200	98.2	98.6	97.9
Ni ²⁺	400, 500, 500	97.1	98.4	96.9
Mn ²⁺	500, 600, 700	97.9	99.3	96.5
Ag ⁺	200, 200, 250	97.8	98.5	97.1
CO ₃ ²⁻ , NO ₃ ⁻ , S ²⁻	700, 900, 900	98.0	97.5	97.8

EOSiP-TS@MWCNTs adsorbent. Finally, the final concentration of mercury in the liquid phase was determined by F-AAS. Due to the results, the mean of adsorption capacities (AC) of the EOSiP-TS@MWCNTs adsorbent for the Cu, Cd, and Pb ions was achieved at 135.6 mg g⁻¹.

3.4.6. Validation in real samples

By the UD- μ -SPE procedure, the Cu, Cd, and Pb ions were extracted based on the EOSiP-TS@

MWCNTs adsorbent in water samples at a pH of 6.0. The results were validated by spiking to the water samples by the UD- μ -SPE procedure. So, the different concentrations of the Cu, Cd, and Pb ions were spiked by standard solutions (Table 3-5). Also, the Cu, Cd, and Pb ions in plant and soil samples were simply measured by F-AAS after acid digested samples and validated by a microwave digestion system (Table 6).

Table 3. Determination of lead (Pb²⁺) in water samples based on the EOSiP-TS@MWCNTs adsorbent by the UD- μ -SPE procedure

Sample	Added ($\mu\text{g L}^{-1}$)	*Found ($\mu\text{g L}^{-1}$)	Recovery (%)
^a Drinking water	-----	ND	-----
	5.0	4.91 \pm 0.15	98.2
^b Well water	-----	15.75 \pm 0.54	-----
	15	29.94 \pm 0.15	94.6
^c Wastewater	-----	765.76 \pm 28.4	-----
	750	1496.32 \pm 56.33	97.4
^d River water	-----	9.54 \pm 0.43	-----
	10	19.85 \pm 0.88	103.1

* Mean of three determinations \pm confidence interval (P= 0.95, n=5)

+ND: Not Detected

^a drinking water prepared from Zabol city

^b well water prepared from agricultural water of Zabol

^c Wastewater prepared from an industrial chemical in Zabol city

^d River water prepared from Helmand river of Zabol

Table 4. Determination of cadmium (Cd²⁺) in water samples based on the EOSiP-TS@MWCNTs adsorbent by the UD- μ -SPE procedure

Sample	Added ($\mu\text{g L}^{-1}$)	*Found ($\mu\text{g L}^{-1}$)	Recovery (%)
^a Drinking water	-----	ND	-----
	1.0	0.95 \pm 0.15	95.0
^b Well water	-----	6.34 \pm 0.22	-----
	5.0	11.46 \pm 0.46	102.4
^c Wastewater	-----	87.26 \pm 3.72	-----
	100	185.82 \pm 8.34	98.6
^d River water	-----	2.54 \pm 0.11	-----
	2.0	4.47 \pm 0.88	96.5

* Mean of three determinations \pm confidence interval (P= 0.95, n=5)

+ND: Not Detected

^a drinking water prepared from Zabol city

^b well water prepared from agricultural water of Zabol

^c Wastewater prepared from an industrial chemical in Zabol city

^d River water prepared from Helmand river of Zabol

Table 5. Determination of copper (Cu^{2+}) in water samples based on the EOSiP-TS@MWCNTs adsorbent by the UD- μ -SPE procedure

Sample	Added ($\mu\text{g L}^{-1}$)	*Found ($\mu\text{g L}^{-1}$)	Recovery (%)
^a Drinking water	-----	4.65 ± 0.23	-----
	5.0	9.61 ± 0.39	99.2
^b Well water	-----	44.94 ± 2.13	-----
	50	93.96 ± 4.32	98.1
^c Wastewater	-----	523.94 ± 20.73	-----
	500	999.87 ± 43.62	95.2
^d River water	-----	13.65 ± 0.47	-----
	10	23.41 ± 1.08	97.6

* Mean of three determinations \pm confidence interval ($P=0.95$, $n=5$)

^a drinking water prepared from Zabol city

^b well water prepared from agricultural water of Zabol

^c Wastewater prepared from an industrial chemical in Zabol city

^d River water prepared from Helmand river of Zabol

Table 6. Validation of acid digested procedure for determination of the Cu, Cd, and Pb ions in plant and soil samples by F-AAS and compared to microwave digestion system coupled to F-AAS

Sample	*Microwave/F-AAS (mg L^{-1})	*Acid digestion/F-AAS (mg L^{-1})	^A Recovery MW (%)
Plant	1.77 ± 0.11	1.82 ± 0.12	102.8
Soil	11.56 ± 0.42	10.96 ± 0.38	94.8
Plant	2.01 ± 0.09	1.93 ± 0.12	96.1
Soil	8.85 ± 0.28	8.66 ± 0.25	97.8

* Mean of three determinations \pm confidence interval ($P=0.95$, $n=5$, $\text{RSD}<2\%$)

^A Recovery MW: Recovery Acid digestion/microwave digestion

4. Conclusions

Today, due to potential adverse ecological effects, soil contamination with heavy metals has become a critical concern for the environment. Results obtained in this research showed that amount of heavy metals is accumulated in soil and some plants. Although, the mentioned plants in this study are used to feed livestock and only in a few cases the wheat is used to prepare flour, but lack of suitable grasslands and pastures in Sistan and water shortage would stimulate ranchers to use wastewater increasingly for farmlands. Also, the Cd, Pb, and Cu were determined in digested plant and soil samples by F-AAS. Moreover, the Cd, Pb, and Cu ions in water and wastewater samples based on EOSiP-TS@MWCNTs adsorbent were determined by F-AAS after the UD- μ -SPE

procedure at pH 6-6.5. The RSD% of results was obtained between 1.23-3.11. The mean absorption capacity (AC) of EOSiP-TS@MWCNTs adsorbent for Cd, Pb, and Cu ions was achieved at 144.8 mg g^{-1} , 127.4 mg g^{-1} , and 134.6 mg g^{-1} , respectively in a static system.

5. Acknowledgments

The authors sincerely appreciate the efforts of the chemistry laboratory of Zabol and the department of health engineering, Zabol University of medical sciences, Zabol, Iran.

6. References

- [1] S. Qayyum, I. Khan, K. Meng, Y. Zhao, C. Peng, A review on remediation technologies for heavy metals contaminated soil, Cent.

- Asian J. Environ. Sci. Technol. Innov., 1 (2020) 21-29. <https://doi.org/10.22034/CAJESTI.2020.01.03>
- [2] .R.R. Kahkha, S. Bagheri, R. Noori, J .Piri, S. Javan, Examining total concentration and sequential extraction of heavy metals in agricultural soil and wheat, Polish J. Environ. Studies, 26 (2017) 2021-2028. <http://yadda.icm.edu.pl/yadda/element/bwmeta1.element.agro-9ee0c900-e068-43b7-8beb-dabd88ca4595>
- [3] B. He, W. Wang, R. Geng, Z. Ding, D. Luo, J. Qiu, G. Zheng, Q. Fan, Exploring the fate of heavy metals from mining and smelting activities in soil-crop system in Baiyin, NW China, Ecotoxicol. Environ. Safe., 207 (2021) 111234. <https://doi.org/10.1016/j.ecoenv.2020.111234>
- [4] F. Elbehiry, H. Elbasiouny, R. Ali, E.C. Brevik, Enhanced immobilization and phytoremediation of heavy metals in landfill contaminated soils, Water Air Soil Pollut., 231 (2020) 1-20. <https://doi.org/10.1007/s11270-020-04493-2>
- [5] T. Hourri, Y. Khairallah, A. Al Zahab, B. Osta, D. Romanos, G. Haddad, Heavy metals accumulation effects on the photosynthetic performance of geophytes in Mediterranean reserve, J. King. Saud. Uni. Sci., 32 (2020) 874-880. <https://doi.org/10.1016/j.jksus.2019.04.005>
- [6] T.M. Minkina, S.S. Mandzhieva, M.V. Burachevskaya, T.V. Bauer, S.N. Sushkova, Method of determining loosely bound compounds of heavy metals in the soil, Methods X, 5 (2018) 217-226. <https://doi.org/10.1016/j.mex.2018.02.007>
- [7] F. Capitelli, F. Colao, M. Provenzano, R. Fantoni, G. Brunetti, N. Senesi, Determination of heavy metals in soils by laser induced breakdown spectroscopy, Geoderma, 106 (2002) 45-62. [https://doi.org/10.1016/S0016-7061\(01\)00115-X](https://doi.org/10.1016/S0016-7061(01)00115-X)
- [8] H.L. Byers, L.J. McHenry, T.J. Grundl, XRF techniques to quantify heavy metals in vegetables at low detection limits, Food Chem. X, 1 (2019) 100001. <https://doi.org/10.1016/j.fochx.2018.100001>
- [9] S. Li, C. Zhang, S. Wang, Q. Liu, H. Feng, X. Ma, J. Guo, Electrochemical microfluidics techniques for heavy metal ion detection, Analyst, 143 (2018) 4230-4246. <https://doi.org/10.1039/C8AN01067F>
- [10] A. Maurya, L. Kesharwani, M.K. Mishra, Analysis of heavy metal in soil through atomic absorption spectroscopy for forensic consideration, Int. J. Res. Appl. Sci. Eng. Technol., 6 (2018) 1188-1192. <http://doi.org/10.22214/ijraset.2018.6173>
- [11] G. Yu, Y. Lu, J. Guo, M. Patel, A. Bafana, X. Wang, B. Qiu, C. Jeffryes, S. Wei, Z. Guo, Carbon nanotubes, graphene, and their derivatives for heavy metal removal, Adv. Compos. Hybrid. Mater., 1 (2018) 56-78. <https://doi.org/10.1007/s42114-017-0004-3>
- [12] M. hirani, A. Semnani, S. Habibollahi, H. Haddadi, Ultrasound-assisted, ionic liquid-linked, dual-magnetic multiwall carbon nanotube microextraction combined with electrothermal atomic absorption spectrometry for simultaneous determination of cadmium and arsenic in food samples, J. Anal. At. Spectrom., 30 (2015) 1057-1063. <https://doi.org/10.1039/c4ja00481g>
- [13] A.A. Mamun, Y.M. Ahmed, M.F.R. AlKhatib, A.T. Jameel, M. AlSaadi, Lead sorption by carbon nanofibers grown on powdered activated carbon—kinetics and equilibrium, NANO: Brief Reports Rev., 10 (2015) 1550017. <https://doi.org/10.1142/s1793292015500174>
- [14] M.F. Mahmoud, N.A. Fekry, M.M.A. El-Latif, Nanocomposites of nanosilica-immobilized-nanopolyaniline and crosslinked nanopolyaniline for removal of heavy metals, Chem. Eng. J., 304 (2016) 679-691. <https://doi.org/10.1016/j.cej.2016.06.110>
- [15] D.C. Culita, C.M. Simonescu, R.E. Patescu, M. Dragne, N. Stanica, O. Oprea, o-Vanillin functionalized mesoporous silica coated

- magnetite nanoparticles for efficient removal of Pb(II) from water, *J. Solid State Chem.*, 238 (2016) 311–320. <https://doi.org/10.1016/j.jssc.2016.04.003>
- [16] P. Pirkwieser, J.A. López-López, W. Kandioller, B.K. Keppler, C. Moreno, F. Jirsa, Novel 3-hydroxy-2-naphthoate-based task-specific ionic liquids for an efficient extraction of heavy metals, *Front. Chem.*, 6 (2018)172. <https://doi.org/10.3389/fchem.2018.00172>
- [17] M. Hossein Habibollahi, Extraction and determination of heavy metals in soil and vegetables irrigated with treated municipal wastewater using new mode of dispersive liquid-liquid microextraction based on the solidified deep eutectic solvent followed by GFAAS, *J. Sci. Food Agric.*, 30 (2019) 656-665. <https://doi.org/10.1002/jsfa.9230>.
- [18] M.G. Kakavandi, M. Behbahani, F. Omid, G. Hesam, Application of ultrasonic assisted-dispersive solid phase extraction based on ion-imprinted polymer nanoparticles for preconcentration and trace determination of lead ions in food and water samples, *Food Anal. Methods*, 10 (2017) 2454–2466. <https://doi.org/10.1007/s12161-016-0788-8>
- [19] M. D. Yadav, K. Dasgupta, Role of sulfur source on the structure of carbon nanotube cotton synthesized by floating catalyst chemical vapour deposition, *Chem. Phys. Lett.*, 748 (2020)137391. <https://doi.org/10.1016/j.cplett.2020.137391>
- [20] V. Kumar, A. Sharma, P. Kaur, G.P.S. Sidhu, A.S. Bali, R. Bhardwaj, A.K. Thukral, A. Cerda, Pollution assessment of heavy metals in soils of India and ecological risk assessment: A state-of-the-art, *Chemosphere*, 216 (2019) 449-462. <https://doi.org/10.1016/j.chemosphere.2018.10.066>.
- [21] B. Jiang, A. Adebayo, J. Jia, Y. Xing, S. Deng, L. Guo, Y. Liang, D. Zhang, Impacts of heavy metals and soil properties at a Nigerian e-waste site on soil microbial community, *J. Hazard. Mater.*, 362 (2019) 187-195. <https://doi.org/10.1016/j.jhazmat.2018.08.060>.
- [22] M. Sulaiman, K. Salawu, A. Barambu, Assessment of concentrations and ecological risk of heavy metals at resident and remediated soils of uncontrolled mining site at Dareta Village, Zamfara, Nigeria, *J. Appl. Sci. Environ. Manage.*, 23 (2019) 187–193. <https://doi.org/10.4314/jasem.v23i1.28>



Application of experimental design methodology to optimize acetaminophen removal from aqueous environment by magnetic chitosan@multi-walled carbon nanotube composite: Isotherm, kinetic, and regeneration studies

Ebrahim Nabatian ^{a, b}, Maryam Dolatabadi ^c, Saeid Ahmadzadeh ^{d, e*}

^a Student Research Committee, Kerman University of Medical Sciences, Kerman, Iran.

^b Department of Chemistry, Faculty of Sciences, Shahid Bahonar University of Kerman, Kerman, Iran.

^c Environmental Science and Technology Research Center, Department of Environmental Health Engineering, School of Public Health, Shahid Sadoughi University of Medical Sciences, Yazd, Iran.

^d Pharmaceutics Research Center, Institute of Neuropharmacology, Kerman University of Medical Sciences, Kerman, Iran.

^e Pharmaceutical Sciences and Cosmetic Products Research Center, Kerman University of Medical Sciences, Kerman, Iran

ARTICLE INFO:

Received 23 Dec 2021

Revised form 20 Feb 2022

Accepted 2 Mar 2022

Available online 29 Mar 2022

Keywords:

Adsorption,
Acetaminophen,
Experimental design,
Isotherm, Kinetic,
Regeneration

ABSTRACT

Acetaminophen is a widely used drug worldwide and is frequently detected in water and wastewater as a high-priority trace pollutant. This study investigated the applicability of the adsorption processes using a composite of magnetic chitosan and multi-walled carbon nanotubes (MCS@MWCNTs) as an adsorbent in the treatment of acetaminophen. The model was well fitted to the actual data, and the correlation coefficients of R^2 were 0.9270 and 0.8885, respectively. The maximum ACT removal efficiency of 98.1% was achieved at ACT concentration of 45 mg L^{-1} , pH of 6.5, MCS@MWCNTs dosage of 400 mg L^{-1} , and the reaction time of 23 min. The result shows that BET specific surface area of $640 \text{ m}^2 \text{ g}^{-1}$. The adsorption isotherms were well fitted with the Langmuir Model ($R^2 = 0.9961$), depicting the formation of monolayer adsorbate onto the surface of MCS@MWCNTs. The maximum monolayer adsorption capacity of 256.4 mg g^{-1} was observed for MCS@MWCNTs. The pseudo-second-order kinetic model well depicted the kinetics of ACT adsorption on MCS@MWCNTs ($R^2 = 0.9972$). Desorption studies showed that the desorption process is favored at high pH under Alkaline conditions. The results demonstrate that the MCS@MWCNTs is an efficient, durable, and sustainable adsorbent in water purification treatment.

1. Introduction

Pharmaceutical pollutants (PPs) are a group of emerging anthropogenic hazard contaminants that contain different groups of human and veterinary medicinal compounds that are used widely all over the globe [1, 2]. Acetaminophen (ACT) is one of

the most frequently used drugs worldwide. ACT is a type of analgesic and antipyretic drug commonly used as a fever reducer and pain reliever. Because of high consumption worldwide, it is one of the most frequently detected drugs in bodies of water and wastewater [3-5]. Overdoses of ACT produce the accumulation of toxic metabolites, which may cause severe and sometimes fatal hepatotoxicity, and nephrotoxicity; generally, due to their bio-accumulation, they pose a potential long-term risk

*Corresponding Author: [Saeid Ahmadzadeh](mailto:Saeid.Ahmadzadeh@kmu.ac.ir)

Email: chem_ahmadzadeh@yahoo.com

<https://doi.org/10.24200/amecj.v5.i01.168>

for aquatic and terrestrial organisms. To improve the water quality and protect human health, the water contaminated with emerging contaminants, including pharmaceuticals, must be efficiently treated using an appropriate technique before being supplied for consumption [6, 7]. Various physical, chemical, and biological technologies can be employed to treat ATC from water and wastewater. Among the different treatments, adsorption technology is attractive due to its effectiveness, efficiency, and economy. The common adsorbents primarily include activated carbons, zeolites, clays, industrial by-products, agricultural wastes, biomass, and polymeric materials. AC is characterized by high porosity and an extensive surface area, enabling it to adsorb many kinds of pollutants efficiently. Despite its high adsorption capacity, the use of AC on a large scale is limited by process engineering difficulties such as the dispersion of the AC powder and the cost of its regeneration. However, these adsorbents described above suffer from low adsorption capacities and separation inconvenience. Therefore, efforts are still needed to investigate new promising adsorbents [8]. Chitosan (CS) has gained considerable attention as a non-conventional adsorbent in water decontamination research due to its favorable properties such as non-toxicity, eco-friendliness, high availability, biodegradability, good biocompatibility, low cost, and good adsorption properties. However, the high solubility of CS at lower pH (i.e., below 4) and poor mechanic properties are the limiting problems for taking advantage of the interaction ability of CS with Pollutant molecules. Thus, it might be not advisable to use untreated CS as an adsorbent in aqueous media [9-12]. One good strategy is to immobilize CS on solid matrixes that can stabilize CS in acid solutions and improve its mechanical strength to overcome these problems. Different kinds of solid organic or inorganic matrixes have been used to form composites with CS, such as glass plates, activated clay, silica, and polymer spheres. Recently, carbon nanotubes (CNTs) have also been used as a matrix to prepare CS/CNTs composites.

CNTs, a fascinating new member of the carbon family, have attracted strong research interest since their discovery because of their unique morphologies and various potential applications, as well as their remarkable mechanical properties [13]. CNTs have been proven to possess excellent adsorption capacity in removing organic and inorganic pollutants because of their hollow and layered nanosized structures with a large specific surface area. Also, CNTs can provide improved mechanical strength and better structural integrity conditions. However, the difficulty in collecting these adsorbents from treated effluents can cause inconveniences in their practical application. As an efficient, fast, and economical method for separating magnetic materials, Magnetic separation technology has received considerable attention in recent years. Imparting magnetic properties to adsorbents can isolate them from the medium using an external magnetic field without the need for complicated centrifugation or filtration steps [11, 14].

The current work aimed to investigate the efficacy of magnetic CS and multi-walled carbon nanotubes (MCS@MWCNTs) as the adsorbent in ACT removal under various operating conditions. Effective parameters on ACT removal such as solution pH, reaction time, ACT concentration, and adsorbent dosage were optimized with response surface method (RSM) using central composite design (CCD). In addition, some extra experiments were performed to study adsorption kinetics and isotherms, and adsorbent reusability.

2. Experimental

2.1. Chemicals

Chitosan (Merck), Multi-walled carbon nanotubes (Sigma-Aldrich), Acetaminophen ($C_8H_9NO_2$, Merck), Ferric chloride ($FeCl_3 \cdot 6H_2O$, Merck), Sodium acetate ($C_2H_3NaO_2$, Merck), Ethylene glycol ($C_2H_6O_2$, Merck), Acetone (C_3H_6O , Merck), Paraffin (C_nH_{2n+2} , Merck), Sodium hydroxide (NaOH, Merck), Hydrochloric acid (HCl, Merck), were of analytical grade. All solutions used in the experiments were prepared with distilled water.

2.2. Preparation of Fe_3O_4 nanoparticles

Typically, 1.35 g of $FeCl_3 \cdot 6H_2O$ and 3.6 g of sodium acetate were dissolved in 40 mL ethylene glycol with stirring and heating simultaneously. The temperature has risen to 80-100 °C. After stirring for 30 min, the yellow-brown color solution was transferred to a Teflon-lined stainless-steel autoclave and heated in the oven at 180°C for 12 h. Then, the autoclave was allowed to cool down to room temperature naturally. The black magnetite particles were washed with acetone and water several times and dried in the oven at 60°C overnight [15].

2.3. Preparation of MCS@MWCNTs

The composites of MCS@MWCNTs were synthesized by a suspension cross-linking approach with some modification. Typically, 0.1 g of chitosan was dissolved in 20 mL of 2% (v/v) acetic acid solution under ultrasonication. Subsequently, 0.2 g of Fe_3O_4 and 0.2 g of MWCNTs were added into the chitosan solution, and the reaction system was further ultrasonicated for 20 min. Then, the above mixture was slowly dispersed in 40 mL of paraffin containing 2 mL of span-80 under stirring. After 30 min of emulsification, 1 mL of 25% (v/v) glutaraldehyde was introduced into the system for the cross-linking of chitosan. Then the mixture was stirred continuously for 1 h at 70 °C. Afterward, the pH value of the reaction solution was adjusted to 9–10 with 1 mol L⁻¹ NaOH and the reaction system was allowed to stir for another 1 h at 80 °C. The particles were washed with petroleum ether, ethanol, and ultrapure water three times, respectively. Finally, MCS@MWCNTs were obtained by magnetic separation and freeze-dried for 12 h [16].

2.4. Characterization of MCS@MWCNTs

The standard BET equation was employed to calculate the Brunauer-Emmert-Teller (BET) surface area from the desorption isotherms. The pore size distribution was determined from desorption isotherms using the Barrett, Joyner, and Halenda (BJH) method. All calculations were performed

automatically by an Accelerated Surface Area and Porosimeter system (ASAP 2010, Micromeritics, U.S.A.). The pH of zero point charge (pH_{zpc}) describes the condition when the charge density on the surface is zero. It is usually determined concerning the pH of the mixtures. Researchers proposed a mass titration method to determine the values of pH_{zpc}: portions of 20 mL NaCl (0.01 M) solution were added into different flasks. The initial pH was adjusted with NaOH or HCl to the desired values between 2 and 12 (metrohm 827 pH/mV lab pH meter). Then, 20 mg of the MCS@MWCNTs sample was suspended into each flask. The flasks with caps were placed in a shaker. After shaking for 24 h, the pH of the solutions was measured and designated as pH_{final}. The pH_{zpc} value is the point where the pH_{initial} = pH_{final} [17].

2.5. Experimental design and statistical analysis

The response surface methodology (RSM) is a set of statistical and mathematical methods used to analyze experimental results. RSM is used in conditions that many input variables affect the performance and response characteristics of the process. A complete description of a process requires that it be modeled as a polynomial function generally of degree 2 or higher. Since operational conditions may be associated with changes, the nonlinear second-order model can describe it. The quadratic regression model was considered in the form of Equation 1 [18-20]:

$$Y = \beta_0 + \sum_{i=1}^k \beta_i X_i + \sum_{i=1}^k \beta_{ii} X_i^2 + \sum_{i=1}^k \sum_{j=1}^k \beta_{ij} X_i X_j + \epsilon$$

(Eq. 1)

where Y represents the response of process, i and j index numbers for factors, X_i and X_j are the design variables, β_i and β_j represents the coefficient of first-order effect, β_{ij} is the coefficient of interaction, β_0 is constant-coefficient, k is the number of factors and ϵ is the model error. In this study, CCD is based on a four-factor design, including ACT concentration (X_1), pH (X_2), adsorbent dosage (X_3), and reaction time (X_4) were discussed. In the

Table 1. Coded and actual values of independent process variables used in the design of an experimental matrix using the RSM-CCD framework.

Coded Variables (X _i)	Factors	Coded Level				
		- α	-1	0	+1	+ α
X ₁	A= ACT Concentration (mg L ⁻¹)	20.0	40.0	60.0	80.0	100.0
X ₂	B= pH	4.00	5.50	7.00	8.50	10.00
X ₃	C= Adsorbent dosage (mg L ⁻¹)	100	200	300	400	500
X ₄	D= Reaction time (min)	5.00	11.25	17.50	23.75	30.00

design of the experiments, each variable with five levels was considered, in accordance with Table 1. The statistical significance of CCD modeling parameters and their combined interactions at certain levels were examined based on their p values. Analysis of variance (ANOVA) was used to check the experimental data and accuracy of the response surface model. The coefficient of variation (C.V. %) and R² values was calculated to evaluate the goodness of fit of the regression model. The model precision associated with the range of predicted values at the given points was also elucidated.

2.6. Adsorption experiments

All adsorption experiments were carried out in 100 mL of pyrex reactor by mixing a given dose of MCS@MWCNTs with a certain concentration of ATC solution in a thermostatic shaker. The initial pH of the ACT solution was adjusted to a certain value using NaOH and HCl solution by pH meter. After adsorption, the mixture was immediately centrifuged, and the supernatant was analyzed for the concentration of ATC was measured using a UV/Vis spectrophotometer (Optizen). The wavelength corresponding to the maximum absorbance of ATC was 242 nm. Each experiment was repeated at least three times, and the average value was recorded. The ACT removal (q_e) and adsorption capacity were calculated by Equations (2) and (3), respectively [15, 21]:

$$\text{ACT Removal (\%)} = \frac{C_0 - C_t}{C_0} \times 100 \quad (\text{Eq. 2})$$

$$q_e = \frac{(C_0 - C_e) \times V}{m} \quad (\text{Eq. 3})$$

Where C₀ is the initial ACT concentration (mg L⁻¹), C_e is the ACT concentration (mg L⁻¹) after the batch adsorption procedure, m is the adsorbent dosage (g L⁻¹), and q_e is the amount of ACT adsorbed by the adsorbent (mg g⁻¹).

2.7. Kinetic and isotherm models

Two widely used kinetics models, pseudo-first-order and pseudo-second-order models were examined to fit the experimental data. The linear expression of pseudo-first-order and pseudo-second-order models are expressed as Equation 4 and 5 [15, 22].

$$\ln(q_e - q_t) = \ln(q_e) - k_1 t \quad (\text{Eq. 4})$$

$$\frac{t}{q_t} = \frac{1}{k_2 q_e^2} + \frac{t}{q_e} \quad (\text{Eq. 5})$$

where k₁ (min⁻¹) is the rate constant of the pseudo-first-order, k₂ (g mg⁻¹ min⁻¹) is the second-order rate constant. q_e and q_t (mg g⁻¹) are the adsorption capacities at equilibrium and time t (min), respectively.

Three commonly used isotherm models, the Langmuir and Freundlich isotherms, are selected to analyze the equilibrium experimental data for the adsorption of ACT onto MCS@MWCNTs. The two models are given as Equation 6 and 7 [23].

$$\frac{C_e}{q_e} = \frac{C_e}{q_m} + \frac{1}{b q_m} \quad (\text{Eq. 6})$$

$$\ln q_e = \ln K_F + \left(\frac{1}{n}\right) \ln C_e \quad (\text{Eq. 7})$$

where C_e (mg L⁻¹) is the equilibrium concentration of the ACT, q_e (mg g⁻¹) is the amount of ACT

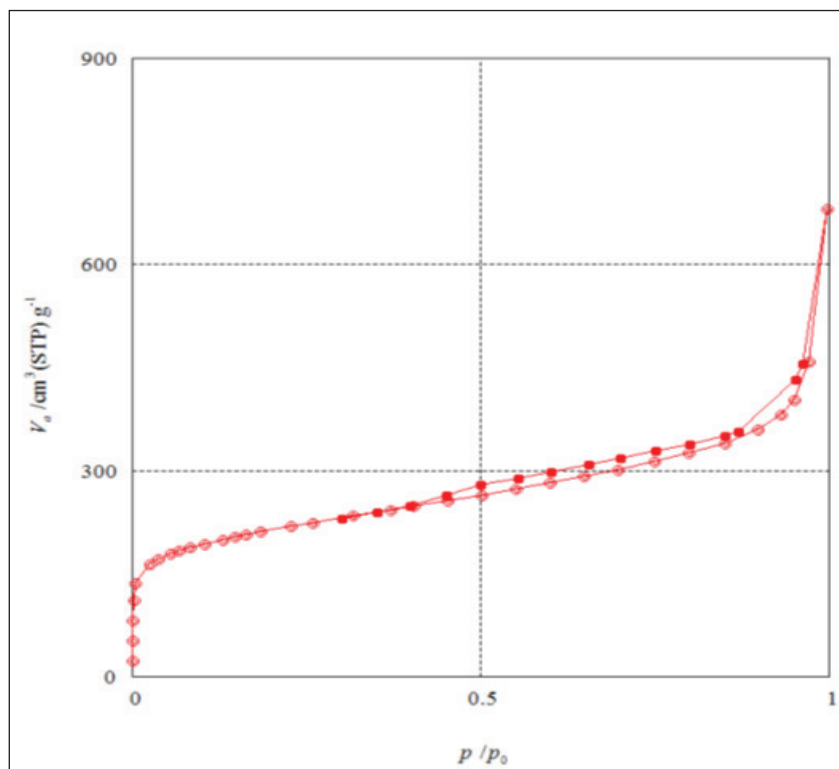


Fig. 1. N₂ adsorption–desorption isotherms of MCS@MWCNTs.

adsorbed under equilibrium, b (L mg⁻¹) is the Langmuir adsorption constant, and q_m (mg g⁻¹) is the maximum adsorption amount. K_F and n are Freundlich constants. n presents the adsorption intensity, assessing the unfavorable adsorption ($n < 1$) or preferential adsorption ($n > 1$), and K_F ((mg g⁻¹ (L mg⁻¹)^{1/n}) is the adsorption capacity of the adsorbent.

The isotherm can predict if an adsorption system is favorable or unfavorable. Researchers pointed out that the essential characteristics of the Langmuir isotherm can be expressed in terms of a dimensionless constant, R_L , as presented in Equation 8.

$$R_L = \frac{1}{1 + bC_0} \quad (\text{Eq. 8})$$

where, R_L is the separation factor or equilibrium parameter, which is a direct function of the Langmuir constant b . The values of R_L indicate the shape of the isotherm: $R_L > 1$ (unfavorable), $R_L = 1$ (linear), $1 > R_L > 0$ (favorable) and $R_L = 0$ (irreversible).

3. Results and discussions

3.1. Characterization of adsorbent

Figure 1 shows the N₂ adsorption-desorption isotherms of MCS@MWCNTs. According to Figure 1, the N₂ adsorption nearly completed at a lower relative pressure of $P/P_0 < 0.1$, suggesting that the sample has the micropore size distribution. In addition, the N₂ hysteresis loop at $P/P_0 > 0.5$ was observed, indicating the presence of mesopores structure. Accordingly, the micropore volume fraction is higher than 79%, confirming the majority of micropores. The MCS@MWCNTs had a high BET-specific surface area of 640 m² g⁻¹.

The adsorbent's pH_{zpc} value was determined to explain the adsorption behavior. This parameter reveals the characteristics of the surface's active sites in a linear range of solution pH. The pH_{zpc} of MCS@MWCNTs was found to be around 6.8, implying that the surface of the adsorbent would be positively charged at solution pH below 6.8 and negatively charged at solution pH above 6.8. Hence, one can conclude that adsorption of cationic molecules is favored at $\text{pH} > 6.8$, while anionic molecules adsorption is favored at $\text{pH} < 6.8$.

3.2. Development and analysis of regression model equation

CCD is considered a reliable method to analyze diagnostic plots, such as the normal probability plot of residuals and to predict versus actual values, to validate the adequacy of the model. The normal

probability plot of the studentized residuals is an excellent graphical representation for the diagnosis of data normality (Fig. 2). The data were well fitted with the line. In addition, the residuals followed a random distribution around zero with a variation of ± 3.0 (Fig. 3).

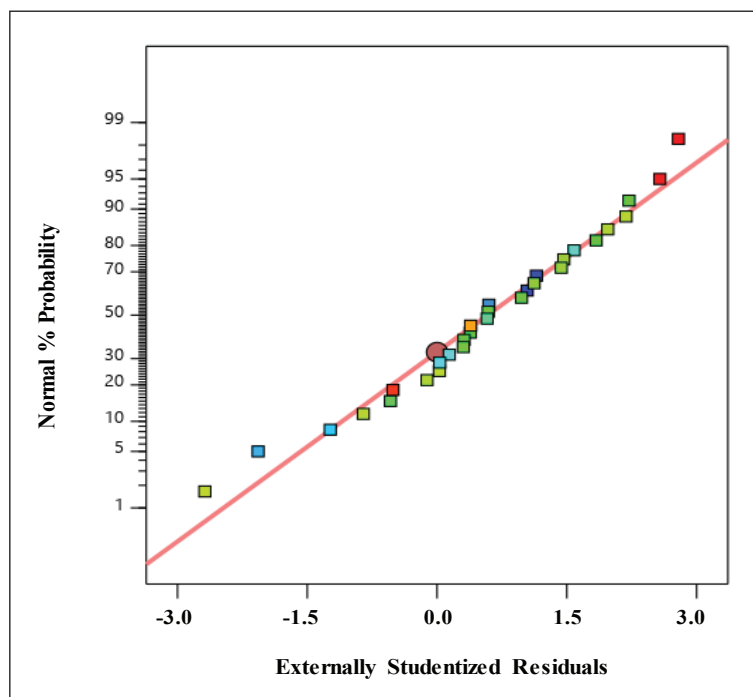


Fig. 2. Normal probability plot of the internally studentized residuals for ACT removal.

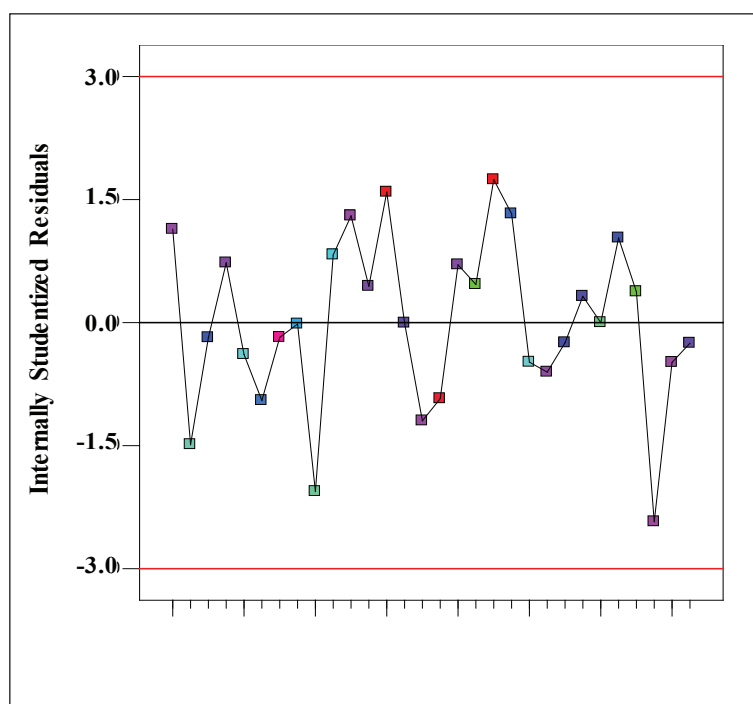


Fig. 3. Run number versus residual data for ACT removal.

The result indicates that the data were normally distributed in the model response. In addition, the corresponding relationship between the residual and the predicted value of the equation also could reflect the reliability of the model. When the points are distributed discretely in the Figure, it could represent the higher reliability of the model.

ANOVA carried out the analysis of obtained experimental data. Table 2 shows ANOVA data for the removal efficiency (Y). F-value in ANOVA implies that the model is significant for the dependent variable. As shown in Table 2, F-value is 87.47 for removal efficiency, which indicates the model is significant. Prob>F or p-value less than 0.05 demonstrates that these model terms are important. The lack of fit F-value of 4.13 with the associated p-value of 0.0612 for the response was insignificant due to relative pure error. The validity of the model is checked by some statistical parameters, including the determination coefficient (R^2), adjusted R^2 , predicted R^2 , adequate precision (AP), and coefficient of variation (CV). R^2 is defined as a measure of the degree of fit. As R^2 approaches unity, the degree of fit increases.

The similarity between R^2 and adjusted R^2 shows the model's compatibility to predict the dependent variable. The difference between predicted R^2 and

adjusted R^2 must be less than 0.2. It is indicated that predicted R^2 is in acceptable agreement with adjusted R^2 . AP is defined as a measure of the ratio of the signal to noise. A ratio greater than 4 is desirable. In our current study, all findings in Table 2 were acceptable, which confirmed the model's fitness with the experimental results.

Overall, the ANOVA analysis was reliable to optimize and determine the level of each factor for removal ACT. Therefore, it is pretty satisfactory to predict the ACT removal efficiency by the second-order polynomial model. In the present study, five model terms (X_1 (ACT concentration), X_2 (pH), X_3 (Adsorbent dosage), X_4 (Reaction time), X_2^2 (quadratic effect of pH)) was most important because of their p-values less than 0.05. These model terms are shown in the model equation. Based on ANOVA results, the empirical model equation in terms of coded variables was developed for the removal efficiency as Equation 9.

$$Y(\%) = 82.72 - 4.84X_1 - 3.27X_2 + 5.71X_3 + 5.57X_4 - 3.87X_2^2 \quad (\text{Eq. 9})$$

The positive sign in the equation indicates the synergistic effect of the corresponding factor on the response, and the negative sign represents

Table 2. Analysis of variance (ANOVA) for regression model.

Source	Sum of Squares	Degree of freedom (df)	Mean Squares	F-Value	Probability P-value > F
Model	2775.21	5	555.04	87.47	< 0.0001
	561.89	1	561.89	88.55	< 0.0001
	256.30	1	256.30	40.39	< 0.0001
	781.29	1	781.29	123.12	< 0.0001
	744.41	1	744.41	117.31	< 0.0001
	431.33	1	431.33	67.97	< 0.0001
Residual	152.30	24	6.35	-	-
Lack of Fit	143.18	19	7.54	4.13	0.0612
Pure Error	9.12	5	1.82	-	-
Cor Total	2927.51	29	-	-	-
Fit Statistics					
R^2	0.9480		SD	2.52	
Adjusted R^2	0.9371		CV	3.16	
Predicted R^2	0.9140		AP	34.40	

the antagonistic effect. The effect of the initial concentration (20-100 mg L⁻¹) was investigated. The removal efficiency for ACT is highly dependent on the initial ACT concentration. Figure 4 illustrated that removal efficiency decreases from 92.3 to 72.6%, increasing ACT concentration from 20 to 100 mg L⁻¹. The effect of initial ACT concentration depends on the immediate relation between the concentration of the ACT and the available sites on an adsorbent surface. In general, the removal efficiency decreases with an increase in the initial ACT concentration due to the saturation of adsorption sites on the adsorbent surface. On the other hand, the increase in initial ACT concentration will cause an increase in the capacity of the adsorbent, which may be due to the high driving force for mass transfer at a high initial ACT concentration.

Figure 4 shows the effect of solution pH ranging from 4 to 10 on the adsorption of ACT onto MCS@MWCNTs. Figure 4 implies that the adsorption of

ACT onto MCS@MWCNTs at pH solution between 4 and 7.0 is a pH-dependent phenomenon, so the adsorption performance was around 85% in all pH ranges. The increase of solution pH to 7.0 caused improvement of the adsorption. A decreasing trend in adsorption of ACT was observed for the solution pH over 7.0. Accordingly, the optimum solution pH at which the maximum adsorption of the ACT under the selected experimental conditions was obtained was found to be 6.5. The effect of solution pH on the adsorption of ACT onto MCS@MWCNTs can be justified considering the pHzpc of MCS@MWCNTs (6.8) and pK_a of ACT (9.4). According to Figure 4, the adsorption of ACT onto MCS@MWCNTs is almost independent of solution pH over the solution pHs between 4.0 and 7.0. At this pH range, the ACT molecules remain mostly neutral and nonionic and thus unfavorable for electrostatic and π - π interactions with the functional groups on the surface of MCS@MWCNTs. Therefore, the hydrophobic

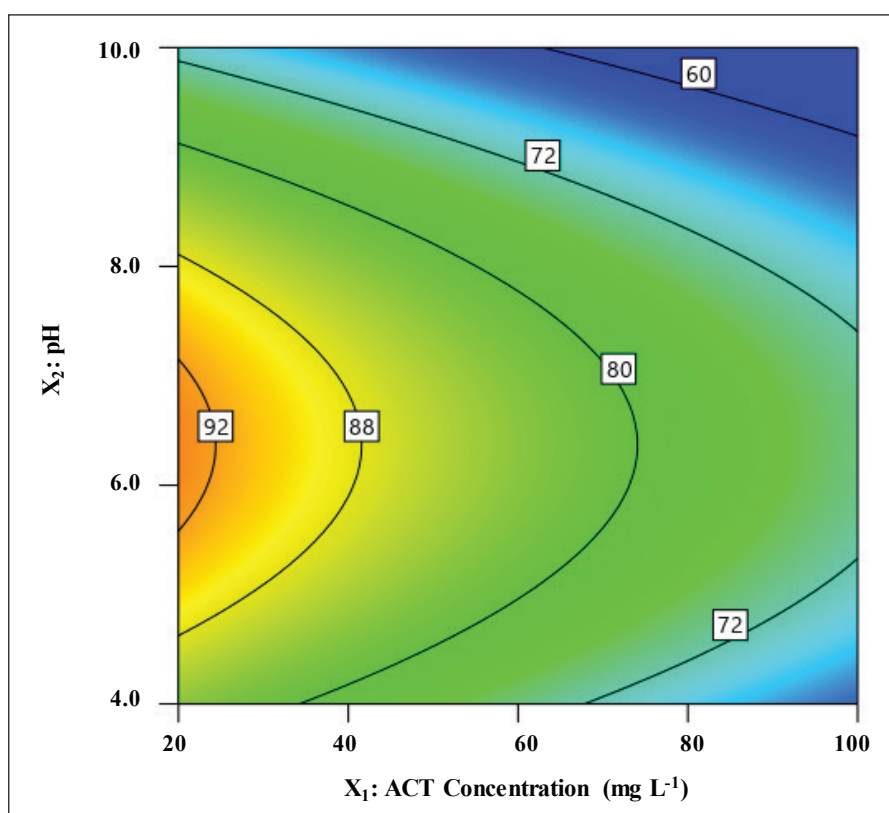


Fig. 4. Contour plot of ACT removal showing the effect of variables of ACT concentration and pH (MCS@MWCNTs dosage of 300 mg L⁻¹ and reaction time of 17.5 min).

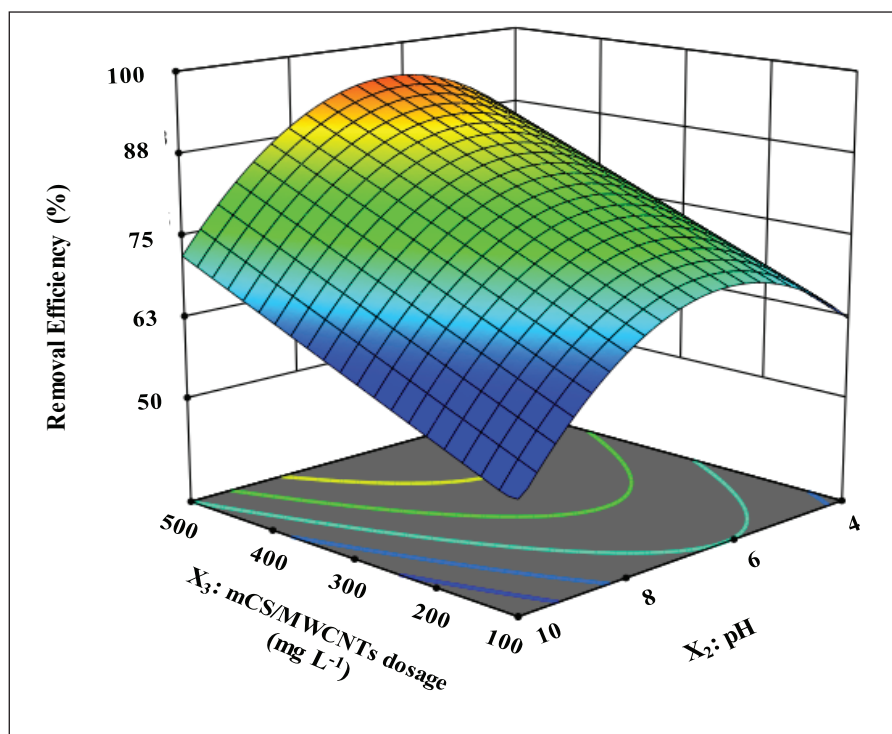


Fig. 5. Response surface plot of ACT removal showing the effect of variables of MCS@MWCNTs dosage and pH (ACT concentration of 60 mg L^{-1} and reaction time of 17.5 min).

interactions might be the primary mechanism anticipated in the ACT adsorption under these conditions. Considering that the pK_a of ACT is 9.4, the main fraction of ACT molecules was in anionic form at solution pHs above this value. In contrast, the surface of MCS@MWCNTs ($\text{pH}_{\text{zpc}} = 6.8$) is negatively charged at alkaline solution pH. Therefore, the reduction of ACT adsorption at the pH over 7.0 can be related to the electrostatic repulsion that occurred between anionic ACT molecules and the negatively charged functional groups on the surface of MCS@MWCNTs. This effect tends to enhance the adsorption of ACT onto MCS@MWCNTs. The greater the solution pH over 7.0, the more negative the surface of MCS@MWCNTs and the more ionized the ACT molecules. Therefore, the greater the repulsive force leads to reduced adsorption. The MCS@MWCNTs dosage as adsorbent was one of the dominant parameters controlling the adsorption of ACT. The relation of MCS@MWCNTs dosage and pH on removal efficiency of ACT is illustrated in [Figure 5](#). Increasing MCS@MWCNTs dosage from

100 to 500 mg L^{-1} leads to an improvement in ACT removal efficiency from 71.4% to 94.2% at ACT concentration of 60 mg L^{-1} , pH of 7, and reaction time 17.5 min. The increase in removal efficiency with increasing adsorbent dose is probably due to the greater adsorbent surface area and pore volume available at higher adsorbent dose providing more functional groups and active adsorption sites that result in higher removal efficiency.

The dependence of the removal efficiency of ACT on reaction time is shown in [Figure 6](#). This Figure shows that removal efficiency increases with time, and adsorption reaches equilibrium in about 25 minutes. It indicates that the rapid increase in removal efficiency is achieved during the first 20 min. The fast adsorption at the initial stage may be due to the higher driving force making an immediate transfer of adsorbate ions to the surface of MCS@MWCNTs particles and the availability of the uncovered surface area and the remaining active sites on the adsorbent. According to the results, an equilibrium time was set to 25 min for adsorption of ACT onto MCS@MWCNTs.

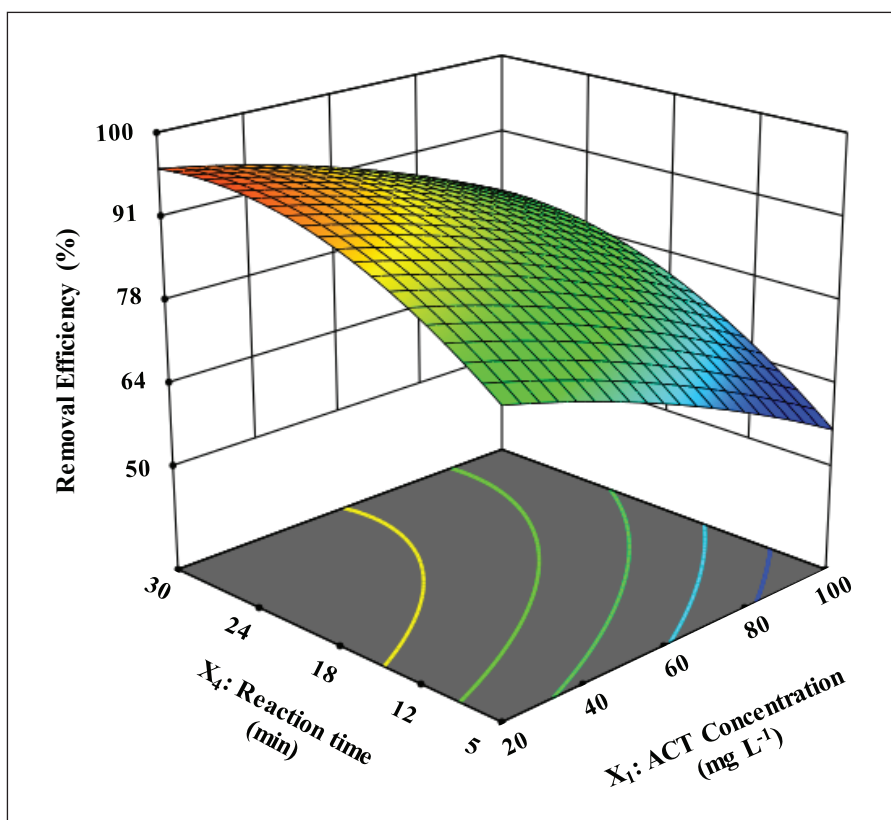


Fig. 6. Response surface plot of ACT removal showing the variables effect of reaction time and ACT concentration (MCS@MWCNTs dosage of 300 mg L^{-1} , and pH of 7).

3.3. Optimization and validation test

The optimization of operating conditions was conducted to determine the optimum values of these parameters required to achieve the highest ACT removal efficiency. Optimization was performed by numerical technique built in the Design-Expert software. The desired goal for the variables was chosen as “in range”, while removal efficiency (response) was chosen as “maximize”. According to the output results, the removal efficiency of ACT could reach a maximum value of 98.1% with the ACT concentration of 45 mg L^{-1} , pH of 6.5, MCS@MWCNTs dosage of 400 mg L^{-1} , and the reaction time of 23 min. An additional experiment was conducted to validate the model prediction (the optimal conditions) in this study. It was found that the results were greatly agreed with the predicted value through the quadratic

model (Table 3). The experimental data were close to predicted data, indicating the accurate prediction ability of the model.

3.4. Adsorption kinetics and isotherms studies

The calculated kinetic parameters for pseudo-first-order and pseudo-second-order models are listed in Table 4. The pseudo-second-order model's correlative coefficient (R^2) was better than that of the pseudo-first-order model. These results indicated that the kinetic data fitted well with pseudo-second-order models. The pseudo-second-order model assumes that the rate-limiting step might be chemical adsorption in the adsorption process.

The adsorption isotherm is critically important in designing an adsorption system. The sorption data were fitted by the Langmuir and Freundlich equations, and the calculated parameters are

Table 3. Optimization and validation tests for ACT removal efficiency.

NO	ACT concentration (mg L ⁻¹)	pH	MCS@MWCNTs dosage (mg L ⁻¹)	Reaction time (min)	Experimental removal efficiency (%)	Predicted removal efficiency (%)
I	45	6.5	400	23	98.7	98.1
II	60	7.0	300	18	84.5	85.3
III	40	8.5	400	12	79.4	80.0
IV	80	8.5	200	25	71.0	69.4

Table 4. Parameters of kinetic equations for the adsorption of ACT.

Pseudo-First-Order model			Pseudo-Second-Order model		
q _c (mg g ⁻¹)	k ₁ (min ⁻¹)	R ²	q _c (mg g ⁻¹)	k ₂ (g mg ⁻¹ min ⁻¹)	R ²
121.47	0.0689	0.9452	217.4	0.0008	0.9972

Table 5. Langmuir and Freundlich constants for the adsorption of ACT.

Langmuir			Freundlich			
q _m (mg g ⁻¹)	b (L mg ⁻¹)	R _L	R ²	K _f (L g ⁻¹)	n	R ²
256.4	0.658	0.026	0.9961	103.1	3.52	0.9542

summarized in Table 5. It was found that the Langmuir model provided a better fit to the observed data for the ACT, with high correlation coefficients ($R^2=0.996$). The maximum ACT sorption capacity (q_m) was 256.4 mg g⁻¹. The values of n and R_L were obtained at 3.52 and 0.026, respectively, suggesting that the adsorbent was favorable for removing ACT from the aqueous solution.

3.5. Regeneration studies

Desorption studies are necessary to complete the investigation of the mechanism involved in the adsorption of an adsorbate by an adsorbent and to regenerate the adsorbent for economic success. In the present study, desorption was explored, varying

the pH from 4.0 to 10.0 and keeping the adsorbent dosage constant at 300 mg L⁻¹. An increase in pH favored ACT desorption from MCS@MWCNTs because of electrostatic repulsion between negatively charged sites on the adsorbent surface and ACT molecules. The feasibility of using MCS@MWCNTs in successive adsorption-desorption cycles was examined by contacting 45 mg L⁻¹ ACT solution with 400 mg L⁻¹ recycled adsorbent at pH 10.0. Under these conditions, ACT removal by MCS@MWCNTs and recycled MCS@MWCNTs was 98.1% and 86.7%, respectively. Such a marked loss of sorption capacity suggests that the reuse of desorbed MCS@MWCNTs would need some regeneration before recycling.

4. Conclusions

The process was optimized using central composite design (CCD), a statistical tool used to optimize response surface methodology (RSM). A second-order polynomial model adequately fit the experimental data with an adjusted R^2 of 0.9270, showing that the model could efficiently predict the ACT removal. It was found that all selected variables significantly affect ACT removal efficiency. Under these conditions, the maximum adsorption capacity for MCS@MWCNTs was found to be 256.4 mg g⁻¹. The results showed that the Langmuir and the pseudo-second-order kinetic models presented better fittings for the adsorption equilibrium and kinetics data. This study showed that MCS@MWCNTs are a useful adsorbent for the removal of ACT from aqueous solutions.

5. Acknowledgements

The authors would like to express their appreciation to the student research committee of Kerman University of Medical Sciences [Grant number 400000753] for supporting the current work.

Funding: This work received a grant from the Kerman University of Medical Sciences [Grant number 400000753].

Conflict of interest: The authors declare that they have no conflict of interest regarding the publication of the current paper.

Ethical approval: The Ethics Committee of Kerman University of Medical Sciences approved the study (IR.KMU.REC.1400.503).

6. References

- [1] B. Zaied, M. Rashid, M. Nasrullah, A. Zularisam, D. Pant, L. Singh, A comprehensive review on contaminants removal from pharmaceutical wastewater by electrocoagulation process, *Sc. Total Environ.*, 726 (2020) 138095. <https://doi.org/10.1016/j.scitotenv.2020.138095>.
- [2] A. Kumar, M. Chandel, A. Sharma, M. Thakur, A. Kumar, D. Pathania, L. Singh, Robust visible light active PANI/LaFeO₃/CoFe₂O₄ ternary heterojunction for the photo-degradation and mineralization of pharmaceutical effluent: Clozapine, *J. Environ. Chem. Eng.*, 9 (2021) 106159. <https://doi.org/10.1016/j.jece.2021.106159>.
- [3] C.-C. Su, C.A. Cada Jr, M.L.P. Dalida, M.-C. Lu, Effect of UV light on acetaminophen degradation in the electro-Fenton process, *Sep. Purif. Technol.*, 120 (2013) 43-51. <https://doi.org/10.1016/j.seppur.2013.09.034>.
- [4] E. Bailey, H. Worthington, P. Coulthard, Ibuprofen and/or paracetamol (acetaminophen) for pain relief after surgical removal of lower wisdom teeth, a Cochrane systematic review, *British Dent. j.*, 216 (2014) 451. <https://doi.org/10.1038/sj.bdj.2014.330>.
- [5] M. Qutob, M. Rafatullah, M. Qamar, H.S. Alorfi, A.N. Al-Romaizan, M.A. Hussein, A review on heterogeneous oxidation of acetaminophen based on micro and nanoparticles catalyzed by different activators, *Nanotechnol. Rev.*, 11 (2022) 497-525. <https://doi.org/10.1515/ntrev-2022-0030>.
- [6] S. Wang, J. Wu, X. Lu, W. Xu, Q. Gong, J. Ding, B. Dan, P. Xie, Removal of acetaminophen in the Fe²⁺/persulfate system: Kinetic model and degradation pathways, *Chem. Eng. J.*, 358 (2019) 1091-1100. <https://doi.org/10.1016/j.cej.2018.09.145>.
- [7] H.N.P. Vo, G.K. Le, T.M.H. Nguyen, X.-T. Bui, K.H. Nguyen, E.R. Rene, T.D.H. Vo, N.-D.T. Cao, R. Mohan, Acetaminophen micropollutant: Historical and current occurrences, toxicity, removal strategies and transformation pathways in different environments, *Chemosphere*, 236 (2019) 124391. <https://doi.org/10.1016/j.chemosphere.2019.124391>.
- [8] Z.B. Khalid, M. Nasrullah, A. Nayeem, Z.A. Wahid, L. Singh, S. Krishnan, Application of 2D graphene-based nanomaterials for pollutant removal from advanced water and wastewater treatment processes, in: *Adapting 2D Nanomaterials for Advanced Applications*, ACS Publications, ACS Symposium Series, 1353 (2020) 191-217.

- <https://doi.org/10.1021/bk-2020-1353.ch009>.
- [9] I. Mustafa, Methylene blue removal from water using H₂SO₄ crosslinked magnetic chitosan nanocomposite beads, *Microchem. J.*, 144 (2019) 397-402. <https://doi.org/10.1016/j.microc.2018.09.032>.
- [10] H. Zeng, L. Wang, D. Zhang, P. Yan, J. Nie, V.K. Sharma, C. Wang, Highly efficient and selective removal of mercury ions using hyperbranched polyethylenimine functionalized carboxymethyl chitosan composite adsorbent, *Chem. Eng. J.*, 358 (2019) 253-263. <https://doi.org/10.1016/j.cej.2018.10.001>.
- [11] S. Wang, Y.-Y. Zhai, Q. Gao, W.-J. Luo, H. Xia, C.-G. Zhou, Highly efficient removal of acid red 18 from aqueous solution by magnetically retrievable chitosan/carbon nanotube: batch study, isotherms, kinetics, and thermodynamics, *J. Chem. Eng. Data*, 59 (2014) 39-51. <https://doi.org/10.1021/JE400700C>.
- [12] M. Abbas, M. Arshad, M. Rafique, A. Altalhi, D. Saleh, M. Ayub, S. Sharif, M. Riaz, S. Alshawwa, N. Masood, Chitosan-polyvinyl alcohol membranes with improved antibacterial properties contained *Calotropis procera* extract as a robust wound healing agent, *Arab. J. Chem.*, (2022) 103766. <https://doi.org/10.1016/j.arabjc.2022.103766>.
- [13] M. Jawaid, A. Ahmad, N. Ismail, M. Rafatullah, *Environmental remediation through carbon based nano composites*, Springer, 2021. <https://www.springer.com/series/8059>
- [14] K. Li, Q. Gao, G. Yadavalli, X. Shen, H. Lei, B. Han, K. Xia, C. Zhou, Selective adsorption of Gd³⁺ on a magnetically retrievable imprinted chitosan/carbon nanotube composite with high capacity, *ACS Appl. Mater. Interfaces*, 7 (2015) 21047-21055. <https://doi.org/10.1021/acsami.5b07560>.
- [15] F. Jamali-Behnam, A.A. Najafpoor, M. Davoudi, T. Rohani-Bastami, H. Alidadi, H. Esmaily, M. Dolatabadi, Adsorptive removal of arsenic from aqueous solutions using magnetite nanoparticles and silica-coated magnetite nanoparticles, *Environ. Prog. Sustain. Energy*, 37 (2018) 951-960. <https://doi.org/10.1002/ep.12751>.
- [16] K. Xu, Y. Wang, H. Zhang, Q. Yang, X. Wei, P. Xu, Y. Zhou, Solid-phase extraction of DNA by using a composite prepared from multiwalled carbon nanotubes, chitosan, Fe₃O₄ and a poly (ethylene glycol)-based deep eutectic solvent, *Microchim. Acta*, 184 (2017) 4133-4140. <https://doi.org/10.1007/s00604-017-2444-4>.
- [17] H. Alidadi, M. Dolatabadi, M. Davoudi, F. Barjasteh-Askari, F. Jamali-Behnam, A. Hosseinzadeh, Enhanced removal of tetracycline using modified sawdust: optimization, isotherm, kinetics, and regeneration studies, *Process Saf. Environ. Prot.*, 117 (2018) 51-60. <https://doi.org/10.1016/j.psep.2018.04.007>.
- [18] A. Fegousse, A. El Gaidoumi, Y. Miyah, R. El Mountassir, A. Lahrichi, Pineapple bark performance in dyes adsorption: optimization by the central composite design, *J. Chem.*, 2019 (2019) 3017163. <https://doi.org/10.1155/2019/3017163>.
- [19] R.A. Khera, M. Iqbal, A. Ahmad, S.M. Hassan, A. Nazir, A. Kausar, H.S. Kusuma, J. Niasr, N. Masood, U. Younas, Kinetics and equilibrium studies of copper, zinc, and nickel ions adsorptive removal on to *Archontophoenix alexandriae*: conditions optimization by RSM, *Desalin. Water Treat.*, 201 (2020) 289-300. <https://doi.org/10.5004/dwt.2020.25937>.
- [20] V.U. Siddiqui, A. Ansari, M.T. Ansari, M. Akram, W.A. Siddiqi, A.M. Alosaimi, M.A. Hussein, M. Rafatullah, Optimization of facile synthesized ZnO/CuO nanophotocatalyst for organic dye degradation by visible light irradiation using response surface methodology, *Catalysts*, 11 (2021) 1509. <https://doi.org/10.3390/catal11121509>.
- [21] S. Noreen, S. Ismail, S.M. Ibrahim, H.S.

- Kusuma, A. Nazir, M. Yaseen, M.I. Khan, M. Iqbal, ZnO, CuO and Fe₂O₃ green synthesis for the adsorptive removal of direct golden yellow dye adsorption: kinetics, equilibrium and thermodynamics studies, *Z. fur Phys. Chem.*, 235 (2021) 1055-1075. <https://doi.org/10.1515/zpch-2019-1599>.
- [22] A. Kausar, K. Naeem, M. Iqbal, H.N. Bhatti, A. Ashraf, A. Nazir, H.S. Kusuma, M.I. Khan, Kinetics, equilibrium and thermodynamics of dyes adsorption onto modified chitosan: a review, *Z. fur Phys. Chem.*, (2021). <https://doi.org/10.1515/zpc-2019-1586>.
- [23] P. Mishra, Z.A. Wahid, R.M. Zaid, S. Rana, S. Tabassum, A. Karim, L. Singh, M.A. Islam, X. Jaing, M. Sakinah, Kinetics and statistical optimization study of bio-hydrogen production using the immobilized photobacterium, *Biomass Convers. Biorefin.*, (2020) 1-12. <https://doi.org/10.1007/s13399-020-00835-6>.



Rapid analysis of chromium (III, VI) in water and wastewater samples based on Task-specific ionic liquid by the ultra-assisted dispersive ionic liquid-liquid microextraction

Vahid Saheb^a and Tayebeh Shamspur^{b,*}

^a Department of Chemistry, College of Science, Shahid Bahonar University of Kerman, Postal code: 7616914111, Kerman, Iran

^b Department of Chemistry, College of Science, Shahid Bahonar University of Kerman, 7616914111, Iran

ARTICLE INFO:

Received 28 Oct 2021

Revised form 10 Jan 2022

Accepted 4 Feb 2022

Available online 27 Mar 2022

Keywords:

Chromium III, VI;
 Water samples;
 2-Mercapto-1-methylimidazole;
 Dispersive ionic liquid-liquid
 microextraction,
 Electrothermal atomic absorption
 spectrometry

ABSTRACT

Exposure to hexavalent chromium (Cr VI) causes cancer in cells of the *human body*. So, the speciation and determination of the Cr (VI) and Cr (III) in water and human samples based on sensitive techniques are necessary. In this research, 2-mercapto-1-methylimidazole a novel Task-specific ionic liquid ($C_4H_6N_2S$; *HS-CH₃-IM*) was used with a new approach for speciation of Cr (III, VI) from water samples by ultra-assisted dispersive ionic liquid-liquid microextraction procedure (USA-D-ILLME). Due to the procedure, 100 mg of *HS-CH₃-IM* and 0.2 mL of acetone were mixed and injected into 10 mL of water or standard Cr (III) and Cr (VI) solution in the conical tube. After stirring for 5 min, the Cr (VI) and Cr (III) were extracted with a positive and negative charge of the thiol group (HS^{2+} , HS^-) in pH 2 or 8 and pH 5, respectively. The mixture of the *HS-CH₃-IM* was collected at the bottom of the conical tube by centrifuging. The upper liquid phase was vacuumed with a peristaltic pump and the Cr (III, VI) loaded on the *HS-CH₃-IM* was back-extracted in a liquid solution. Finally, the concentration of the Cr (III, VI) ions in a remained solution were measured with ET-AAS after dilution up to 0.5 mL with DW. The total chromium was determined in water samples by summarizing the Cr (VI) and Cr (III) contents. All parameters such as the amount of *HS-CH₃-IM*, the sample volume, pH, and the shaking/centrifuging time were optimized. Under the optimal conditions, good linear range (LR), LOD, and enrichment factor (EF) were obtained 0.05–1.7 $\mu\text{g L}^{-1}$, 15 ng L^{-1} , and 19.82 respectively (RSD% < 1.45). The procedure was validated by spiking samples and good accuracy and precision results were achieved.

1. Introduction

Heavy metals have a toxic effect on environmental matrixes (air, soil, water). they can enter from waters, food, or vegetables and accumulate in brain, liver, or renal tissues. A trace amount of heavy

metals can cause cellular damage in the human body. Chromium(VI) is a major pollutant for the environment and enters from many sources such as chemical industries, steelworks, and electroplating. The chromium cause diseases such as gene mutations, carcinogen effect, and DNA lesions in human [1,2]. Two different oxidation forms of chromium exist in the environment (Cr III and Cr VI). Cr (III)

*Corresponding Author: Tayebeh Shamspur

Email: tsh@uk.ac.ir

<https://doi.org/10.24200/amecj.v5.i01.170>

compounds have an important role in the metabolism of glucose and protein in humans [3]. Moreover, the Cr (VI) has carcinogenic effects in cell tissues with a strong oxidation potential in the human body which enables to provide damage to DNA. Also, Cr (VI) is harmful to the lungs and kidneys [4,5]. Chromium values in drinking water are lower than $2 \mu\text{g L}^{-1}$ [6]. The World Health Organization (WHO) was reported that the genotoxicity of Cr (VI) in humans is $50 \mu\text{g L}^{-1}$. The ACGIH announced the normal range for chromium levels in human blood and urine were achieved at $1.8 \mu\text{g L}^{-1}$ and $2.0 \mu\text{g L}^{-1}$, respectively [7,8]. The Federal Committee on drinking water (FCDW) has reported new information on Cr(III, VI) and guideline technical documents on Cr(III, VI) in drinking water. The FCDW showed a maximum acceptable concentration (MAC) of $50 \mu\text{g L}^{-1}$ to Cr(VI). This document focuses on the health effects of Cr(VI) and total chromium considered about $100 \mu\text{g L}^{-1}$. Some of the analytical methods measure the total chromium Cr(III, VI) in drinking water at the lower limit of the reported MAC [9]. Many sample preparations based on adsorbents or ligands were used for extraction chromium from water samples. In addition, Cr(III) is likely to be converted to oxidized form [Cr(VI)] after sample preparation. Therefore, it is important to analyze chromium species and total chromium (TCr) in waters. In conventional studies, the best method for the treatment TCr is coagulation based on filtration and ion exchange [10]. Coagulation-based filtration and ion exchange are favorite methodologies for extracting Cr(VI) from drinking water. The drinking water treatment technologies able to be certified to international standards for reduction of TCr, Cr(VI), and Cr(III) individually, include adsorption, reverse osmosis, and distillation [11]. Recently, the different techniques, include, ion chromatography (IC), inductively coupled plasma mass spectrometry (ICP-MS) [12], stripping voltammetry (SV) [13], co-precipitation [14], flame atomic absorption spectrometry (F-AAS) [15], inductively coupled plasma optical emission spectrometry (ICP-OES) [16], ion chromatography inductively coupled plasma-mass spectrometry (IC-ICP-MS) [17] and

electrothermal atomic absorption spectrometry (ETAAS) [18] were used for determination of chromium species in water samples. Due to difficulty matrixes and low detection for chromium in water samples, treatment process such as liquid-liquid extraction (LLE) [19], dispersive liquid-liquid microextraction (DLLME) [20], magnetic solid-phase extraction (SPE) [21], dithiocarbamate-modified magnetite nanoparticles (DC-MNPs) [22] and cloud point extraction (CPE) [23] are developed. Dispersive liquid-liquid microextraction (DLLME) is a conventional technique, where the extraction phase (a microliter of hydrophobic solvent) was dispersed in the water sample. Many organic solvents (ethanol, methanol, toluene) were used in the extraction phase. Recently, ionic liquids (IL) as green solvent, low vapor pressure, high stability, and large viscosity have been used in LLE [24,25].

The aim of this study is the speciation of Cr (III) and Cr (VI) in water samples based on HS-CH₃-IM by the USA-D-ILLME procedure. The important parameters for the extraction of chromium were optimized and the concentration of chromium was determined by ET-AAS.

2. Experimental

2.1. Instrumental

Chromium was determined with an atomic absorption spectrometer (AAS, GBC Plus 932, Australia) using a graphite furnace accessory (GF3000, ET-AAS). The main parameters such as temperature (ash, atomized, drying), auto-sampler into graphite tube, flowrate Ar gas, and temperature programming for the chromium were adjusted by the book manufacturer. A hollow cathode lamp of chromium (HCLcr) tuned at a current (6 mA) and a wavelength of 357.9 nm with a slit of 0.2 nm was used. The linear range ($1.5\text{--}33 \mu\text{g L}^{-1}$) and sample injection of $20 \mu\text{L}$ was used (Peak Area). The pH of samples was controlled by a digital pH meter (Metrohm 744). A centrifuge and shaker (Germany, Product N: SIAL311GZ2F) was used for dispersing and separating IL from samples. For validation results, ICP-MS (Perkin Elmer) was used for ultra-trace determination of chromium in standard and water samples.

2.2. Reagents and materials

Ultra-trace reagents with HPLC or AAS analytical grade purchased from Merck or Sigma Co. (Germany). The modifier for chromium [$\text{Mg}(\text{NO}_3)_2$] for increasing ashing temperature, hexane, ethanol, acetone, HNO_3 , H_2SO_4 , and HCl were prepared from Merck, Germany. The standard solution of Cr (III) was prepared from an appropriate amount of $\text{Cr}(\text{NO}_3)_3$ in $0.01 \text{ mol L}^{-1} \text{ HNO}_3$ ($1000 \text{ mg L}^{-1} \text{ Cr III}$, 1.0 g L^{-1}). The standard solution of Cr (VI) was purchased from Merck which was prepared by 1.0 g of K_2CrO_4 in 1% HCl ($1000 \text{ mg L}^{-1} \text{ CrVI}$). The standard solutions for the or calibration curve of chromium ($0.1, 0.2, 0.4, 0.5, 1.0, 1.5 \mu\text{g L}^{-1}$) were prepared daily by dilution of the stock solution. The pH adjustments were made using appropriate buffer solutions including sodium phosphate for pH 2.0-2.5, ammonium acetate for pH 4.0-5.5 and ammonium chloride for pH 8-10 (Merck). 2-Mercapto-1-methylimidazole as Task-specific ionic liquid was purchased from Sigma, Germany ($\text{HS-CH}_3\text{-IM}$, CAS N: 60-56-0, 25 g). Ultra-pure water (DW) was obtained from a pure Water System (RIPI).

2.3. Water Sampling

The glass tubes were washed with HNO_3 solution (1 M) for two days and rinsed 10 times with DW. Due to low concentrations of chromium in water samples, even trace contamination, and sample storage caused to affect the accuracy of the results. The acidified water sample was put into the conical tube ($10\text{-}20 \text{ mL}$) and kept at -20°C . After filtering, water samples were prepared from river water from Karaj, well water from Varamin city, drinking water

from Tehran city, industrial wastewater, Tehran, Iran prepared by ASTM procedure for waters.

2.4. Extraction Procedure

A pre-concentration procedure based on $\text{HS-CH}_3\text{-IM}$ by the USA-D-ILLME was performed as follows: first, 100 mg of $\text{HS-CH}_3\text{-IM}$ as a TSIL, 0.2 mL of acetone were mixed and injected into 10 mL of water and chromium standard samples (Fig.1). After shaking for 5 min , the Cr VI and Cr III were extracted by thiol group of $\text{HS-CH}_3\text{-IM}$ at pH 2 and 5, respectively. For optimizing, 10 mL of $0.1 - 1.5 \mu\text{g L}^{-1} \text{ Cr (III)}$ and Cr (VI) standard solutions as the lower and upper limit of quantification was used instead of water samples in a conical centrifuge tube. First, 100 mg of $\text{HS-CH}_3\text{-IM}$ dispersed in 0.2 mL of acetone in a 1 mL syringe and injected to 10 mL of chromium standard in a conical tube. The pH was adjusted at 2 and 5 by the buffer solutions, then the mixture solution was shaken for 5 min , and chromium extracted by TSIL at 25°C . To separation phase, the turbid solution was centrifuged for 5 min at 4000 rpm and the liquid phase was vacuumed with an autosampler. Then, Cr (III) and Cr (VI) were back-extracted from TSIL in acidic and basic by adding 0.25 mL of $1.2 \text{ mol L}^{-1} \text{ HNO}_3$ and 0.2 mL of $1.0 \text{ mol L}^{-1} \text{ NaOH}$, respectively. Finally, the remained aqueous phase was determined by ET-AAS after dilution with DW up to 0.5 mL . In the optimum pH conditions, total chromium was calculated by summarizing Cr (VI) to Cr (III) contents. The blank solutions proceeded in the same way and were used for the calibration ET-AAS. The extraction conditions based on the $\text{HS-CH}_3\text{-IM}$ (IL) for chromium speciation were shown in Table 1.



Fig.1. The extraction and speciation chromium based on $\text{HS-CH}_3\text{-IM}$ by the USA –D-ILLME procedure

Table 1. Extraction conditions for chromium (III, VI) based on *HS-CH₃-IM* by the USA –D-ILLME method

Parameters	Value
pH	4 for Cr(III) and 2 for Cr(VI)
Sample volume	10 mL
Volume of back-extraction reagents	0.2 mL for KOH/0.25 mL for HNO ₃
Volume of Buffer (0.1-0.2 mol L ⁻¹)	1 mL
Concentration of back-extraction	1.0 mol L ⁻¹ for KOH/1.2 mol L ⁻¹ for HNO ₃
Amount of IL	100 mg
Volume of Acetone	200 mL
Shaking time	5 min
Centrifugation time	5 min

3. Results and discussion

The TSIL (*HS-CH₃-IM*) with the USA-D-ILLME procedure was used for chromium speciation in the standard solution and water samples. The results showed us, the mean concentrations of Cr (III and VI) in wastewater samples were significantly higher than water samples [(5.13 ± 0.22 µg L⁻¹, 3.92 ± 0.18 µg L⁻¹) and (0.19 ± 0.02µg L⁻¹, 0.12 ± 0.01 µg L⁻¹)], respectively.

The extraction recovery (Equation 1) was obtained as the percentage of the ratio of the extraction chromium (C_{ex}) into the IL phase vs total chromium in water (C_{total}).

$$\text{Extraction Recovery} = \left(\frac{C_{ex}}{C_{total}} \right) \times 100 = \left[\frac{C_{ex} V_{coil}}{C_r V_{aq}} \right] \times 100 \quad (\text{Eq. 1})$$

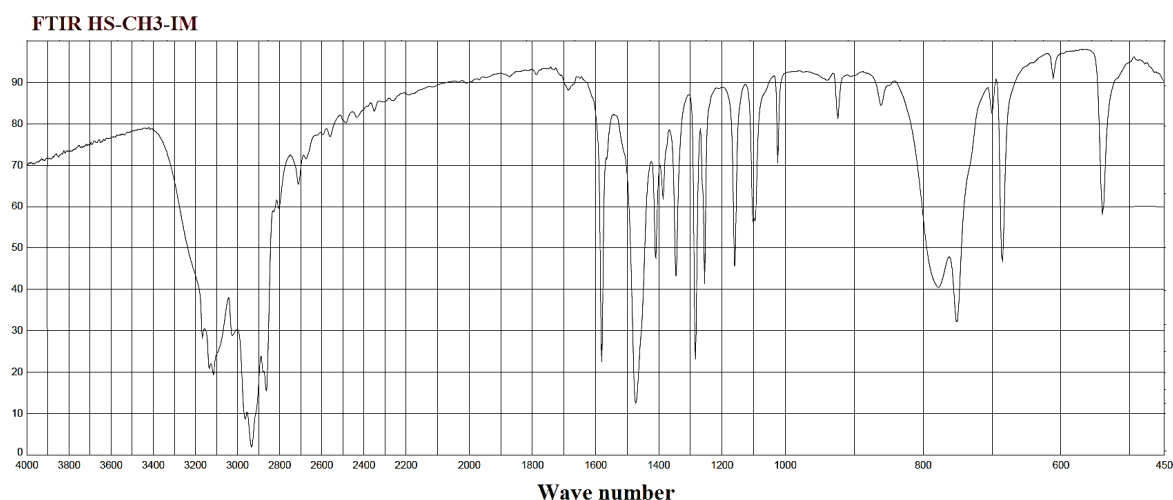
3.1. FTIR spectrum

The FT-IR spectra of *HS-CH₃-IM* are presented in Figure 2. The peak of FT-IR spectra at 1600 cm⁻¹

is related to C=O bond vibration of the carboxylic acid groups. The spectrum shows a band around 3100 cm⁻¹ which can be attributed to the hydroxyl groups. In addition, bands around 2900 cm⁻¹ are due to regular C-H stretching of the CH₂ groups of *HS-CH₃-IM*.

3.2. PH effect

The effect of pH on extraction of Cr (III) and Cr(VI) ions on the *HS-CH₃-IM* as a TSIL was investigated using different pH from 2 to 12 for 0.1 µg L⁻¹ Cr (III) and Cr(VI) ions as a lower LOQ and 1.5 µg L⁻¹ Cr (III) and Cr(VI) ions as upper LOQ. The extraction was strongly dependent on the pH of solutions and subsequently affected recovery. The results show that the highest extraction efficiency for Cr (III) was achieved at pH 4 to 6 by the thiol group of the *HS-CH₃-IM* and the Cr (VI) extracted at pH 2-3. Thus, the procedure was applied to speciation of two forms of chromium at pH 5 and 2 for the Cr (III)

**Fig.2.** FTIR spectra for *HS-CH₃-IM*

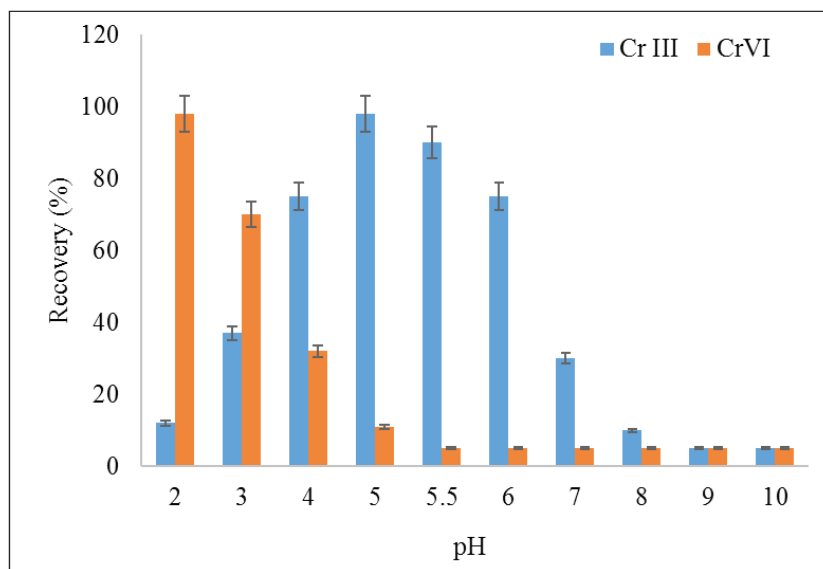


Fig.3. Effect of pH on extraction and speciation of Cr (III) and Cr(VI) ions based on *HS-CH₃-IM* by the USA –D-ILLME procedure

and Cr(VI), respectively (Fig. 3). The mechanisms of Cr (III) and Cr(VI) ions on the *HS-CH₃-IM* were obtained by complex formation between Cr (III) and Cr(VI) ions and HS groups of the *HS-CH₃-IM* at optimized pH. The HS can be deprotonated (SH^-) at a wide range of pH from 4 to 9. The extraction efficiency of Cr (III) can be attributed to the affinities of HS of the *HS-CH₃-IM* as a TSIL for the Cr^{3+} cations existing at pH from 4 to 6. The different anionic species of Cr (VI) exist at low and high pH (pH=2 and pH > 8), namely HCrO_4^- , CrO_4^{2-} and $\text{Cr}_2\text{O}_7^{2-}$ and negatively charged of anionic species can be extracted by positive charges of SH^{2+} group.

3.3. Sample volume

Sample volume is the main parameter for the extraction of chromium in the water sample. So, the effect of sample volume was studied in a range of 2- 25 mL for 0.1 - 1.5 $\mu\text{g L}^{-1}$ of Cr (III) and Cr(VI), respectively. High extraction was obtained between 2 mL and 12 mL of the water sample. At more volumes, the extraction efficiency was decreased. On the other hand, TSIL can be soluble partially in water at higher sample volumes and cause non-reproducible results. Therefore, a sample volume of 10 mL was used for this study with *HS-CH₃-IM* by the USA-D-ILLME method (Fig. 4).

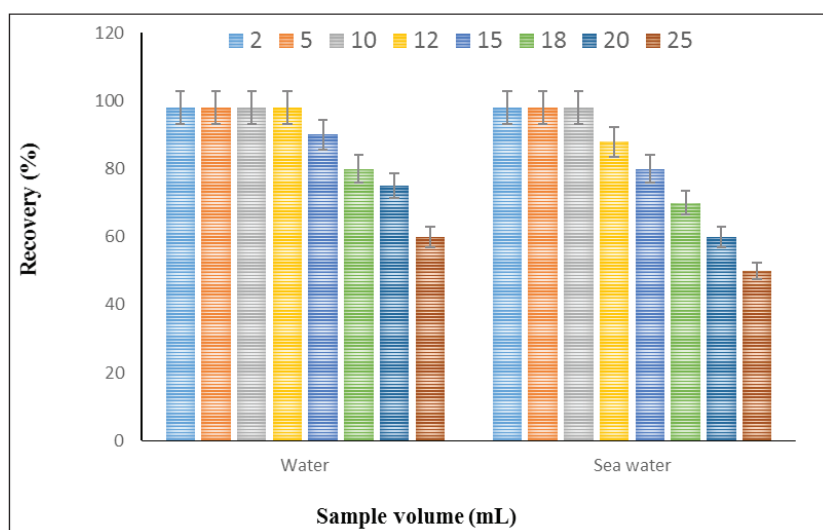


Fig. 4. Effect of sample volume on extraction and speciation of Cr (III) and Cr(VI) ions based on *HS-CH₃-IM* by the USA –D-ILLME procedure

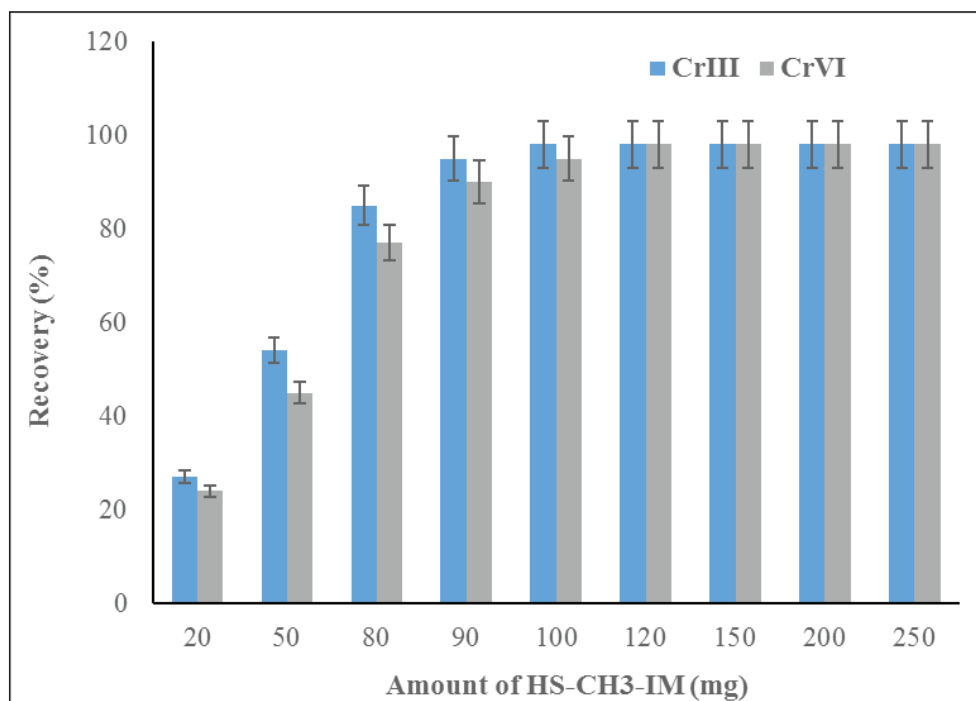


Fig. 5. Effect of *HS-CH₃-IM* on extraction and speciation of Cr (III) and Cr(VI) ions by the USA –D-ILLME procedure

3.4. Amount of *HS-CH₃-IM*

The results showed us that the extraction efficiency of Cr (III) and Cr(VI) ions was remarkably affected by the amount of TSIL. Therefore, the amount of TSIL was evaluated within the range of 50–250 mg. The extraction recovery was observed at more than 80 mg TSIL. So, 100 mg of TSIL (*HS-CH₃-IM*) was chosen as optimum IL for extraction of Cr (III) and Cr(VI) ions in water samples at pH 2 and 5 by the HS group (Fig. 5). For salty water such as seawater, 120 mg of TSIL for 10 mL of seawater must be used at optimized pH.

3.5. Centrifuge and sonication time

The sonication and centrifuge time are crucial to achieving an efficient extraction based on *HS-CH₃-IM* by the USA-D-ILLME procedure. In this research, the various sonication and centrifuge times between 1-10 min was evaluated for chromium extraction in water samples. The result showed us, by increasing the sonication time the relative response for extraction of chromium

increased and reached the maximum value at 4.5 seconds for *HS-CH₃-IM*, and then remained constant. Therefore, the ultrasonic times of 5.0 minutes for the Cr (III) and Cr(VI) extraction was used. Also, the centrifuge time of 5.0 minutes was selected for Cr (III) and Cr(VI) extraction in water.

3.6. Effect of reagents on back-extraction

Due to the viscosity and organic structure of ionic liquids, injection of IL into the graphite tube of the furnace of ETAAS was not possible. So, based on the USA-D-ILLME procedure, Cr (III) and Cr(VI) were back-extracted from the *HS-CH₃-IM* with acid and base reagents. Due to previous research, decreasing pH leads to dissociation and releasing of chromium ions released into the aqueous phase by decreasing or increasing pH. So, the different concentrations of reagents such as HCl, HNO₃, H₂SO₄, KOH (0.5 -2.0 mol L⁻¹) were used for chromium back-extraction from the TSIL (Fig. 9). The research showed that 1.2 mol L⁻¹ of HNO₃

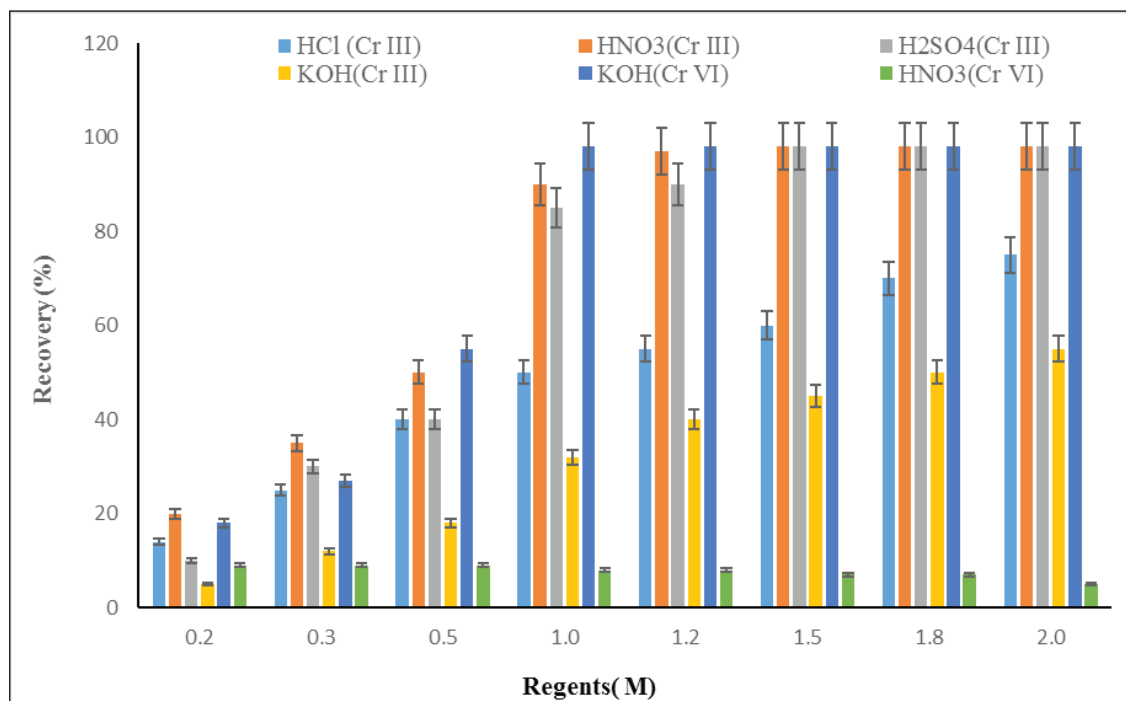


Fig. 6. Effect of reagents (acid and base) on back-extraction of Cr (III) and Cr(VI) ions by the USA –D-ILLME procedure

(0.25 mL) can be back-extracted Cr (III) from the HS-CH₃-IM to the liquid phase. Also, 1.0 mol L⁻¹ of KOH (0.2 mL) can be back-extracted Cr (VI) from the HS-CH₃-IM phase. After back-extraction, the resultant solution was adjusted to 0.5 mL with DW in a centrifuge conical tube before determining by ET-AAS (Fig. 6).

3.7. Validation of methodology

The USA –D-ILLME method was applied to determine Cr (VI) and Cr (III) found in 10 mL of water samples. The Cr (VI) and Cr (III) in wastewater and water samples were evaluated (20 n). The mean concentration of Cr (VI) and Cr (III) in wastewater was higher than in water samples. Also, the mean concentration of Cr (VI) in well water was lower than Cr (III) concentration. The coloration analysis was achieved between Cr (III) and Cr (VI) in industrial water and drinking waters and there was a high correlation ($r > 0.66$). In addition, in drinking waters, no correlation and regression were shown between Cr (III) and Cr

(VI) ($r > 0.12$). The spiked water and wastewater samples were used to demonstrate the reliability and validation of the method for speciation and determination of Cr (III) and Cr (VI) (Table 2). By back-extraction process, the remaining solution was spiked with standard solutions of Cr (VI) and Cr (III) and analyzed with ET-AAS after extraction based on the HS-CH₃-IM by the USA-D-ILLME method (Table 3). The recovery of spiked samples is satisfactory results, which shows the ability of the procedure for determination and speciation of the Cr (VI) and Cr (III)

in water samples. For validation of the proposed method, certified reference materials in waters (CRM) were obtained by ICP-MS. The spiking CRM with the chromium standard solution showed us the validation of methodology for speciation and determination of Cr (VI) and Cr (III) in water samples (Table 4). Due to results, high efficiency and accuracy were achieved for the determination and speciation of Cr (VI) and Cr (III) in water samples.

Table 2. The coloration analysis for chromium determination of wastewater and water samples in different cities, Iran (n=20, $\mu\text{g L}^{-1}$)

City	*Wastewater (n=20)		water (n=20)		Wastewater	
	Cr ^{III}	Cr ^{VI}	Cr ^{III}	Cr ^{VI}	r	P-value
Tehran	1.07 ± 0.77	4.28 ± 0.04	0.09 ± 0.22	0.11 ± 0.02	0.098	<0.002
Karaj	2.51 ± 0.03	2.03 ± 0.69	0.14 ± 0.02	0.07 ± 0.04	0.331	<0.001
Kerman	0.75 ± 0.13	1.94 ± 0.81	0.10 ± 0.11	0.06 ± 0.05	0.113	<0.005

*Wastewater diluted with DW up to 50 mL (1:5)

Table 3. Validation of chromium speciation based on the HS-CH₃-IM with spiking water samples by the USA-D-ILLME method

Sample*	Added ($\mu\text{g L}^{-1}$)		*Found ($\mu\text{g L}^{-1}$)		Total	Recovery (%)	
	Cr (III)	Cr (VI)	Cr (III)	Cr (VI)		Cr (III)	Cr (V)
Water 1	---	---	1.235 ± 0.034	1.028 ± 0.037	2.263 ± 0.088	---	---
	1.0	---	2.205 ± 0.104	1.055 ± 0.032	3.260 ± 0.126	97.0	---
	---	1.0	1.229 ± 0.029	1.996 ± 0.097	3.225 ± 0.127	---	96.8
Water 2	---	---	0.224 ± 0.012	0.188 ± 0.013	0.412 ± 0.022	---	---
	0.2	---	0.419 ± 0.019	0.191 ± 0.012	0.610 ± 0.028	97.5	---
	---	0.2	0.226 ± 0.011	0.393 ± 0.021	0.619 ± 0.031	---	102.5
**Wastewater 1	---	---	4.213 ± 0.186	2.450 ± 0.105	6.663 ± 0.298	---	---
	2.0	---	6.197 ± 0.304	2.447 ± 0.094	8.644 ± 0.386	99.2	---
	---	2.0	4.198 ± 0.191	4.406 ± 0.178	8.604 ± 0.411	---	97.8
**Wastewater 2	---	---	2.155 ± 0.086	3.175 ± 0.128	5.330 ± 0.237	---	---
	2.0	---	4.163 ± 0.204	3.179 ± 0.132	7.342 ± 0.335	100.4	---
	---	3.0	2.162 ± 0.094	6.104 ± 0.275	8.266 ± 0.403	---	97.6
Water 5	---	---	0.532 ± 0.025	0.082 ± 0.004	0.614 ± 0.031	---	---
	0.5	---	1.026 ± 0.045	0.079 ± 0.003	1.105 ± 0.048	98.8	---
	---	0.1	0.528 ± 0.024	0.177 ± 0.005	0.705 ± 0.032	--	95.0

*Mean of three determinations ± confidence interval (P = 0.95, n = 5)

**wastewater diluted with DW (1:5), so the result calculated after dilution factor (DF × 5)

Water 1: River water from Karaj

Water 2: Drinking water from Tehran city

Water 5: Well water from Varamin city

Table 4. Comparing chromium speciation and determination based on the HS-CH₃-IM/ET-AAS with CRM analysis by ICP-MS

CRM	ICP-MS ($\mu\text{g L}^{-1}$)			HS-CH ₃ -IM ($\mu\text{g L}^{-1}$)		
	Cr ^{III}	Cr ^{VI}	Total	Cr ^{III} Found	Cr ^{VI} Found	Total
SS ^a	0.205 ± 0.012	0.198 ± 0.010	0.403 ± 0.019	0.195 ± 0.013	0.211 ± 0.014	0.406 ± 0.021
	0.714 ± 0.031	0.508 ± 0.024	1.222 ± 0.048	0.698 ± 0.034	0.494 ± 0.026	1.192 ± 0.055
Water	---	---	1.321 ± 0.054	1.005 ± 0.054	0.318 ± 0.014	1.323 ± 0.068
	0.50	---	1.804 ± 0.086	1.493 ± 0.069	0.305 ± 0.018	1.798 ± 0.087
	---	0.50	1.818 ± 0.081	1.012 ± 0.051	0.811 ± 0.042	1.823 ± 0.093

*Mean of three determinations ± confidence interval (P = 0.95, n = 5)

^aSS: Standard Solution

4. Conclusions

In this study, a novel method based on HS-CH₃-IM as TSIL was used for the speciation and determination of the Cr (III) and Cr (VI) in water samples by the USA-D-ILLME procedure. The important factors for high extraction were optimized. By procedure, a sensitive, efficient, low cost, and simple method for speciation and preconcentration of the Cr (III) and Cr (VI) in water samples were achieved. Under optimized conditions, the working range (WR), LOQ, and RSD% were obtained 0.05–3.6 $\mu\text{g L}^{-1}$, 50 ng L^{-1} , and 1.45, respectively. The performance of the method for quantification analysis of chromium in water samples was obtained. The analytical performances of detection of Cr (III) and Cr (VI) in water samples are comparable to previously reported methods. Finally, the speciation chromium based on HS-CH₃-IM was revealed that most of Cr (VI) and Cr (III) exist in industrial wastewaters.

5. Acknowledgments

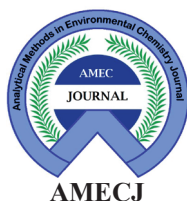
The authors thank from Department of Chemistry, College of Science, Shahid Bahonar University of Kerman, Iran

6. References

- [1] World Health Organization, Manganese in drinking-water: background document for development of WHO guidelines for drinking-water quality, World Health Organization, Geneva, 2004. <https://apps.who.int/iris/handle/10665/75376>.
- [2] J. Briffa, E. Sinagra, R. Blundell, Heavy metal pollution in the environment and their toxicological effects on humans, *Heliyon*, 6 (2020) e04691. <https://doi.org/10.1016/j.heliyon.2020.e04691>.
- [3] W. Feng, G. Mao, Q. Li, W. Wang, Y. Chen, T. Zhao, F. Li, Y. Zou, H. Wu, L. Yang, X. Wu, Effects of chromium malate on glycometabolism, glycometabolism-related enzyme levels and lipid metabolism in type 2 diabetic rats: A dose–response and curative effects study, *J. Diabetes. Investig.*, 6 (2015) 396-407. <https://doi.org/10.1111/jdi.12350>.
- [4] A. Houldsworth, W. R. A. Fisher, D. A. A. Millward, Proposed Relationships between the degree of insulin resistance, serum chromium Level/BMI and renal function during pregnancy and the pathogenesis of gestational diabetes mellitus, *Int. J. Endocrinol. Metab. Disord.*, 3 (2017)1-8. <http://dx.doi.org/10.16966/2380-548X.132>.
- [5] P. Baszuk, B. Janasik, S. Pietrzak, W. Marciniak, E. Reszka, K. Białkowska, E. Jabłońska, M. Muszyńska, M. Lesicka, R. Derkacz, T. Grodzki, J. Wójcik, M. Wojtyś, T. Dębniak, C. Cybulski, J. Gronwald, B. Kubisa, N. Wójcik, J. Pieróg, D. Gajci, P.

- Waloszczyk, R.J. Scott, W. Wąsowicz, A. Jakubowska, J. Lubiński, M.R. Lener, Lung cancer occurrence-correlation with serum chromium levels and genotypes, *Biol. Trace Elem. Res.*, 199 (2021) 1228-1236. <https://doi.org/10.1007/s12011-020-02240-6>.
- [6] G.B. Post, Recent US state and federal drinking water guidelines for per- and polyfluoroalkyl substances, *Environ. Toxicol. Chem.*, 40 (2021) 550-563. <https://doi.org/10.1002/etc.4863>.
- [7] American conference of governmental industrial hygienists, threshold limit values (ACGIH TLVs), new document for chemical substances, USA, 2018. <https://www.acgih.org/science/tlv-bei-guidelines/>.
- [8] National Institute for Occupational Safety and Health (NIOSH), occupational exposure to hexavalent chromium, centers for disease control and prevention, 2018. <https://www.cdc.gov/niosh/topics/hexchrom/default.html>.
- [9] R. Bevan, The first draft of the background document on chromium in drinking-water for the development of the WHO guidelines for drinking-water quality, World Health Organization. Geneva, 2019. https://www.who.int/water_sanitation_health/water-quality/guidelines/chemicals/draft-chromium-190924.pdf.
- [10] H. Peng, J. Guo, Removal of chromium from wastewater by membrane filtration, chemical precipitation, ion exchange, adsorption electrocoagulation, electrochemical reduction, electrodialysis, electrodeionization, photocatalysis and nanotechnology: a review, *Environ. Chem. Lett.*, 18 (2020) 2055-2068. <https://doi.org/10.1007/s10311-020-01058-x>.
- [11] A. Mnif, I. Bejaoui, M. Mouelhi, B. Hamrouni, Hexavalent chromium removal from model water and car shock absorber factory effluent by nanofiltration and reverse osmosis membrane, *Int. J. Anal. Chem.*, 2017 (2017) 7415708. <https://doi.org/10.1155/2017/7415708>.
- [12] D. Spanu, D. Monticelli, G. Binda, C. Dossi, L. Rampazzi, S. Recchia, One-minute highly selective Cr (VI) determination at ultra-trace levels: An ICP-MS method based on the on-line trapping of Cr (III), *J. Hazard. Mater.*, 412 (2021) 125280. <https://doi.org/10.1016/j.jhazmat.2021.125280>.
- [13] N. Thi Hue, N. Van Hop, H. Thai Long, N. Hai Phong, T.H. Uyen, L. Quoc Hung, N. Nhi Phuong, Determination of chromium in natural water by adsorptive stripping voltammetry using in situ bismuth film electrode, *J. Environ. Public Health*, 2020 (2020) 1347836. <https://doi.org/10.1155/2020/1347836>.
- [14] N.A. Yazid, Y.C. Joon, Co-precipitation synthesis of magnetic nanoparticles for efficient removal of heavy metal from synthetic wastewater, *AIP Conf. Proc.*, 2124 (2019) 020019. <https://doi.org/10.1063/1.5117079>.
- [15] E. Kazemi, A.M. Haji Shabani, S. Dadfarnia, F. Izadi, Speciation and determination of chromium ions by dispersive micro solid phase extraction using magnetic graphene oxide followed by flame atomic absorption spectrometry, *Int. J. Environ. Anal. Chem.*, 97 (2017) 1080-1093. <https://doi.org/10.1080/03067319.2017.1381693>.
- [16] T.S. Munonde, N.W. Maxakato, P.N. Nomngongo, Preconcentration and speciation of chromium species using ICP-OES after ultrasound-assisted magnetic solid phase extraction with an amino-modified magnetic nanocomposite prepared from Fe₃O₄, MnO₂ and Al₂O₃, *Microchim. Acta*, 184 (2017) 1223-1232. <https://doi.org/10.1007/s00604-017-2126-2>.
- [17] B.-H. Chen, S.-J. Jiang, A.C. Sahayam, Determination of Cr (VI) in rice using ion chromatography inductively coupled plasma mass spectrometry, *Food. Chem.*, 324 (2020) 126698. <https://doi.org/10.1016/j.foodchem.2020.126698>.
- [18] D.J. Butcher, Recent highlights in graphite furnace atomic absorption spectrometry,

- Appl. Spectrosc. Rev., 52 (2017) 755-773. <https://doi.org/10.1080/05704928.2017.1303504>.
- [19] M.B. Arain, I. Ali, E. Yilmaz, M. Soylak, Nanomaterial's based chromium speciation in environmental samples: A review, *TrAC, Trends Anal. Chem.*, 103 (2018) 44-55. <https://doi.org/10.1016/j.trac.2018.03.014>.
- [20] N. Campillo, P. Viñas, J. Šandrejová, V. Andruch, Ten years of dispersive liquid-liquid microextraction and derived techniques, *Appl. Spectrosc. Rev.*, 52 (2017) 267-415. <https://doi.org/10.1080/05704928.2016.1224240>.
- [21] Y.-W. Wu, J. Zhang, J.-F. Liu, L. Chen, Z.-L. Deng, M.-X. Han, X.-S. Wei, A.-M. Yu, H.-L. Zhang, Fe₃O₄@ZrO₂ nanoparticles magnetic solid phase extraction coupled with flame atomic absorption spectrometry for chromium (III) speciation in environmental and biological samples, *Appl. Surf. Sci.*, 258 (2012) 6772-6776. <https://doi.org/10.1016/j.apsusc.2012.03.057>.
- [22] A. Saboori, A nanoparticle sorbent composed of MIL-101(Fe) and dithiocarbamate-modified magnetite nanoparticles for speciation of Cr (III) and Cr (VI) prior to their determination by electrothermal AAS, *Microchim. Acta*, 184 (2017) 1509-1516. <https://doi.org/10.1007/s00604-017-2155-x>.
- [23] K.M. Diniz, C.R.T. Tarley, Speciation analysis of chromium in water samples through sequential combination of dispersive magnetic solid phase extraction using mesoporous amino-functionalized Fe₃O₄/SiO₂ nanoparticles and cloud point extraction, *Microchem. J.*, 123 (2015) 185-195. <https://doi.org/10.1016/j.microc.2015.06.011>.
- [24] E. Yıldız, H. Çabuk, Dispersive liquid-liquid microextraction method combined with sugaring-out homogeneous liquid-liquid extraction for the determination of some pesticides in molasses samples, *J. Sep. Sci.*, 44 (2021) 4151-4166. <https://doi.org/10.1002/jssc.202100551>.
- [25] F.C. Pinheiro, M.Á. Aguirre, J.A. Nóbrega, N. González-Gallardo, D.J. Ramón, A. Canals, Dispersive liquid-liquid microextraction based on deep eutectic solvent for elemental impurities determination in oral and parenteral drugs by inductively coupled plasma optical emission spectrometry, *Anal. Chim. Acta*, 1185 (2021) 339052. <https://doi.org/10.1016/j.aca.2021.339052>.



Sensitive voltammetry method for analysis of the antioxidant pyrogallol using a carbon paste electrode with CdS nanoparticle

Hamideh Asadollahzadeh^{a,*} and Mahdieh Ghazizadeh^a

^a Department of Chemistry, Faculty of Science, Kerman branch, Islamic Azad University, Kerman, Iran,
P. O. Box 7635131167, Kerman, Iran

ARTICLE INFO:

Received 12 Dec 2021

Revised form 7 Feb 2022

Accepted 28 Feb 2022

Available online 29 Mar 2022

Keywords:

Pyrogallol,
Analysis,
Carbon paste electrode,
Differential pulse voltammetry (DPV),
Cyclic voltammetry (CV),
CdS nanoparticles

ABSTRACT

A voltammetry method for the determination of pyrogallol (PY) was developed employing a carbon paste electrode (CPE) modified with CdS nanoparticle that was synthesized by microwave. The effect of different parameters i.e. time and irradiation power on the morphology and the sample's particle size have been investigated. The synthesized nanostructures were characterized by X-ray diffraction and scanning electron microscopy. The optimized condition for time and power consumption to prepare CdS nanoparticles was obtained 4 min and 360 W. Cyclic voltammetry study of the modified electrode indicated that the oxidation potential shifted towards a lower potential by approximately 106 mV and the peak current was enhanced by 2 fold in comparison to the bare CPE. The effect of pH and interferences from some inorganic salts and organic compounds were studied. The usability of this method for the quantification of pyrogallol was investigated with differential pulse voltammetry (DPV). Under the optimal conditions, the peak current was proportional to pyrogallol concentration in the range of 7.0×10^{-7} to 3.0×10^{-4} mol L⁻¹ with a detection limit of 4.8×10^{-7} mol L⁻¹. These values are satisfactory for application to real samples. Finally, the developed method was successfully used for the analysis of real samples.

1. Introduction

Pyrogallol is an important kind of polyphenol with a strong reduction property and has been widely used as a useful antioxidant and scavenger free radicals. Free radicals are chemical species possessing an unpaired electron that can be considered as fragments of molecules that are generally very reactive [1]. Oxidative stress is a phenomenon caused by an imbalance between the production and accumulation of oxygen reactive species (ROS) in cells and tissues and the ability of a biological

system to detoxify these reactive products. Oxidative stress is the cause of many human diseases like diabetes, thyroid disorders, hypertension, arthritis, etc [2, 3]. Antioxidants are compounds that act as inhibitors of oxidative damage [1]. Therefore, the determination of pyrogallol is very important in chemistry, environment, clinic, and biological system. There are several methods have been developed for the determination of pyrogallol, such as UV spectrophotometry [4], chromatography [5], electrochemiluminescence [6]. However, these instrumental methods have suffered some disadvantages such as being time-consuming, solvent usage intensive, and requiring expensive devices and maintenance [1]. Electroanalytical methods

*Corresponding Author: [Hamideh Asadollahzadeh](mailto:Hamideh.Asadollahzadeh@iaukerman.ac.ir)

Email: asadollahzadeh90@yahoo.com

<https://doi.org/10.24200/amecj.v5.i01.171>

represent a cheaper alternative with the possibility of field analysis. Modified electrodes have been widely used in sensitive and selective analytical methods for the detection of trace amounts of antioxidants [7-10]. These modified electrodes have shown good electrocatalytic properties, high surface-to-volume ratios, high stabilities, and fast electron transfer rates [8]. Nanomaterials may be mixed with electrode materials or may be attached to the electrode surface [11]. Carbon paste electrode has been extensively modified with nanomaterials and has been used to measure a wide range of compounds. This is due to modified electrodes with nanoparticles that can enhance the electrocatalytic property, stability, fast reaction rate, and reproducibility in the results. Various types of nanoparticles such as metal nanoparticles [12], metal oxides [13], and even composite nanoparticles [14-16] have been used to modify the electrodes. Several strategies based totally on bodily and chemical methods have been advanced for the synthesis of controlled size and form nanoparticles [17]. Examples of these procedures involve solvothermal techniques, template-assisted, kinetic increase management; sonochemical reactions, and thermolysis of unmarried-supply precursors in ligating solvents [17]. Microwave Irradiation (MWI) methods provide simple and speedy routes to the synthesis of nanoparticles on account that no excessive temperature or excessive strain is needed. The heating effect is generated by the interaction of the dipole moment of the molecules with electromagnetic radiation at high frequency. Moreover, MWI is specifically beneficial for a managed huge-scale synthesis that minimizes the thermal gradient consequences [18-20]. To our knowledge, no study has reported the electrocatalytic oxidation of pyrogallol by using CdS modified carbon paste electrode.

Thus, in the present work, CdS nanoparticles have been synthesized using a microwave irradiation process. In this process, changes in power and time of microwave irradiation caused different CdS morphologies. A modified carbon paste electrode is fabricated by using CdS nanoparticles for the determination of pyrogallol.

2. Experimental

2.1. Chemicals and Reagents

Pure pyrogallol, thioacetamide (TAA), sodium dihydrogen orthophosphate (NaH_2PO_4), disodium hydrogen phosphate (Na_2HPO_4), sodium phosphate (Na_3PO_4), orthophosphoric acid (H_3PO_4), sodium hydroxide (NaOH), hydrochloric acid (HCl), $\text{Cd}(\text{NO}_3)_2 \cdot 4\text{H}_2\text{O}$ and graphite powder were obtained from Merck. The buffer solutions were prepared from orthophosphoric acid and its salts in the pH range of 1 to 7. All the aqueous solutions were prepared by using double distilled water. High viscosity paraffin ($d = 0.88 \text{ kg L}^{-1}$) from Merck was used as the pasting liquid for the preparation of the carbon paste electrodes.

2.2. Apparatus

Electrochemical studies were performed using a Metrohm polarograph potentiostat-galvanostat (Metrohm Computrace 797-VA). Three-electrode system consisted of a bare CP and CdS/CP electrode as the working electrode, Ag/AgCl (3 M KCl) as the reference electrode, and a platinum wire as the auxiliary electrode. A Metrohm 691 pH/Ion meter was used for pH measurements. Solutions were degassed with nitrogen for 10 min prior to the recording of the voltammogram. X-ray diffraction (XRD) patterns were recorded by a Philips, X-ray diffractometer using Ni filtered Cu K α radiation. Scanning electron microscopy (SEM) images were obtained from LEO instrument model 1455VP.

2.3. Synthesis of CdS Nanoparticles

To synthesize CdS nanoparticles, 1mmol of $\text{Cd}(\text{NO}_3)_2$ was solubilized in 10 mL of water and stirred for 10 min. Subsequently, 0.1 mmol of thioacetamide has added to the solution and stirred for 15 min. Then the mixture was left for the reaction to proceed by cyclic microwave radiation at 360 W power for 4 min. Each cycle was 90 s long, and composed of 30 and 60 s for the on and off periods, respectively. The final precipitate was washed with water and ethanol, dried at 80 °C for 24 h.

2.4. Preparation of bare carbon paste electrode and modified carbon paste electrode

The modified carbon paste electrode was prepared by hand mixing 0.2 g of CdS nanoparticles with 0.9 g graphite powder with a mortar and pestle. Then paraffin was added to the above mixture and mixed for 30 min until a uniformly wetted paste was obtained. This paste was then packed into the end of a glass tube (ca. 3.35 mm i.d. and 10 cm long). Electrical connection implemented by a copper wire leads fitted into the tube. A fresh electrode surface was obtained by squeezing out a small portion of paste and polishing it with filter paper until a smooth surface was obtained. Unmodified CPE was prepared in the same way without adding CdS nanoparticles.

2.5. General procedure for the determination of pyrogallol

A 25 ml aqueous solution of analyte-containing 5 ml of 0.1 M phosphate buffer at pH 6 and a

specific amount of sample solution was added to the cell and purged with purified nitrogen for 5 min to remove oxygen (Fig 1) and CV and DPV voltammograms were recorded. The scanning potential was varied from 0 to 0.8 V. Cyclic voltammogram was recorded by the anodic potential scanning at scan rate 50 mVs⁻¹. A renewed surface electrode was used for each measurement.

3. Results and discussion

3.1. XRD analysis

The XRD pattern of the as-obtained CdS nanoparticles was shown in Figure 2. The diffraction peaks observed can be indexed to pure cubic phase CdS with cell constants $a = b = c = 5.3580 \text{ \AA}$ (JCPDS No. 05-0731). The XRD results proved the high crystallinity and purity of the products synthesized by this method. According to XRD data, the crystallite size

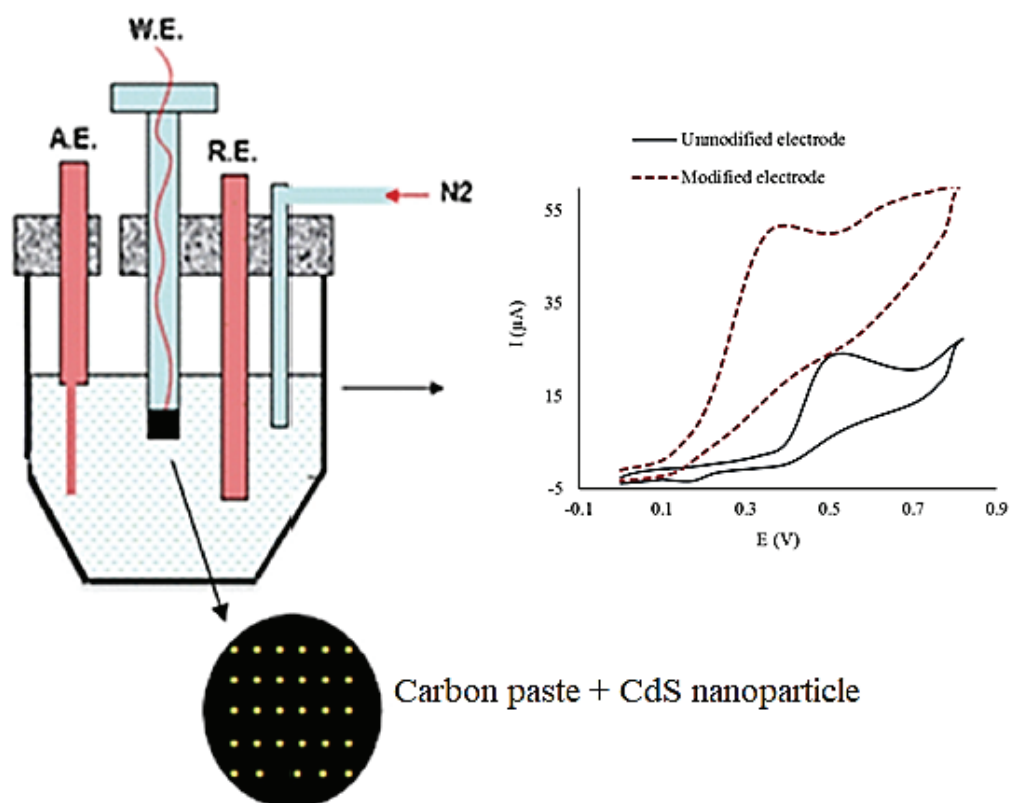


Fig 1. The procedure of voltammetry for determination of pyrogallol

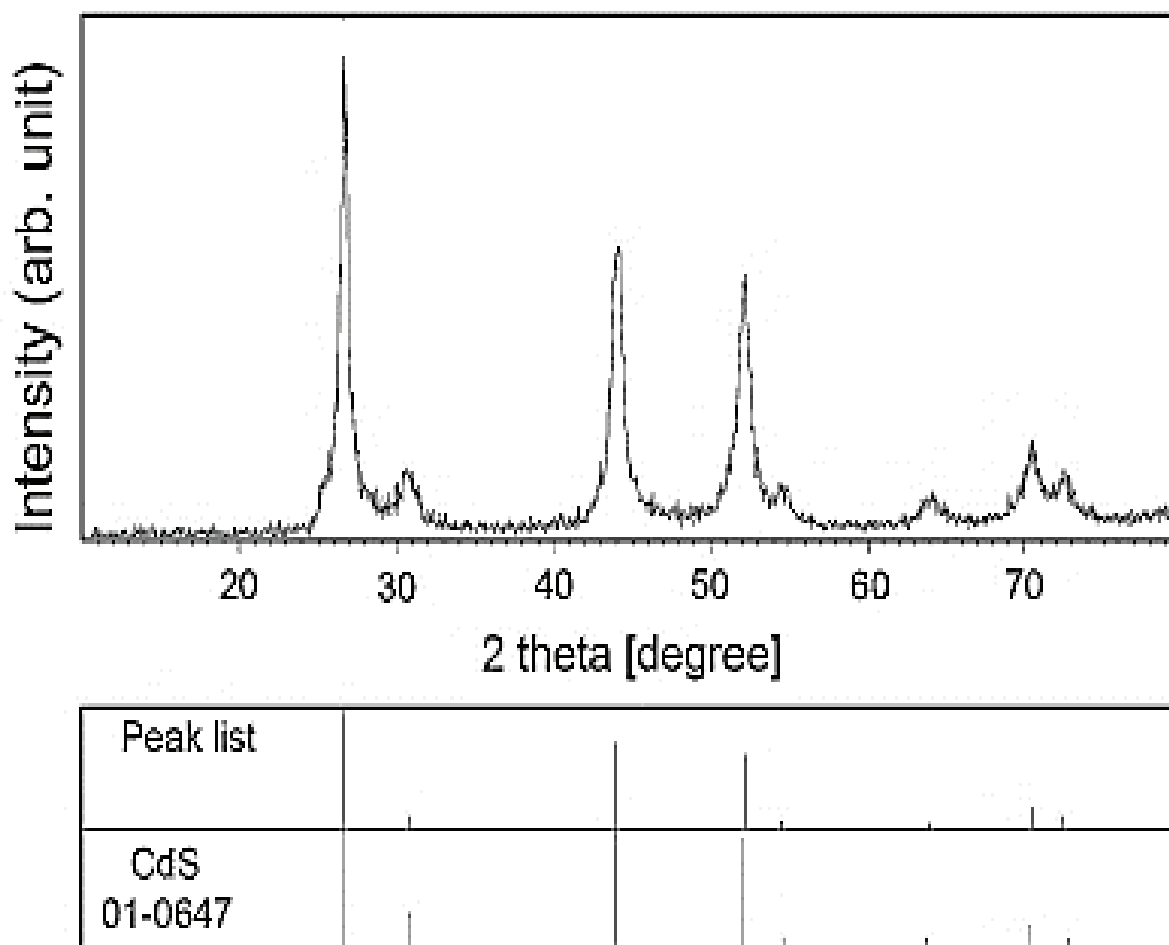


Fig. 2. XRD patterns of the synthesized CdS prepared by microwave irradiation

(Dc) of CdS nanoparticles can be determined by using the Debye-Scherrer formula. The obtained average particle size was found to be 45 nm. The dependence of morphology and the average particle sizes of the products on the irradiation power was also investigated.

3.2. Scanning electron microscopy

SEM images of the CdS obtained with thioacetamide in different powers of 180, 360, and 540 W are shown in Figure 3a–d respectively. As can be seen from SEM images, at 180 W power, due to the insufficient heat of the reaction, cohesive particles are formed. At 540 W, due to the very high energy produced in this power,

the nucleation of the particles is increased, and since the particles have a very active surface, large and cohesive masses are obtained in all test conditions. However, at 360 power, the reaction is faster due to the generation of more free radicals in solution and increased heat production due to the rotation of these active species. The formed nanoparticles have relatively smaller sizes and better distribution. Therefore, the sample prepared in 360 W power and 4 min time due to the creation of nanoparticles in nanometer size according to the scale of images and homogeneous distribution is an optimized condition for time and power consumption to prepare of CdS nanoparticles.

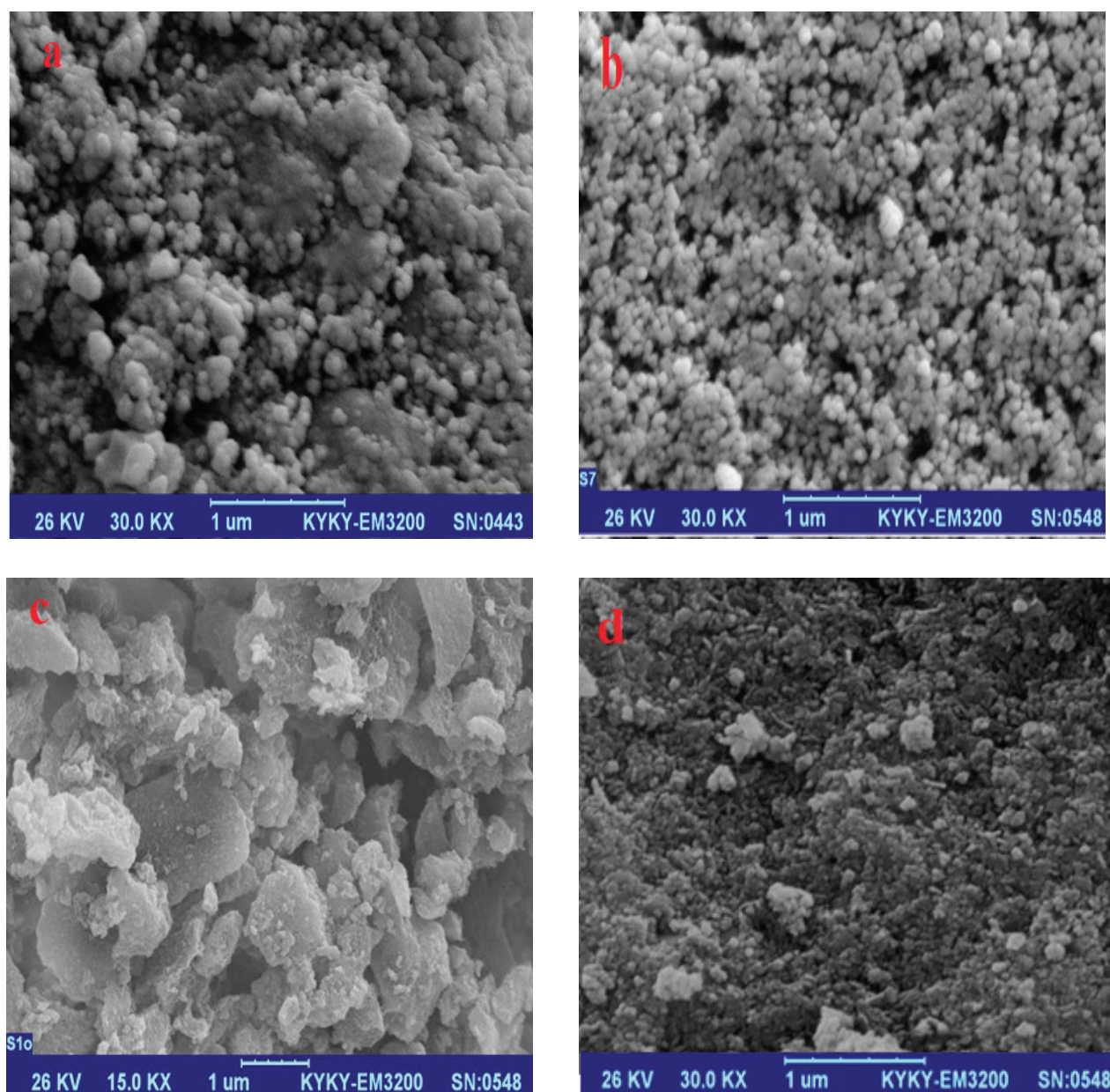


Fig. 3. SEM images of the CdS nanoparticles at (a) 180 W, (b) 360 W and (c, d) 540W

3.3. Electrochemical behavior of pyrogallol at the CdS/CPE

The electrochemical behavior of pyrogallol has been studied in two electrodes. Cyclic voltammetry (CV) was applied to investigate the electrochemical behavior of 0.4 mM pyrogallol in 0.1 M phosphate buffer at pH 6 with a bare CPE and a CdS/CPE (Fig. 4).

As shown in this Fig 3, in the presence of pyrogallol, an irreversible oxidation peak at 0.520

V on the bare CPE attributed to the electrochemical oxidation of pyrogallol. In the case of the CdS / CPE, the oxidation peak of pyrogallol decreased to 0.355 V and the peak current increased by 2.0 times compared with that for the bare CPE. These results suggested that CdS obviously accelerate the electron transfer at the electrode surface and improve the electrochemical performance accordingly.

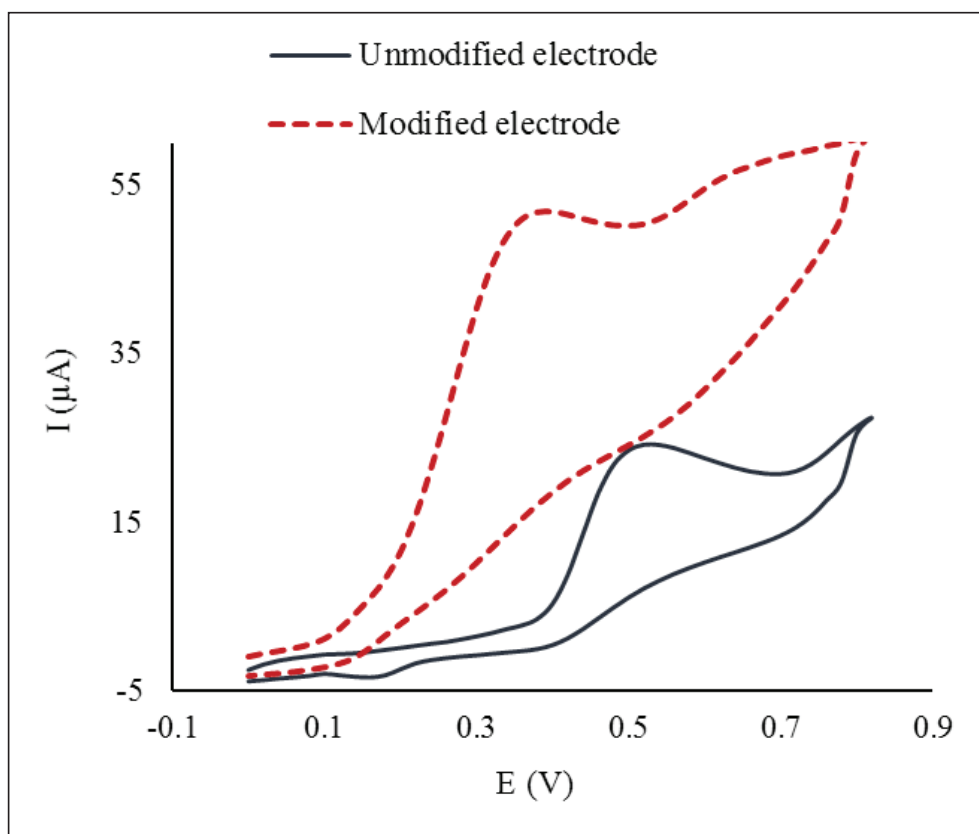


Fig. 4. Cyclic voltammograms of CPE and CdS/CPE at the presence of 0.4 mM pyrogallol in 0.1 phosphate buffer solution (pH 6) at scan rate 50 mVs⁻¹

3.4. Effect of pH

The effect of the pH of the solution on the electrochemical response of pyrogallol was investigated from pH 1.0 to 7. Due to [Figure 5](#), the anodic peak current of pyrogallol increased with increasing pH and the highest peak current was obtained at a pH of 6.0. Additionally, anodic potential peaks shifted by 165 mV to a more negative potential upon increasing pH, which is better for pyrogallol oxidation. Thus, a buffer solution with a pH of 6.0 was selected for further studies. In addition, the relationship between oxidation peak potential (E_{pa}) and pH value was also investigated and the results are shown in [Figure 5](#). As pH value increases from 1.0 to 7.0, the E_{pa} shifts linearly to a more negative potential, obeying the following equation: $E_{pa} = 631.3 - 55.4 \text{ pH}$, $R^2 = 0.9979$. (1) The slope of E_{pa}/pH is -55.4 mV , suggesting that the number of electrons and protons involved in the oxidation of pyrogallol is equal.

3.5. Effect of scan rate

The effect of scan rate on the electrocatalytic oxidation of pyrogallol at the CdS/CPE was investigated by cyclic voltammetry. As can be seen in [Figure 6a](#), the scanning potential increases the peak pyrogallol oxidation shifts to more positive potentials, which imposes a kinetic constraint on the electrochemical reaction. [Figure 6b](#) illustrates that a linear relationship existed between the oxidation peak currents of pyrogallol and the square root ($v^{1/2}$) of the scan rate in the range from 10 to 150 mVs⁻¹, indicating a diffusion-controlled process. The linear regression equation was expressed as $I_{(\mu\text{A})} = 4.178v^{1/2} + 10.657$ ($R^2 = 0.9925$).

3.6. Calibration curve

In order to develop a voltammetric method for the determination of the drug, the DPV mode is selected, because the peaks are sharper and better defined at lower concentrations of pyrogallol

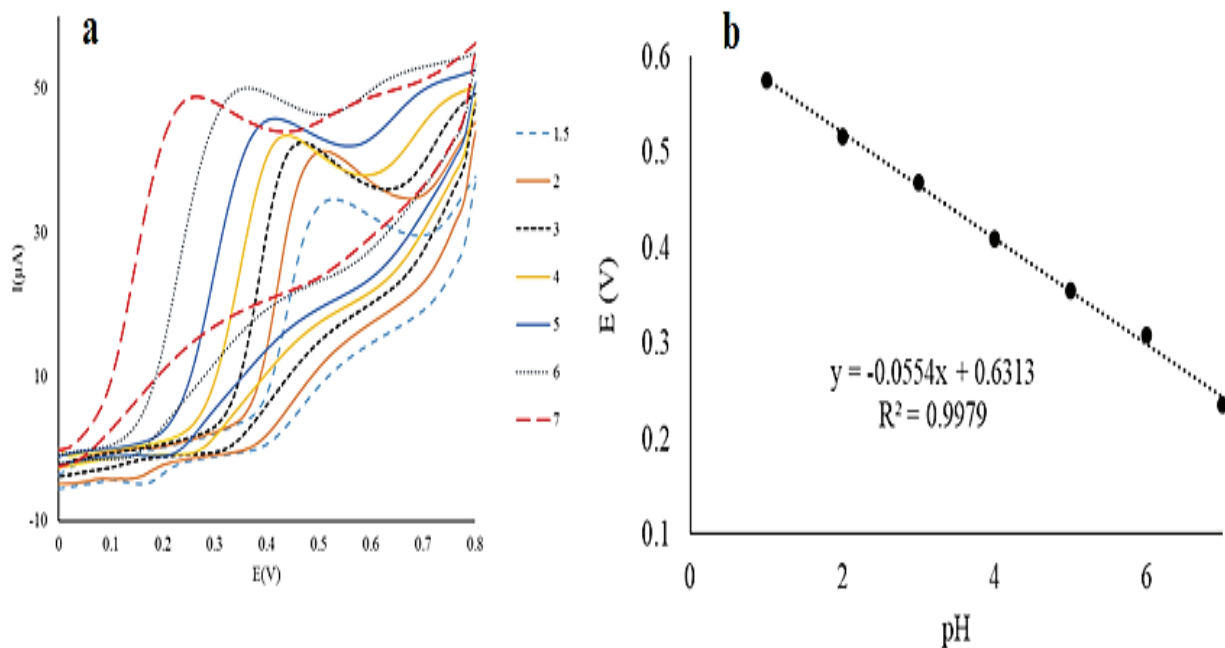


Fig.5. a) Cyclic voltammogram of pyrogallol at different pH
b) Relationship between the peak potential of pyrogallol and pH

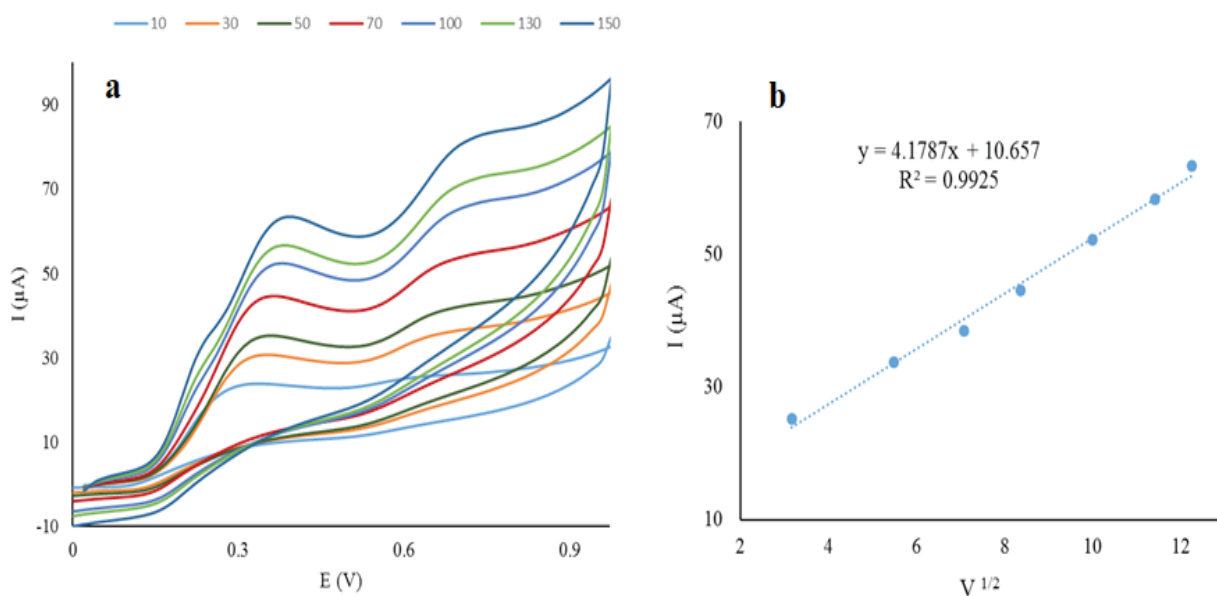


Fig. 6. (a) Cyclic voltammograms of Cds/CPE in the presence of 0.4 mM of pyrogallol in 0.1 phosphate buffer solution (pH 6) at different scan rates (from inner to outer): 10, 30, 50, 70, 100, 130 and 150 mV s⁻¹.
(b) peak current vs. square root of scan rate ($v^{1/2}$).

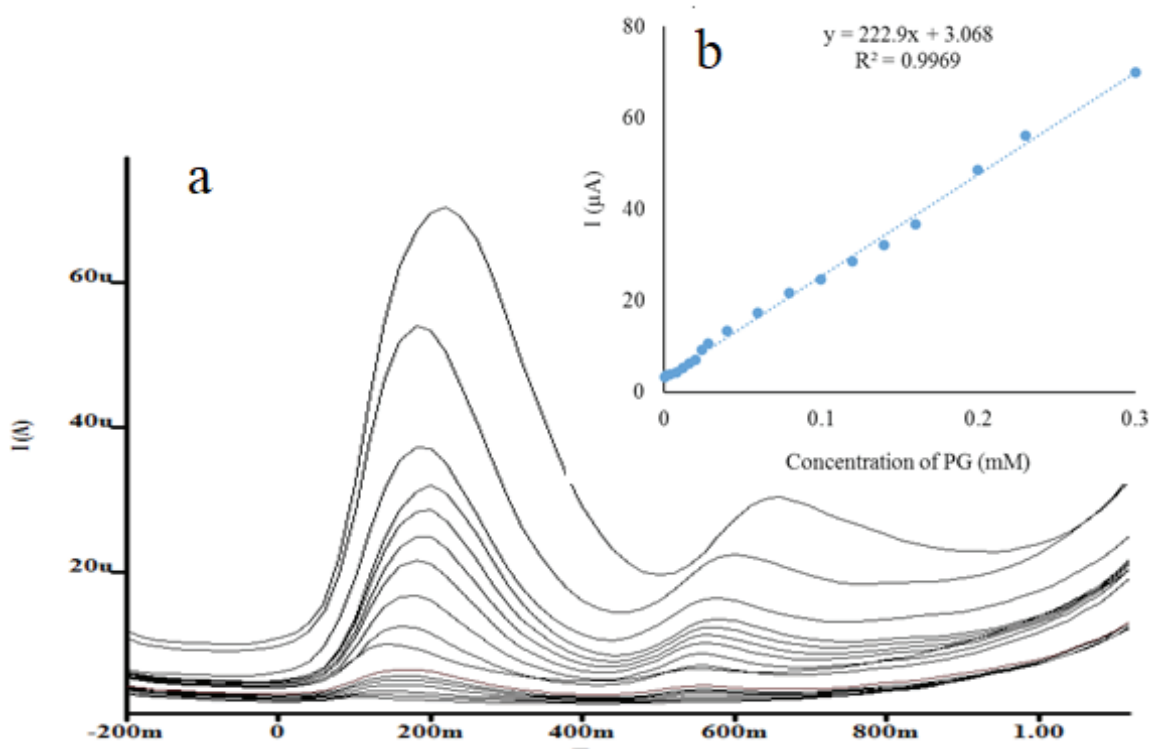


Fig. 7. (a) DPV obtained at a CdS/CPE for different concentrations of pyrogallol (0.7 to 300 μM). Inset: (b) linear relationship between the peak current and concentration of pyrogallol, scan rate: 50 mV s^{-1}

than those obtained by cyclic voltammetry, with a lower background current, resulting in improved resolution. According to the obtained results, it was possible to apply this technique to the quantitative analysis of pyrogallol. The phosphate buffer solution of pH 6 was selected as the supporting electrolyte for the quantification of pyrogallol as it gave maximum peak current at pH 6. DPV obtained with increasing amounts of pyrogallol showed that the peak current increased linearly with increasing concentration, as shown in Figure 7. Using the optimum conditions described previously, linear calibration curves were obtained for pyrogallol in the range of 7×10^{-8} to 3×10^{-4} M. (Fig. 7 Inset). The linear equation $I = 222.9x + 3.068$ ($R^2 = 0.9969$). The limit of detection (LOD), defined as $DL = 3S_b/m$ (where DL , S_b , and m are the limits of detection, the standard deviation of the blank and slope of the calibration graph, respectively) was found to be 0.48 μM of pyrogallol.

3.7. Interference study

To assess the prospects of the electroanalytical assays, several possible interferences of organic and inorganic chemicals were added into the 100 μM pyrogallol solutions to evaluate their effects on the current responses. The results were shows no significant signal change (below 5%) when 1000-fold phenol and hydroquinone Ca^{2+} , urea, Mg^{2+} , and 500 fold of glucose, caffeine, Na^+ , K^+ , Cl^- , and 100 fold of Zn^{2+} , Fe^{2+} , 10-fold folic acid, ascorbic acid were added.

3.8. The repeatability and stability

The repeatability of the CdS/CPE was examined by the determination of 0.8 mM of pyrogallol in 0.1 M phosphate buffer solution at pH=6 with the same electrode 5 times. A relative standard deviation (RSD) value of 3.92% was observed, indicating good reproducibility of CdS/CPE for pyrogallol determination. Furthermore, the

operational stability of CdS/CPE was investigated by the CV method every 2 days in 23 weeks. Only a small decrease of current (about 4.0%) for 0.1 mM pyrogallol was observed, which can be attributed to the good stability of the modified electrode.

3.9. Analysis of real samples

In order to evaluate the applicability of the proposed method in the real sample analysis, it was used to detect pyrogallol in tap water and green tea. The concentration of pyrogallol in these samples was obtained according to the calibration curve, and the results are listed in Table 1. In addition, the accuracy was evaluated by performing a recovery test after spiking the samples. The recovery is between 96.0 and 103.7 %, indicating that the determination of pyrogallol CdS/CPE is accurate and feasible. Analytical parameters obtained here

were compared with results obtained by other methods which show that they are comparable or better than the values reported by other groups (Table 2).

4. Conclusion

The CdS nanoparticles were synthesized via the microwave method. This method is rapid, simple, and can be easily controlled. The influence of different power on the morphology of the products was investigated. Cyclic voltammetry and differential pulse voltammetry determination of pyrogallol was successfully performed using CPE modified with CdS, which has shown an electrocatalytic effect on the oxidation of pyrogallol. The proposed electrode exhibited good sensitivity and stability for the determination of pyrogallol, with reduced overpotential. The pyrogallol peak current is linear

Table 1. Results of the recovery tests for pyrogallol using the CdS

Row	Sample	Spiked (μM)	Found (μM)	Recovery (%)
1	Tap water	0	Not detected	-
		40	38.4	96
		150	155.6	103.7
2	Green Tea	0	Not detected	-
		40	41.3	103.25
		150	153.1	102

Table 2. Comparison of detection limits and linear ranges obtained with the proposed electrode for determination of pyrogallol with those obtained by others

Working system	Linear range (μM)	Detection limit (μM)	Ref.
Pretreated Pt electrode	1-100	0.6	21
Au/CNT/PPY/HRP	1.6-22.4	1.24	22
GCE/poly(PPY-CD)	1 - 10	1.8	23
SPCE	10-1000	0.33	24
SiO ₂ -CPE	2-300	0.7	25
CdS-CPE	0.7-300	0.485	This work

from a concentration range of 0.7 μM to 300 μM with an excellent R^2 value of 0.9969. The detection limit of this modified electrode was found to be 0.48 μM and good reproducibility, high stability was obtained for the determination of pyrogallol using this electrode. The content of pyrogallol in tap water and green tea was successfully determined with CdS/CPE, which indicated the modified electrode is useable for the determination of pyrogallol concentration in real samples.

5. Acknowledgment

The author is grateful to Islamic Azad University, Kerman Branch, for financial assistance of this work.

6. References

- [1] A. Bao, N. Xiao, Y. Zhu, S. Xin, H. Zhang, The electrochemical catalytic behavior of pyrogallol at 8-hydroxyquinoline-Aluminum complex modified carbon paste electrode and its detection in tomato, *RSC Adv.*, 5 (2015) 12710-12716. <https://doi.org/10.1039/C4RA14842H>
- [2] M. Sharifi-Rad, N. V. Anil Kumar, Lifestyle, Oxidative stress, and antioxidants: Back and forth in the pathophysiology of chronic diseases, *Front. Physiol.*, 11 (2020) 694. <https://doi.org/10.3389/fphys.2020.00694>
- [3] G. Pizzino, N. Irrera, Oxidative Stress: harms and benefits for human health, *Oxid. Med. Cell. Longev.*, 2017 (2017) 8416763. <https://doi.org/10.1155/2017/8416763>
- [4] M. Mudasir, H. Ngatidjo, Spectrophotometric determination of pyrocatechol and pyrogallol based on their redox reaction with iron(III)/phenanthroline system, *Indo. J. Chem.*, 2 (2002) 161-163. <https://doi.org/10.22146/ijc.21911>
- [5] J. Dutschke, M. Suchowski, J. Pietsch, Simultaneous determination of selected catechins and pyrogallol in deer intoxications by HPLC-MS/MS, *J. Chromatogr. B*, 1180 (2021) 122886. <https://doi.org/10.1016/j.jchromb.2021.122886>
- [6] L. Zhang, X. Zheng, A novel electrogenerated chemiluminescence sensor for pyrogallol with core-shell luminol-doped silica nanoparticles modified electrode by the self-assembled technique, *Anal. Chim. Acta*, 570 (2006) 207-213. <https://doi.org/10.1016/j.aca.2006.04.018>
- [7] A. Cardenas, C. Frontana, Evaluation of a carbon ink chemically modified electrode incorporating a copper-neocuproine complex for the quantification of antioxidants, *Sens. Actuators B: Chem.*, 313 (2020) 128070. <https://doi.org/10.1016/j.snb.2020.128070>
- [8] D. Ersin, S. Ahmet, T. K. Mouhoum, D. Erhan, A. Hassan, Electrochemical evaluation of the total antioxidant capacity of Yam food samples on a polyglycine-glassy carbon modified electrode, <https://doi.org/10.2174/1573411014666180619143729>
- [9] G. Ziyatdinova, Y. Zelenova, H. Budnikov, Novel modified electrode with immobilized galvinoxyl radical for the voltammetric determination of antioxidant activity, *J. Electroanal. Chem.*, 856 (2020) 113677. <https://doi.org/10.1016/j.jelechem.2019.113677>
- [10] MM. Becker, EB. Ribeiro, O. Marques, Development of a highly sensitive xanthine oxidase-based biosensor for the determination of antioxidant capacity in Amazonian fruit samples, *Talanta*, 204 (2019) 626-632. <https://doi.org/10.1016/j.talanta.2019.06.002>
- [11] M. Amelia, C. Lincheneau, S. Silvi, A. Credi, Electrochemical properties of CdSe and CdTe quantum dots, *Chem. Soc. Rev.* 41 (2012) 5728-5743. <https://doi.org/10.1039/C2CS35117J>
- [12] J. Mariya George, A. Antony, B. Mathew, Metal oxide nanoparticles in electrochemical sensing and biosensing: a review, *Microchim. Acta*, 185 (2018) 358. <https://doi.org/10.1007/s00604-018-2894-3>
- [13] A. M Fekry, M. Shehata, S. M. Azab, A. Walcarius, Voltammetric detection of caffeine in pharmacological and beverages samples based on simple nano-Co (II, III) oxide modified carbon paste electrode in aqueous and micellar media, *Sens. Actuators. B*, 302 (2020) 127172. <https://doi.org/10.1016/j.snb.2019.127172>

- [14] N.P. Shetti, D.S. Nayak, G.T. Kuchinad, Electrochemical behavior of thiosalicylic acid at γ -Fe₂O₃ nanoparticles and clay composite carbon electrode, *Electrochim. Acta*, 269 (2018) 204-211. <https://doi.org/10.1016/j.electacta.2018.02.170>
- [15] B. Su, H. Shao, N. Li, X. Chen, Z. Cai, X. Chen, A sensitive bisphenol A voltammetric sensor relying on AuPd nanoparticles/graphene composites modified glassy carbon electrode, *Talanta*, 166 (2017) 126-132. <https://doi.org/10.1016/j.talanta.2017.01.049>
- [16] SD Bukkitgar, NP Shetti, RM Kulkarni, Construction of nanoparticles composite sensor for atorvastatin and its determination in pharmaceutical and urine samples, *Sens. Actuators B: Chem.*, 255 (2018) 1462-1470. <https://doi.org/10.1016/j.snb.2017.08.150>
- [17] N. P. Herring, A. B. Panda, Kh. AbouZeid, S. H. Almahoudi, Ch. R. Olson. Microwave synthesis of metal oxide nanoparticles, metal oxide nanomaterials for chemical sensors, Springer, (2013) 245-284. <https://link.springer.com/book/10.1007/978-1-4614-5395-6?noAccess=true>
- [18] A.R. Siamaki, A.E. Khder, V. Abdelsayed, M.S. El-Shall, B.F. Gupton, Microwave assisted synthesis of palladium nanoparticles supported on graphene: a highly active and recyclable catalyst for carbon-carbon cross-coupling reactions, *J. Catal.*, 279 (2011) 1-11. <https://doi.org/10.1016/j.jcat.2010.12.003>
- [19] F. Foroughi, M. Rahsepar, MJ. Hadianfard, H. Kim, Microwave-assisted synthesis of graphene modified CuO nanoparticles for voltammetric enzyme-free sensing of glucose at biological pH, *Microchim. Acta*, 185 (2017) 57. <https://doi.org/10.1007/s00604-017-2558-8>
- [20] M.S. Jagadeesan, K. Movlaee, T. Krishnakumar, S.G. Leonardi, G. Neric, One-step microwave-assisted synthesis and characterization of novel CuO nanodisks for non-enzymatic glucose sensing, *J. Electroanal. Chem.*, 835 (2019) 161-168. <https://doi.org/10.1016/j.jelechem.2019.01.024>
- [21] P. S. Feng, S.M. Wang, W.Y. Suand, S.H. Cheng, Electrochemical oxidation, sensitive determination of Pyrogallol at Preanodized screen-printed carbon electrodes, *J. Chin. Chem. Soc.*, 59 (2011) 1-8. <https://doi.org/10.1002/jccs.201100384>
- [22] N. Izaoumen, D. Bouchta, H. Zejli, M. Kaoutit, A. Stalcup. Electrosynthesis and analytical performances of functionalized poly (pyrrole/ β -cyclodextrin) films, *Talanta*, 66 (2005) 111-117. <https://doi.org/10.1016/j.talanta.2004.10.003>
- [23] S. Korkut, B. Keskinler, E. Erhan, An amperometric biosensor based on multiwalled carbon nanotube-poly (pyrrole)-horseradish peroxidase nanobiocomposite film for determination of phenol derivatives, *Talanta*, 76 (2008) 1147-1152. <https://doi.org/10.1016/j.talanta.2008.05.016>
- [24] S. Kanwal X. Fu, X. Su, Highly sensitive flow-injection chemiluminescence determination of pyrogallol compounds, *Spectrochim. Acta, part A*, 74 (2009) 1046-1049. <https://doi.org/10.1016/j.saa.2009.08.047>
- [25] J. Tashkhourian. S. M. Ghaderizadeh, SiO₂-modified carbon paste electrode for electrochemical determination of pyrogallol, *Rus. J. Electrochem.*, 50 (2014) 1066-1074. <https://doi.org/10.1134/S1023193514100139>